CHARGE MIGRATION THROUGH DUPLEX DNA: A STUDY OF THE MECHANISM FOR CHARGE MIGRATION AND OXIDATIVE DAMAGE

A Dissertation
Presented to
The Academic Faculty

by

Nathan William Schlientz

In Partial Fulfillment
of the Requirements for the Degree
Doctor of Philosophy in the
School of Chemistry and Biochemistry

Georgia Institute of Technology
August 2006

CHARGE MIGRATION THROUGH DUPLEX DNA: A STUDY OF THE MECHANISM FOR CHARGE MIGRATION AND OXIDATIVE DAMAGE

Approved by:

Dr. Gary B. Schuster, Advisor
School of Chemistry and Biochemistry
Georgia Institute of Technology

Dr. Laren Tolbert
School of Chemistry and Biochemistry
Georgia Institute of Technology

Dr. David Collard
School of Chemistry and Biochemistry
Georgia Institute of Technology

Dr. Uzi Landman
College of Physics
Georgia Institute of Technology

Dr. Nick Hud
School of Chemistry and Biochemistry
Georgia Institute of Technology

Date Approved: May 05, 2006

This dissertation is in dedication to my family.

To my parents, William and Mary Ann,

who have always been there for me, with all the love and support

i could ever ask for. I love you very much!

To my brothers and sisters,

Dejah, Jason, Christa, Graham, and Anna,

who have always been encouraging and a source of inspiration.

And finally to my wife, Leah,

for without her love and support none of this would have been possible.

She has guided me and loved me through these years and for that I will always be

grateful. I love you very much!

ACKNOWLEDGEMENTS

I wish to thank many people for my wonderful experiences at Georgia Institute of Technology. First, I would like to thank my advisor Professor Gary B. Schuster for allowing me to conduct research in his laboratory. The research opportunities he provides are tremendously inspirational and educational. His guidance and patience are second to none, and I am grateful to have worked under his tutelage.

Second, I would like to thank my doctoral committee for their support and useful suggestions. Third, I would like to thank the researchers from Schuster's lab. I couldn't have asked for a more enjoyable group of labmates to work alongside. Special thanks to Dr. Edna Boone for her assistance in teaching me how to use the lab equipment and perform the general experiments used in our laboratory; Dr. Sriram Kanvah for the synthesis of DNA oligomers as well as his support and guidance; Dr. Abraham Joy and Dr. Rick Redic for their support and helpful discussions and suggestions; and the remaining group members, Dr. Rochelle Bradford, Dr. Chu-Sheng Liu, Dr. Joshy Joseph, Dr. Bhaskar Datta, Dr. Santhosh Unni, Dr. Huachuan Cao, Dr. Lezah Roberts, Dr. Thabisile Ndlebe, Gozde Guler, Frank Onyemauwa, Prolay Das, Avik Ghosh, and Chiko Umeweni for their memorable moments in and out of the lab as well as their inspiration and motivation.

Lastly, I thank my friends and family for all of their support.

TABLE OF CONTENTS

LIST OF TABLES

LIST OF FIGURES

LIST OF SYMBOLS AND ABBREVIATIONS

α	alpha
Å	Angstrom(s)
A	Adenine
AQ	Anthraquinone
$AQ^{\cdot -}$	Anthraquinone radical anion
ATP	5'-adenosine triphosphate
b	path length
bpy'	4-butyric acid-4'-methyl bipyridyl
C	Cytidine
ºC	degree(s) Celcius
c_3C	3-deazacytidine
CD	Circular Dichroism
CV	Cyclic Voltammetry
cm	centimeter(s)
cpm	count(s) per minute
δ	delta
δA/δT	change in absorbance with respect to the change in temperature
D_2O	deuterium oxide
DFT	density functional theory
DMT	4,4'-methoxytrityl
DNA	Deoxyribonucleic Acid
dppz	dipyridophenazine
dsDNA	double-stranded DNA
ε	extinction coefficeint

ESI	Electrospray Ionization
F_5C	5-fluorocytidine
γ	gamma
G	Guanine
$G^{\cdot+}$	guanine radical cation
h	hour
hole	radical cation
HPLC	High-Performance Liquid Chromatography
in vacuo	in a vacuum
k_h	rate of hopping
k_t	rate of trapping
μ	micro (10-6)
M	molar
MALDI	Matrix-Assisted Laser Desorption Ionization
min	minute(s)
mM	millimolar
nm	nanometer(s)
phen	1,10-phenanthroline
phi	9,10-phenanthrenequinone diimine
PNK	polynucleotide kinase
Rh	Rhodium
ROS	Reactive oxygen species
Ru	Ruthenium
ssDNA	single-stranded DNA
T	Thymine

TdT	terminal dinucleotide transferase
Tm	melting temperature
TMSOTf	Trimethylsilyl Triflate
TOF	Time-of-Flight
UV	Ultraviolet
Vis	Visible

SUMMARY

Damage to endogenous DNA has been implicated in cancers, aging, and apoptosis. One-electron oxidation of duplex DNA leads to the migration of a "hole" through the duplex DNA, where it gets trapped predominantly at G_n (n = 2, 3, etc.) sites within the DNA. Hole-trapping at guanine results in further oxidation and damage of the guanine, which during DNA replication can lead to miscoding errors and eventually mutations. To better understand the one-electron oxidation of duplex DNA, several methods have been developed to abstract an electron from the duplex DNA allowing for charge migration. Our research has focused primarily on the charge injector anthraquinone (AQ). The AQ molecules excited state is energetic enough to abstract an electron from any of the four natural DNA bases. Upon abstraction of an electron, the "hole" migrates through the DNA until it is quenched by reaction predominantly at guanine. Analysis of charge migration through varying duplex DNA systems has led to a detailed understanding of the properties that govern charge migration through DNA.

It has been determined that charge migration through duplex DNA is highly sequence specific without regard for the length of DNA. Some studies have indicated that because of the sensitivity of DNA sequence, charge migration through DNA could be used as a sensor for mismatched base pairs. It has been shown that under certain circumstances, base pair mismatches retard the charge migration through DNA. Our studies have focused on two distinct mispairs within duplex DNA: contiguous A•A and T•T mismatch regions. The T•T mismatch base pair contains no purines, which are

believed to act as charge carriers during migration through DNA, and therefore it is expected these sequences would inhibit the charge to migrate beyond the mismatch region. However, the contiguous A•A mismatch region forms a "zipper-like" base pair conformation allowing for π-orbital overlap of the purine bases throughout the mismatch region and would potentially permit charge migration through the "zipper-like" region. Results of these studies will further demonstrate the degree of sensitivity of charge migration towards mismatch base pairs as well as gain insight into the mechanism of charge migration through duplex DNA.

Charge migration through duplex DNA leads to oxidative damage at G_n (n = 2, 3, etc.) steps. The mechanism of oxidative damage at guanine is not fully understood in duplex DNA, therefore studies to elucidate this mechanism have led to the belief that 8-oxo-guanine is an intermediate in the oxidation of guanine by charge migration. The reaction pathway for oxidation of guanine is hypothesized to take one of two different pathways (Figure 4.1). To probe the whether one pathway is preferred, studies have been conducted to increase the pKa of cytidine to inhibit the proton transfer from the N1 of guanine to the N3 of cytidine. These studies revealed that oxidation of guanine base paired with 5-fluoro-cytidine (F_5C) severely reduces the extent of oxidative damage at the paired guanines. However, it was also shown that the charge migration efficiency beyond the site of G:F_5C was not affected.

We have synthesized the cytidine analogue 3-deaza-2'-methoxycytidine for the purposes of base pairing it with guanine and measuring its effects on charge migration

efficiency as well as oxidative damage at the gaunines. Removal of the hydrogen bond acceptor reduces the number of hydrogen bonds from three to two, and potentially imposes steric hindrance on the base stacking at the site of modification. These studies will further enhance the understanding of the mechanism of oxidative damage at guanine by eliminating one of the possible reaction pathways predicted to govern the oxidative damage of guanine in duplex DNA.

CHAPTER 1

INTRODUCTION

From the early discovery that DNA is the carrier of genetic information[1] to the elucidation of its secondary structure by Watson and Crick in 1953[2], DNA has motivated scientists and biochemists alike to study its vast chemical and physical properties. With the elucidation of the secondary structure of duplex DNA, it was immediately postulated that the nature of base stacking could facilitate the migration of a charge through the DNA. For nearly two decades scientists have been rigorously investigating the process of charge migration through DNA. This intensive investigation is motivated in part by its relevance to two important subjects. First, charges moving through DNA may result in oxidative damage, which has been implicated in aging, apoptosis, and cancer.[3-6] A better understanding of the properties managing charge migration and the resulting damage of DNA may lead to greater insight into damage prevention and repair.[7] Second, the property of charge migration through DNA has led to the hypothesis that DNA would be a reasonable conductor for "molecular electronics" applications.[8]

Charge migration through duplex DNA is the migration of a radical cation, "hole", or an electron through the DNA. Hole migration through DNA has been shown to travel over 200 Å where it then reacts with water or molecular oxygen.[9] Although it is acknowledged that the charge can migrate to sites distant from its origin, the mechanism by which this migration process occurs has produced some controversy.

Previously, several competing theories of the mechanism of charge migration through DNA prompted detailed investigations including experimental and theoretical studies.[10-12] This hopping mechanism is believed to occur via one of two basic processes. The first process is based upon a hole-resting site model where the charge resides on guanines, the base with the lowest oxidation potential, and tunnels through A:T bridges to the nearest guanine.[13] There are several proposed mechanism that involve this tunneling process[14, 15], however, experimental evidence has restricted this model to bridges of only three A:T base pairs, and anything larger than three base pairs must occur through some other hopping mechanism. The second proposed migration process involves hopping of the charge through the DNA from one low energy site to the other, requiring sufficient energy to overcome the activation barrier. In this process it is proposed that the radical cation resides on the A/T bridge as it crosses the barrier. There are two prominent mechanisms that have evolved from this process, one of which is widely gaining support as the most probable mechanism for charge transport in DNA.[14, 15]

The phonon-assisted polaron hopping model[16] (discussed in Chapter 2) is widely gaining acceptance as the most likely candidate for the mechanism of charge migration through DNA. The charge migration efficiency is greatly affected by the sequence of the DNA, as the extent of charge delocalization and the height of the activation barrier are determined by the DNA sequence. Several studies have been conducted in an attempt to verify this model, including studies that vary the size of the polaron and/or the activation barrier as well as altering the environment surrounding the radical cation.

Here we report two studies intended to examine the extent of polaron formation as well as the efficiency of charge migration and charge trapping. First, we have introduced two mismatched base pair regions that have been found to adopt distinctly different conformations at the site of mispairs. These two variable regions are made of either contiguous A:A or T:T mismatches. The A:A mismatch region adopts a zipper-like conformation[17], where the T:T mismatch region adopts a wobble base pair structure.[18, 19] Notably, the A:A zipper-like region contains only purine bases whereas the T:T wobble base pair region contains only pyrimidines, which is significant because purines are believed to act as charge carriers for charge migration. Second, we have investigated the effect of introducing a cytidine analogue, 3-deazacytidine, opposite a GG step in the DNA. This analogue is designed to eliminate the central hydrogen bond between the normal G:C base pair, removing the possibility of proton transfer from G to C during charge migration and oxidation.

The DNA Double Helix

Elucidation of the Secondary Structure of DNA

In 1871, the German medical researcher Friedrich Miescher published the first report of nuclein[20], an isolated substance that was later purified further to DNA. Despite this discovery, for years it was believed that the coding of genetic information was held within the complex array a protein structures. Proteins are comprised of 20 amino acids that can adopt a vast number of sequences and therefore it was thought these amino acids made up the alphabet for genetic information. However, inspired by experiments by

Frederick Griffith in 1928[21], Oswald Avery in 1944 determined that DNA was responsible for carrying genetic information, not proteins.[1] Around the time of this discovery, advances in X-ray diffraction techniques allowed scientists Maurice Wilkins and Rosalind Franklin to obtain the first clear diffraction patterns of duplex DNA molecules.[22, 23] In the late 1940's Erwin Chargaff discovered a roughly equivalent relationship between the ratio of adenines and thymines as well as between guanines and cytosines.[24] However, it wasn't until two Cambridge scientists, Dr. James Watson and Francis Crick, were able to successfully interpret the X-ray diffraction patterns and available data regarding DNA that an accurate model of the secondary structure of DNA was reported.[2]

The X-ray diffraction data obtained by Wilkins and Franklin made it clear that DNA was helical in nature.[22, 23] The atomic components and their approximate orientations were believed to be known, and it was shown that the sugar-phosphate backbone was repetitive throughout the entire sequence. Watson and Crick were able to construct a model of the secondary structure of DNA from all of the data available. In 1953 it was reported that DNA consists of two helical chains each coiled around the same axis. The chains were made of phosphate diester groups joining β-D-deoxyribofuranose residues with 3', 5' linkages. The two chains are right handed helices running in opposite directions with water and cations associating with the DNA molecules. One of the most novel features of the Watson and Crick model was the base pairing between purines and pyrimidines. They show that adenine pairs with thymine and guanine with cytosine, and that these base pairs are held together by hydrogen bonds that are specific for each pair.

The elucidation of the secondary structure of DNA was sufficient in answering the question of how DNA could possibly be the carrier of genetic information with only four base pairs. Watson and Crick also reported that the complementarity of duplex DNA leads to the ability of self-replication, resulting in the creation of identical pairs of DNA.[2]

Structural Components

Deoxyribonucleic acid, DNA, is a relatively simple polymeric biomolecule, which is the carrier of human genetic information. It is comprised of a repeating monomer unit made up of a furanose ring (sugar) with phosphate linkages and a nitrogenous base. The sugar and phosphates make up the backbone of DNA with the phosphates attached to the 5'-CH_2OH and 3'-OH of the sugar, giving rise to a 5' and 3' terminus to DNA single strands (Figure 1.1). DNA differs from RNA within the sugar in that RNA contains a hydroxyl group at the 2' position, known as a ribose unit, whereas DNA has a CH at the 2' position, referred to as a 2'-deoxyribose. The sugar of both DNA and RNA adopt the β-D-conformation meaning both the substituents at the 1' and the 4' position are facing "up", or above the plane of the ring, whereas the 2' (RNA only) and 3' substituents are below the plane of the ring (Figure 1.2).

The sugar's five-membered ring is very important in determining the overall secondary structure of the DNA helix. One of the atoms in the ring tends to "pucker" out of the plane of the ring, potentially affecting the overall shape of the double helix (Figure 1.3). For the majority of DNA the sugar pucker is 2'-*endo*, which means the C2 position

is above the plane of the ring. In RNA the sugar pucker is 3'-*endo*, which means the C3 position is above the plane of the ring.

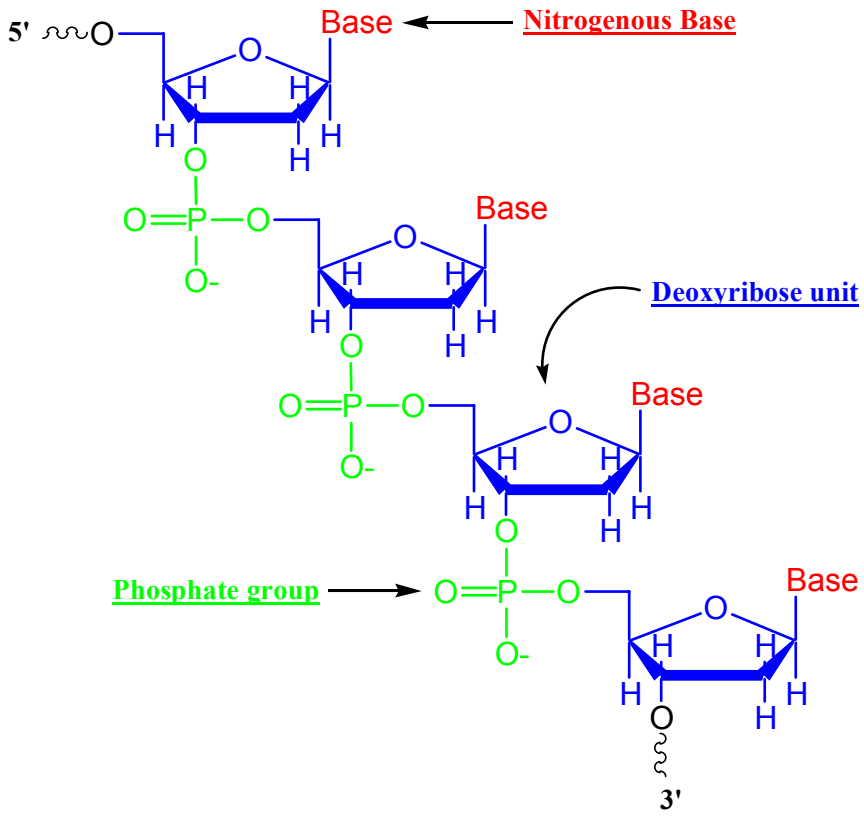

Figure 1.1. DNA Components.

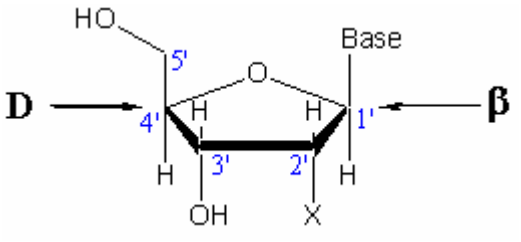

Figure 1.2. Ribose Unit of DNA. Numbering of the carbon atoms is in blue. X is OH for RNA and H for DNA.

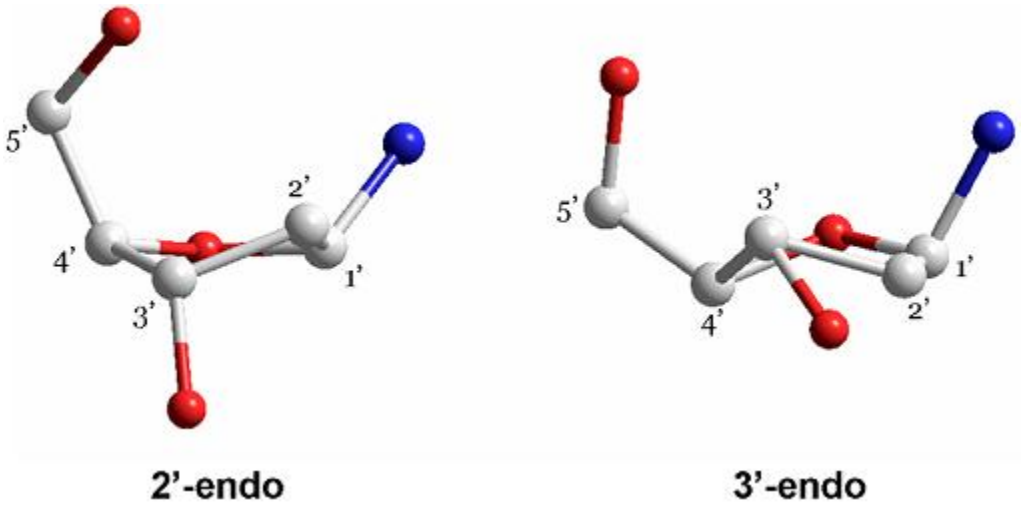

Figure 1.3. DNA Ribose Sugar-Puckering. Blue molecules are Nitrogen, red molecules are Oxygen, and white molecules are Carbon (Hydrogens are not shown).

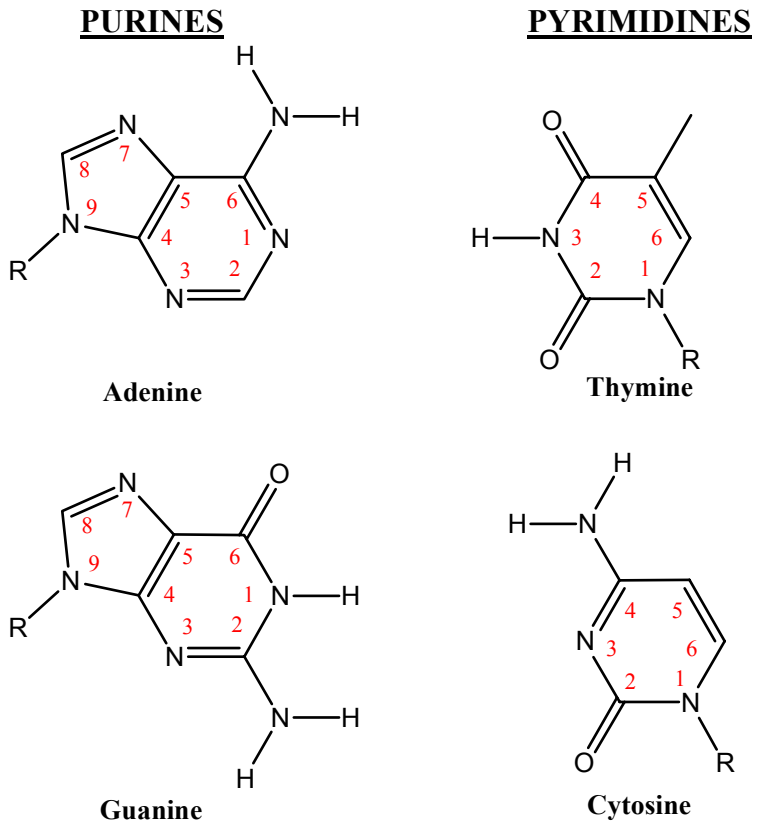

Figure 1.4. Heterocyclic Bases of DNA. Numbering of the ring atoms is shown in red. R is the deoxyribose unit.

The heterocyclic bases of DNA are attached to the 1' position of the furanose ring via an amine linkage and consist of either a purine or pyrimidine ring. There are two purine bases, adenine (A) and guanine (G), and two pyrimidine bases, thymine (T) and cytidine (C) as shown in Figure 1.4. These four aromatic bases make up the sequence of the DNA and are responsible for the complementarity of the duplex. The purine bases are paired with pyrimidine bases, but more specifically adenine pairs with thymine and guanine pairs with cytidine (Figure 1.5).

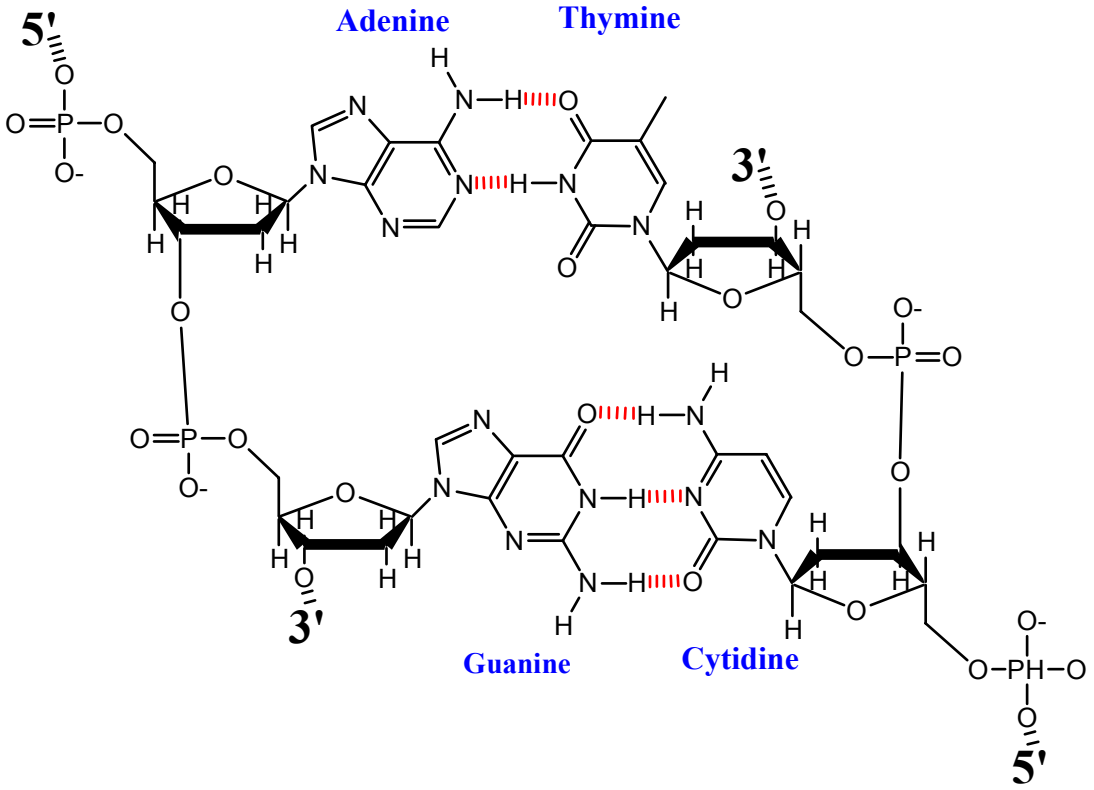

Figure 1.5. DNA Base Pairing.

Base pairing of DNA is sequence specific and allows for the coding of genetic information. The specific base pairs result from hydrogen bonds, H-bonds, between the functional groups of bases. The A:T base pair consists of two H-bonds: one H-bond between the C6-NH_2 of A and C4-O of T and one H-bond between N1 of A and N3-H of T. The G:C base pair consists of three H-bonds: an H-bond between C6-O of G and C4-NH_2 of C, an H-bond between N1-H of G and N3 of C, and an H-bond between C2-NH_2 of G and C2-O of C. These base pairs allow for the replication of DNA where an exact replica is created of each strand because the enzyme recognizes the specific base and places the complement opposite that position. Therefore, DNA replication occurs by transcribing the complement of the strand that is being "read" by the enzyme, and when both strands are copied a new duplex is formed with exactly the same sequence as the parent duplex.

Structural Motifs: A, B, and Z DNA

Under physiological conditions, DNA exists as a double helical polymer with each strand coiled around the same axis. The two strands run antiparallel to each other with the 5' end of one strand matching up with the 3' end of its complementary strand. The development of DNA synthetic techniques[25] made it possible for the first time to prepare tens of milligrams of pure DNA oligomers of predetermined sequence, and to obtain crystals suitable for x-ray analysis. From these studies it has been determined that the secondary structure of duplex DNA varies based on the environment with fundamental differences in the way in which the base pairs are stacked and the sugar-phosphate backbones are wrapped around the helix axis.[26] Three varying conformations

for DNA, A, B, and Z form duplex DNA, have been confirmed from both solution studies as well as x-ray diffraction analysis of pure crystals (Figures 1.6-1.8).

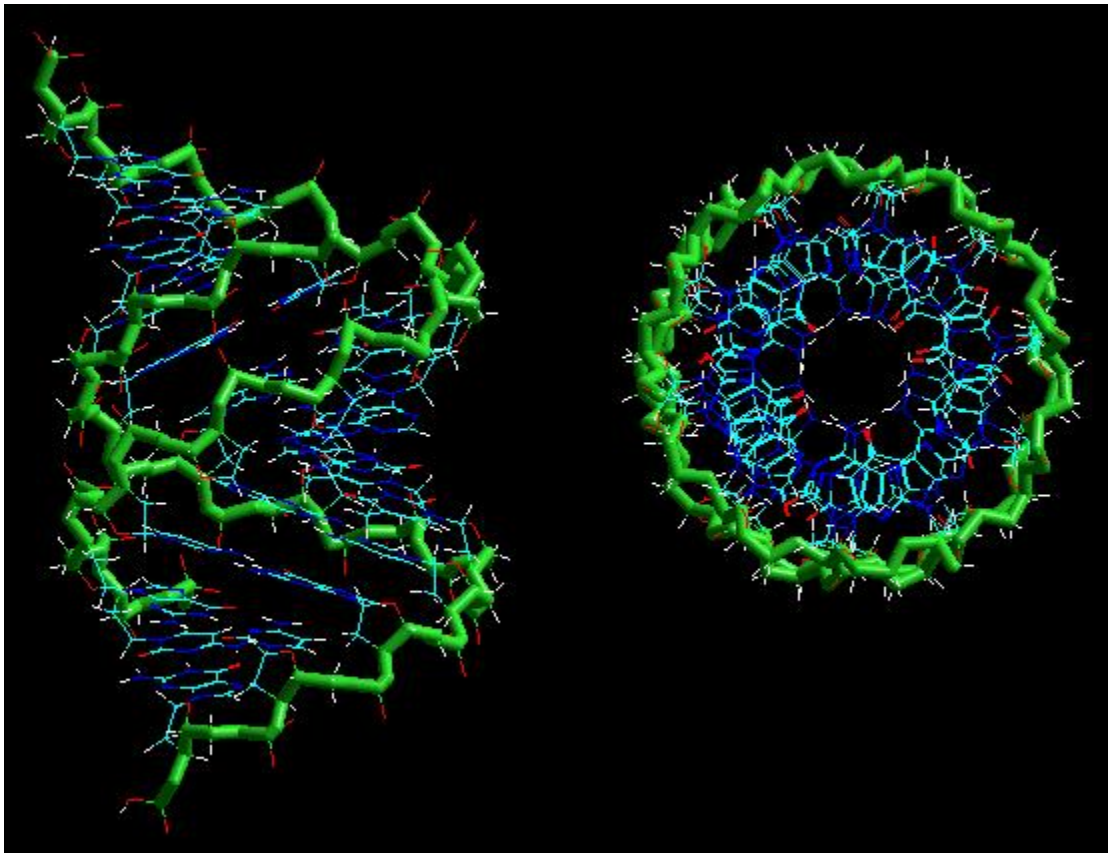

Figure 1.6. Hyperchem Modeling Image of A Form DNA.

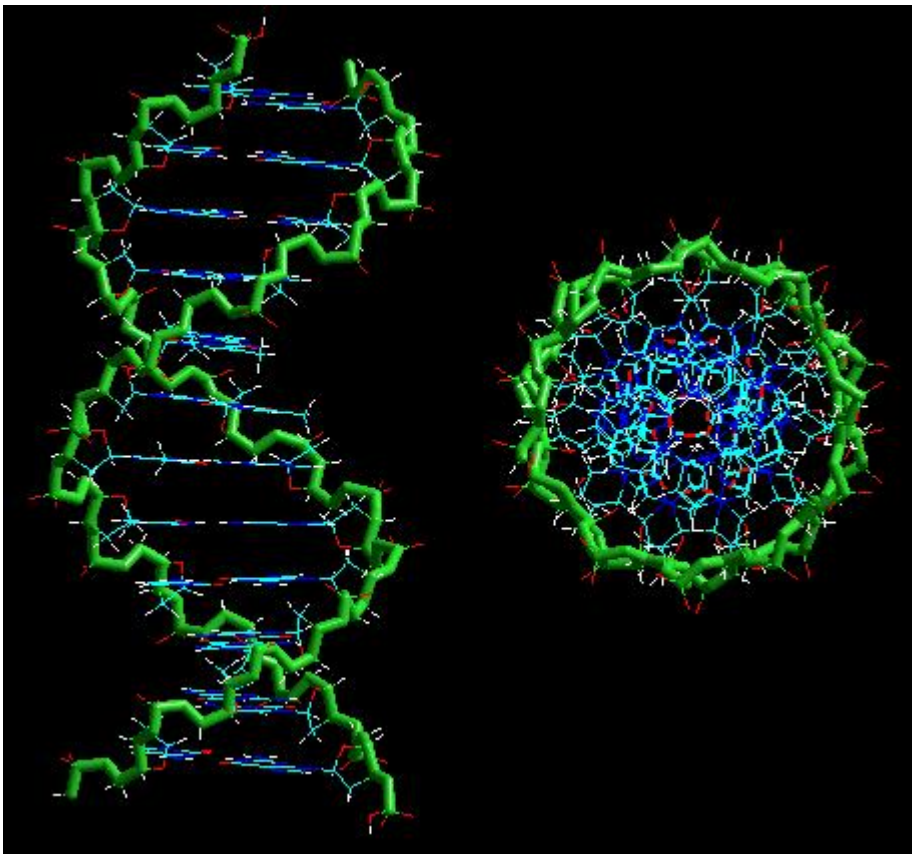

Figure 1.7. Hyperchem Modeling Image of B Form DNA.

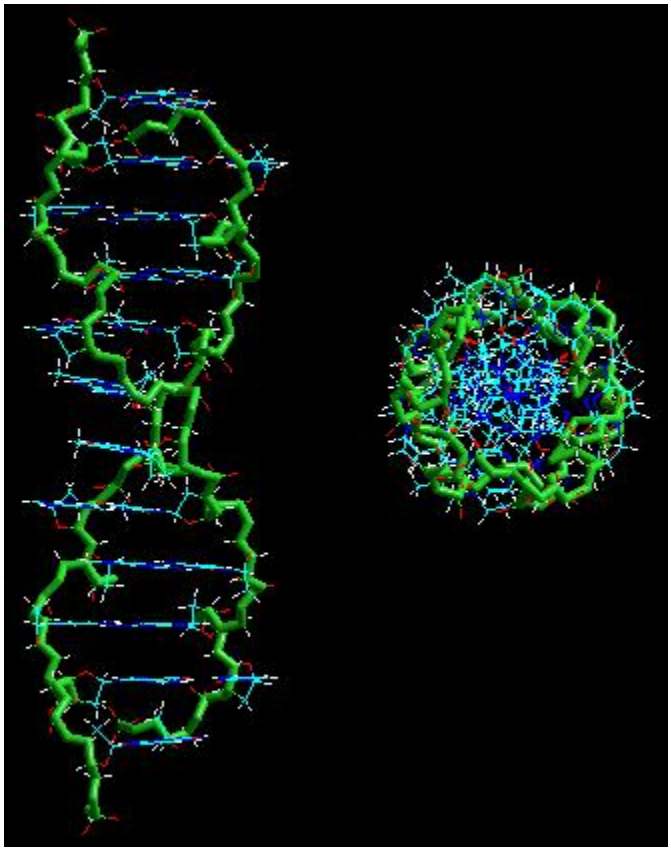

Figure 1.8. Hyperchem Modeling Image of Z Form DNA.

Duplex DNA structures crystallized under varying salt, alcohol, and humidity conditions have helped to define the parameters of each of the secondary structures, as shown in Table 1. The secondary structures A-, B-, and Z-DNA vary drastically as a result of the hydration of the phosphate backbone, differing sugar-pucker conformations and stacking interactions between the base pairs. A-DNA is a wider, shorter right-handed helix with the bases tilted sharply with respect to the helix axis (Figure 1.6). The two helical sugar-phosphate backbones of DNA form two varying grooves in duplex DNA, known as the major and minor grooves. In A-DNA the major groove is very deep and the minor groove is so shallow it is hardly even considered a groove at all. B-DNA is also a right-handed helix, but it is slimmer and more elongated than A-DNA with the planes of the bases essentially perpendicular to the helix axis (Figure 1.7). The grooves of B-DNA are also different that A-DNA in that the major groove and minor groove are nearly equivalent in depth, with the major groove being wider than that of the minor groove (Figure 1.9). The major and minor grooves of B-DNA can also be determined by the direction the bases are facing. The N7 and C6 of A and G as well as the C5 of C and T point towards the major groove, while the N3 of A and G as well as the C2-O of C and T point towards the minor groove. Z-DNA is even slimmer and more elongated, but the most drastic difference is that Z-DNA is a left-handed helix (Figure 1.8). In Z-DNA the minor groove is very deep and the major groove is completely flattened out on the surface of the molecule. The key features of Z-DNA are the left-handed helix and the use of two consecutive nonequivalent base pairs as the helical repeating unit (alternating *syn* and *anti* conformations at guanine and cytosine, respectively), yielding the zigzag configuration for the sugar-phosphate backbone which gives rise to the name Z-DNA.

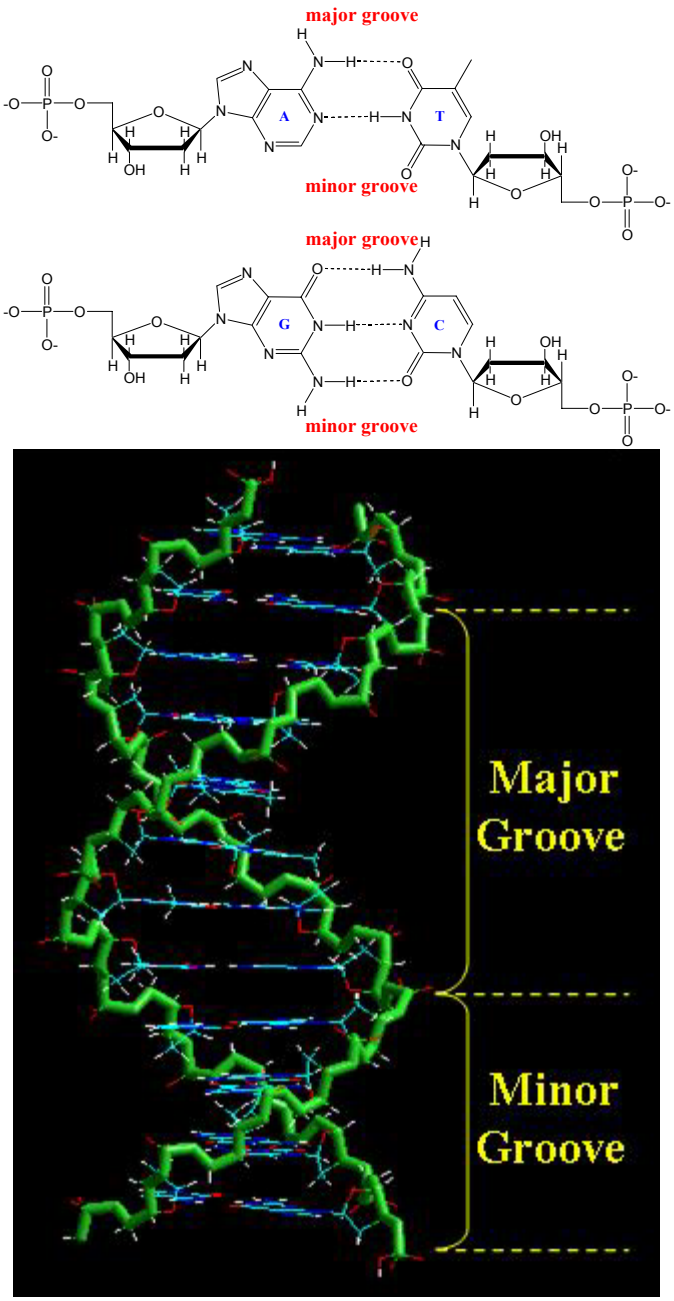

Figure 1.9. Schematic Illustration of the Major and Minor Grooves of B-DNA. Top View: grooves in relation to the functional groups of the base pairs. Bottom View: grooves with respect to the double-stranded DNA molecule.

Table 1.1.[26] Parameters of Polynucleotide Helices. * Mean and standard deviation over 36 bases or 33 base steps in three independently refined dodecamers: CGCGAATTCGCG with bent helix axis, and CGCGAATT^{Br}CGCG (where ^{Br}C is 5-bromocytosine) under conditions in which its axis is bent and straight. The quantity t_g is the global twist angle as measured from outside the helix, whereas t_t is the local value considering the two base pairs in isolation. They differ because the local helix axis frequently deviates from the best overall axis.

Property	Helix		
	A Form	B Form	Z Form
Helix sense	Right-handed	Right-handed	Left-handed
Repeating helix unit	One base pair	One base pair	Two base pairs
Rotation per base pair	33.6°	t_t = 38.0° (4.4°)* t_g = 35.9° (4.2°)*	-60°/2
Mean base pairs per turn	10.7	10.0 (1.2)*	12
Inclination of base normals to helix axis	+19°	-1.2° (4.1°)*	-9°
Rise per base pair along helix axis	2.3 Å	3.32 Å (0.19 Å)*	3.8 Å
Pitch per turn of helix	24.6 Å	33.2 Å	45.6 Å
Mean propeller twist	+18°	+16° (7°)*	~ 0°
Glycosyl angle conformation	*anti*	*anti*	*anti* at C, *syn* at G
Sugar pucker conformation	C3'-*endo*	O1'-*endo* to C2'-*endo*	C2'-*endo* at C C2'-*exo* to C1'-*exo* at G

Geometry of B_DNA

The double stranded nature of DNA is a result of several variables, most notably the hydrophobic interactions that occur between the bases of the DNA and the aqueous environment. The polyanionic backbone of DNA is solvated and neutralized by counterions, such as sodium and magnesium, in solution. However, it is energetically unfavorable for the hydrophobic bases to reside within the aqueous environment and they are therefore aligned within the central portion of the duplex, essentially being mostly shielded from the water molecules by the sugar-phosphate backbone and base to base

stacking interactions. The bases are collapsed and stack on top of each other, known as base stacking, within the central portion of the helix. This stacking is held together by the hydrophobic interactions as well as π-interactions between neighboring bases. Essentially, each base along the entire length of the DNA is stacked with π-orbital overlap between the bases on either side. However, the edges of the bases have functional groups that can potentially hydrogen bond with water molecules.

Extensive studies and x-ray crystallographic information has shown that water molecules bind with a degree of specificity to the major and minor grooves of DNA.[27] A detailed crystallographic investigation of the dodecamer $d(CGCGAATTCGCG)_2$ revealed 72 ordered water molecules associated with the DNA, most of which associate with polar N and O atoms at the edges of the DNA base-pairs.[28] Binding of water molecules also occurs much more tightly with the phosphate-backbone, but tends not to be ordered, except where they are confined by the 5-methyl group of T.

Binding of water molecules to the minor groove of DNA have been shown to form a well-ordered spine of hydration (Figure 1.10). This spine of hydration is composed of two well-ordered layers, primary and secondary layers, where the primary layer interacts directly with the functional groups of the DNA and the secondary layer interacts with the primary layer. The primary and secondary layers of hydration serve as a foundation for disordered outer layers that span beyond the radius of the phosphate backbone. The spine of hydration is especially well-ordered at the A/T rich region of the DNA, where the water molecules bridge across the minor groove from one DNA strand

to the other. Specifically, each water molecule in the A/T region bridges the N3 of A to the 3'-neighboring C3-O of T or C, as illustrated in Figure 1.11. Within the G/C region of the DNA the G introduces an amino group at the C2 position that resides within the minor groove. The presence of this amino group partially disrupts the spine of hydration by pushing it away from the "floor" of the groove by shifting the coordination from the N3 to the C2-NH_2 of G. This effectively dries the outer layers of hydration near the G/C rich region when compared to the A/T rich region.

The major groove of DNA has one layer of ordered water molecules, the majority of which exhibit monodentate binding. Within the major groove of DNA the base pairs expose three polar groups, N and O atoms (Figure 1.9), that associate with the water molecules (Figure 1.12). Within the A/T rich region of the dodecamer, three of the four A's have a water molecule with bidentate association with both C6-NH_2 and N7. To a lesser extend, a few of the water molecules bridge the base and phosphate groups. Within the G/C rich region, the C4-NH_2 of C and C6-O of G associate with water molecules independently, and the N7 of G is generally less hydrated.

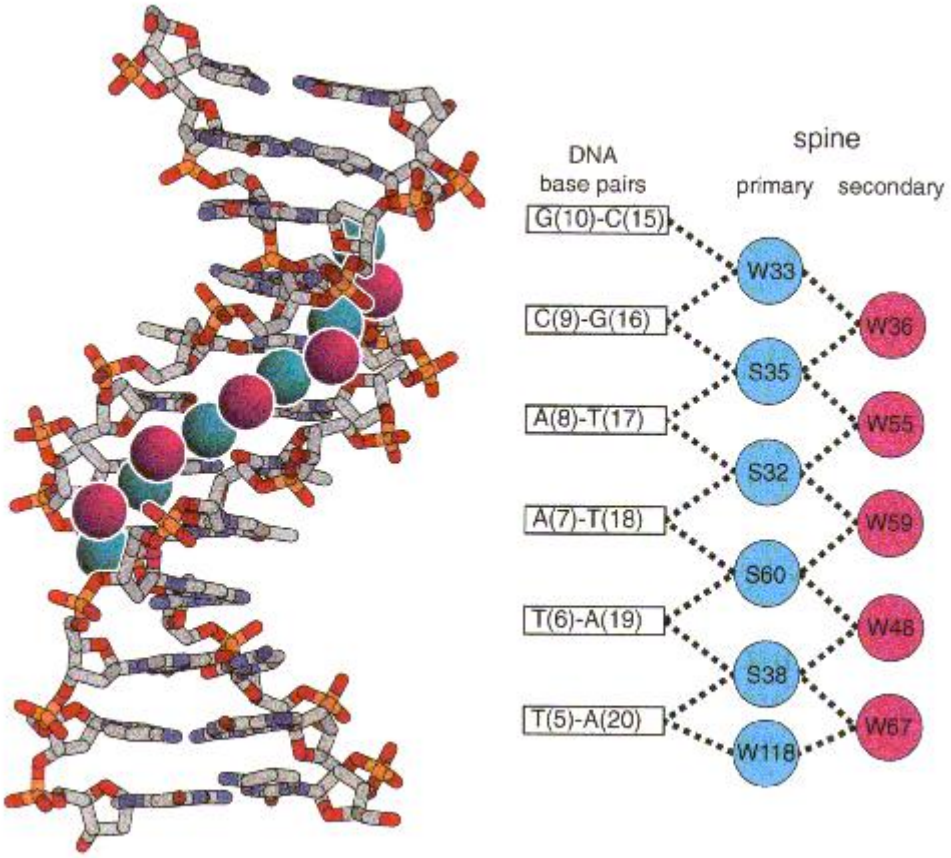

Figure 1.10.[28] DNA Minor Groove Spine of Hydration. The DNA duplex is the dodecamer, d(CGCGTTAACGCG)$_2$. Primary spine is cyan and secondary spine is magenta.

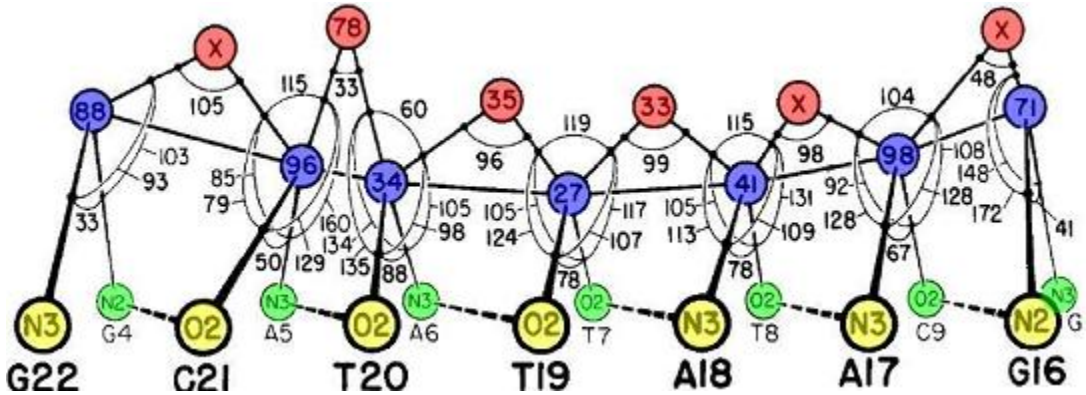

Figure 1.11.[27] Illustration of the Spine of Hydration. Duplex structure is d(CGCGAATTCGCG)$_2$. Dashed lines represent base-pairs, and DNA-H_2O and H_2O-H_2O bond angles show near tetrahedral geometry for the primary layer H_2O molecules (blue). Secondary layer water molecules are shown in red, DNA base functional groups shown in green and yellow.

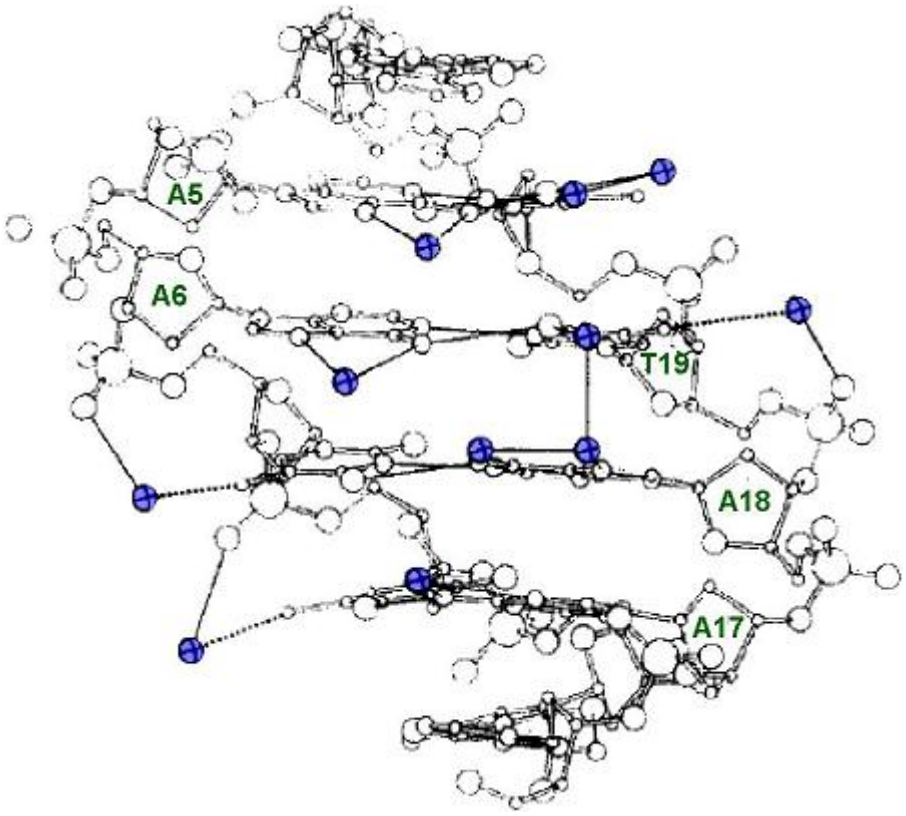

Figure 1.12.[27] Major Groove Hydration at the A/T-rich Region. Water molecules are blue and bases are numbered in green.

Dickerson and Drew were able to hypothesize based on their x-ray crystal data that the hydration of DNA is one of the most influential stabilizing factors. Particularly, the ordered spine of hydration within the minor groove of B-DNA is shown to be one of the main elements in its helix stability compared to A and Z-DNA. This is evident in the fact that the absence of G prohibits the transition from B to A-DNA (Table 1.2), as A's and T's form a much more defined spine of hydration and G's tend to disrupt the spine. Studies where C's are base paired with inosine (I), a purine with the C2-NH_2, help to further support the hypothesis that G's are responsible for the ability of duplex DNA to transition from B to A-DNA. When the duplex contains I's and C's, in the complete absence of G's, the DNA was unable to transition from B to A-DNA, thereby confirming the influence the spine of hydration has on the formation and stability of B-DNA.

Table 1.2.[27] Spine of Hydration Influence on DNA Conformation Stability. * Z-DNA is only formed in alternating purine-pyrimidine base pair duplexes.

Spine of Hydration Influence on DNA Conformation		
DNA Base Pairs	Purine C2-NH_2	DNA Conformation
A/T and I/C	NO	B-DNA only
A/T and G/C	YES	A, B and Z*-DNA

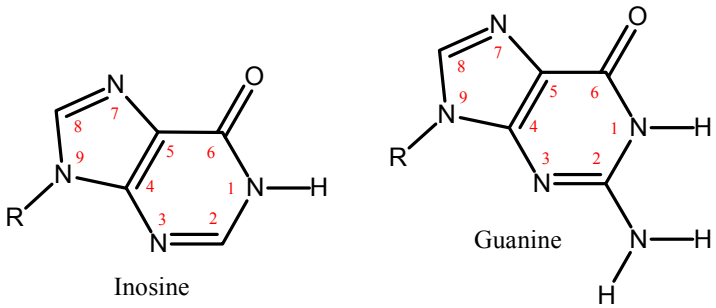

Figure 1.13. Structural Comparison of Inosine and Guanine.

REFERENCES

[1] Avery, Oswald T.; MacLeod, Colin M.; McCarty, Maclyn, Studies on the Chemical Nature of the Substance Inducing Transformation of Pneumococcal Types: Induction of Transformation by a Desoxyribonucleic Acid Fraction Isolated from Pneumococcus Type III. *The Journal of Experimental Medicine* 1944, 79, 137-158.

[2] Watson, James. D.; Crick, Francis H. C., Molecular Structure of Nucleic Acids: A Structure for Deoxyribose Nucleic Acid. *Nature* 1953, 171, 737-738.

[3] Ames, Bruce N.; Lee, Frank D.; Durston, William E., An Improved Bacterial Test System for the Detection and Classification of Mutagens and Carcinogens. *PNAS* 1973, 70, (3), 782-786.

[4] Demple, B.; Harrison, L., Repair of Oxidative Damage to DNA - Enzymology and Biology. *Annual Review of Biochemistry* 1994, 63, 915-948.

[5] Friedman, K. A.; Heller, A., On the Non-Uniform Distribution of Guanine in Introns of Human Genes: Possible Protection of Exons against Oxidation by Proximal Intron Poly-G Sequences. *J. Phys. Chem. B* 2001, 105, (47), 11859-11865.

[6] Poulsen, H. E.; Prieme, H.; Loft, S., Role of Oxidative DNA Damage in Cancer Initiation and Promotion. *European Journal of Cancer Prevention* 1998, 7, (1), 9-16.

[7] Boiteux, Serge; Gellon, Lionel; Guibourt, Nathalie, Repair of 8-oxoguanine in Saccharomyces Cerevisiae: Interplay of DNA Repair and Replication Mechanisms. *Free Radical Biology and Medicine* 2002, 32, (12), 1244-1253.

[8] Ventra, M. Di; Zwolak, M., DNA Electronics. In *Encyclopedia of Nanoscience and Nanotechnology*, Nalwa, H. S., Ed. American Scientific Publishers: 2004; Vol. 2, pp 475-493.

[9] Beratan, David N.; Priyadarshy, Satyam; Risser, Steven M., DNA: Insulator or Wire? *Chemistry and Biology* 1997, 4, 3-8.

[10] Giese, B., Long-Distance Charge Transport in DNA: The Hopping Mechanism. *Acc. Chem. Res.* 2000, 33, (9), 631-636.

[11] Liu, C. S.; Hernandez, R.; Schuster, G. B., Mechanism for Radical Cation Transport in Duplex DNA Oligonucleotides. *J. Am. Chem. Soc.* 2004, 126, (9), 2877-2884.

[12] O'Neill, M. A.; Barton, J. K., DNA Charge Transport: Conformationally Gated Hopping through Stacked Domains. *J. Am. Chem. Soc.* 2004, 126, (37), 11471-11483.

[13] Murphy, C. J.; Arkin, M. R.; Jenkins, Y.; Ghatlia, N. D.; Bossmann, S. H.; Turro, N. J.; Barton, J. K., Long-Range Photoinduced Electron Transfer Through a DNA Helix. *Science* 1993, 262, (5136), 1025-1029.

[14] Topics in Current Chemistry. In *Long-range Charge Transport in DNA I*, Schuster, G. B., Ed. Springer Berlin / Heidelberg: 2004; Vol. 236, pp 1-204.

[15] Topics in Current Chemistry. In *Long-range Charge Transport in DNA II*, Schuster, G. B., Ed. Springer Berlin / Heidelberg: 2004; Vol. 237, pp 1-228.

[16] Henderson, Paul T.; Jones, Denise; Hampikian, Gregory; Kan, Yongzhi; Schuster, Gary B., Long-Distance Charge Transport in Duplex DNA: The Phonon-Assisted Polaron-Like Hopping Mechanism. *PNAS* 1999, 96, (15), 8353-8358.

[17] Shepard, W.; Cruse, W. B.; Fourme, R.; de la Fortelle, E.; Prange, T., A Zipper-Like Duplex in DNA: the Crystal Structure of d(GCGAAAGCT) at 2.1 A Resolution. *Structure* 1998, 6, (7), 849-861.

[18] Peyret, N.; Seneviratne, P. A.; Allawi, H. T.; SantaLucia, J., Nearest-Neighbor Thermodynamics and NMR of DNA Sequences with Internal A·A, C·C, G·G, and T·T Mismatches. *Biochemistry* 1999, 38, (12), 3468-3477.

[19] Trotta, E.; Paci, M., Solution Structure of DAPI Selectively Bound in the Minor Groove of a DNA T.T Mismatch-Containing Site: NMR and Molecular Dynamics Studies. *Nucl. Acids Res.* 1998, 26, (20), 4706-4713.

[20] Miescher, Friedrich, *Med Chem Untersuchun* 1871, 4, 441-460.

[21] Griffith, Frederick, The Significance of Pneumococcal Types. *J. Hyg.* 1928, 27, 113-159.

[22] Franklin, Rosalind Elsie; Goslin, R. G., Evidence for a 2-chain Helix in the Crystalline Structure of Sodium Deoxyribonucleate. *Nature* 1953, 172, 156.

[23] Franklin, Rosalind Elsie; Goslin, R. G., The Structure of Sodium Thymonucleate Fibres: I. The Influence of Water Content. II. The Cylindrically Symmetrical Patterson Function. *Acta Crystallography* 1953, 6, 673-685.

[24] Chargaff, Erwin, Composition of Human Desoxypentose Nucleic Acid. *Nature* 1950, 165, 756.

[25] Itakura, K.; Katagiri, N.; Bahl, C. P.; Wightman, R. H.; Narang, S. A., Improved Triester Approach for the Synthesis of Pentadecathymidylic Acid. *Journal of the American Chemical Society* 1975, 97, (25), 7327-7332.

[26] Dickerson, R. E.; Drew, H. R.; Conner, B. N.; Wing, R. M.; Fratini, A. V.; Kopka, M. L., The Anatomy of A-, B-, and Z-DNA. *Science* 1982, 216, (4545), 475-485.

[27] Drew, Horace R.; Dickerson, Richard E., Structure of a B-DNA Dodecamer , : III. Geometry of Hydration. *Journal of Molecular Biology* 1981, 151, (3), 535-556.

[28] Shui, X.; McFail-Isom, L.; Hu, G. G.; Williams, L. D., The B-DNA Dodecamer at High Resolution Reveals a Spine of Water on Sodium. *Biochemistry* 1998, 37, (23), 8341-8355.

CHAPTER 2

CHARGE MIGRATION THROUGH DUPLEX DNA

When the secondary structure of DNA was finally realized[1], the nature of base stacking immediately allowed for the hypothesis that duplex DNA could serve as a potential molecule for the shuttling of charges.[2, 3] It was believed that the π-orbital overlap of the base pairs separated by 3.4 Å within the central portion of the duplex DNA might act as "a one-dimensional aromatic crystal" allowing for electrons to traverse the length of the DNA. It took 40 years before the first experimental evidence for charge migration through DNA was presented.[4] Early skepticism of the mechanism by which the charge migrates through the DNA has led to over a decade of research to gain insight into the factors influencing charge transfer kinetics.

Introduction to Charge Migration through DNA

Biological processes, such as oxygen metabolism in all aerobic organisms, readily produce reactive oxygen species (ROS) that can interact with DNA resulting in oxidatively damaged DNA products (Figure 2.1). Oxidative damage to endogenous DNA has been revealed to produce a number of modifications including base and sugar lesions, strand breaks, DNA-protein cross-links and base-free sites.[5-8] These modifications are known to lead to mutagenesis, carcinogenesis, and a number of degenerative diseases.[9-11] Along with several biological processes that can lead to

oxidative damage to DNA, there are three known chemical sources resulting from photosensitization that can oxidize DNA: hydrogen atom abstraction from an intermediate free radical[12], singlet oxygen or hydroxyl radical generated from an excited photonuclease[13], and loss of an electron from a nucleobase generating a radical cation.[14]

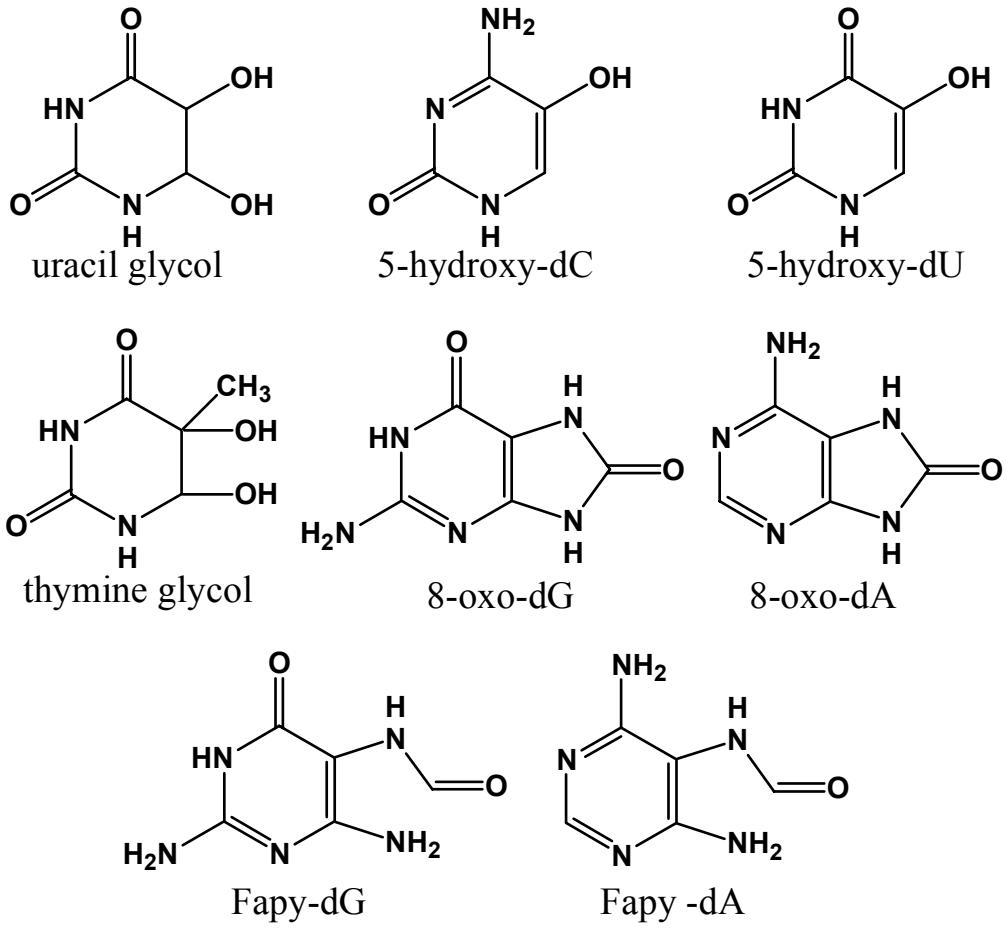

Figure 2.1. Chemical Structures of Some of the Stable Oxidative DNA Base Lesions.

Photosensitization of DNA leading to loss of an electron from a nucleobase has been extensively studied over the past 15 years, in part because of its biological relevance, but also because of DNA's potential application in molecular electronic devices. The loss of an electron from the nucleobase forms a radical cation on the base, which can then potentially migrate through the DNA to a distal site (a site that is more than one base away from the original ionized base). Initial reports of charge migration through DNA led to skepticism about the mechanism by which the charge travels through the DNA. To gain a more detailed understanding of the properties that govern charge transfer through DNA, studies have been performed to investigate the three key components of charge transfer: charge injection into the DNA (removal of an electron from the DNA base), charge transfer through the DNA (movement of the radical cation to distal sites), and finally oxidative damage of the DNA (reaction of the ionized nucleobase resulting in "damaged" DNA).

Charge Injection

To adequately study the properties of charge migration through DNA, a sufficient method for the one-electron oxidization of at least one of the DNA bases must first be determined. Close association of the photosensitizers with the DNA base-pairs is required to facilitate the transfer of an electron from the DNA to the sensitizer. To obtain this critical association with DNA, several photosensitizers have been developed that either intercalate between the base-pairs, bind in the major or minor grooves, or "end-cap" the terminal base-pairs.

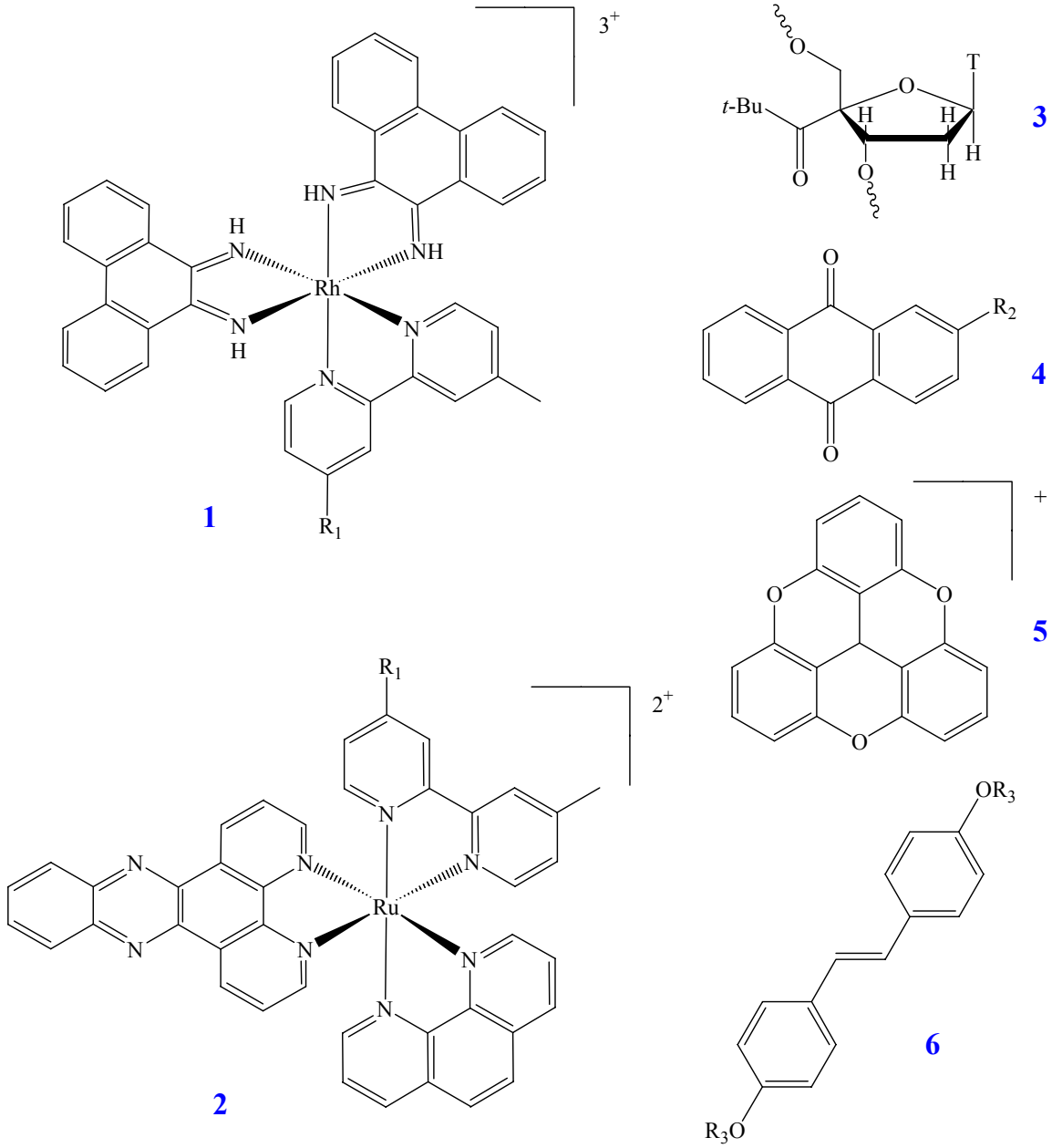

Figure 2.2. Charge Injectors.

Numerous studies have shown a variety of photosensitizing agents that adequately remove an electron from DNA, and a number of these molecules have been used to probe charge transfer through DNA (Figure 2.2). Barton and coworkers have used the metallointercalators $[Rh(phi)_2(bpy')]^{3+}$ and $[Ru(phen)(bpy')(dppz)]^{2+}$ (**1** and **2**); phi, 9,10-phenanthrenequinone diimine; bpy', 4-butyric acid-4-methyl bipyridyl; phen, 1,10-phenanthroline; dppz, dipyridophenazine), which have been covalently tethered to the DNA via the bpy' ligand, to induce charge transfer through DNA.[15, 16] These metallointercalators have been shown to oxidize the DNA bases, however, it has been revealed that under certain circumstances aggregation can occur[17, 18], complicating the interpretation of the results obtained.

Lewis and Wasielewski have employed a hairpin conformation of DNA with the photosensitizer joining the 5'-end of one DNA strand with the 3'-end of the complimentary strand. They have focused mainly on the use of stilbene derivatives (**6**) for the process of charge injection into DNA.[19] Although the excited singlet state of the stilbene derivatives has sufficient energy to oxidize the DNA bases, they have a short half life and don't intersystem cross efficiently. As a result, only short-range charge transfer is observed because the back electron transfer is very rapid. Similarly, trioxatriangulenium ion (**5**) ($TOTA^+$) is an intercalator with a preferential binding site of G/C base pairs that has been shown to be a relatively inefficient sensitizer[20]. This is believed to be a result of $TOTA^+$ reacting with DNA from the singlet excited state, and therefore competition with back electron transfer inhibits the charge transfer process.

As opposed to the use of an aromatic molecule that associates with the bases of the DNA, Giese has focused his interests on a method of photolysis for charge injection.[21] Attaching a pivaloyl group to the 4'-position of a thymine sugar (**3**), followed by photolysis injects a radical cation into the DNA. The formation of a radical cation in the DNA via this photolysis reaction competes with several alternate reactions, namely reaction with O_2 and H_2O, yielding irreversible side products.

The photochemistry of anthraquinone (**4**) has been well established[22] and therefore we have focused our research on using this photosensitizer. The direction the carboxamide linker is attached to the anthraquinone chromophore determines the electronic configuration of the reacting excited state. It has been shown that the desired linker has the chromophore linked to the carbonyl followed by the amine group. This orientation gives the lowest excited state of $\pi\pi^*$ or charge-transfer character.[14] This anthraquinone moiety (AQ) is easily synthesized[12] (Figure 2.3) and can be tethered to the 5'-terminus of a DNA single-strand (Figure 2.4) via standard phosphoramidite chemistry. Attaching an AQ to the terminus of a DNA single-strand, followed by hybridization with its complementary sequence, results in "end-capping" of the DNA duplex. Molecular modeling and spectroscopic experiments have shown this "end-capping" of the DNA (Figure 2.5) permits π-orbital overlap with the DNA, but doesn't yield structural distortions to the DNA that can be caused by intercalation.[23]

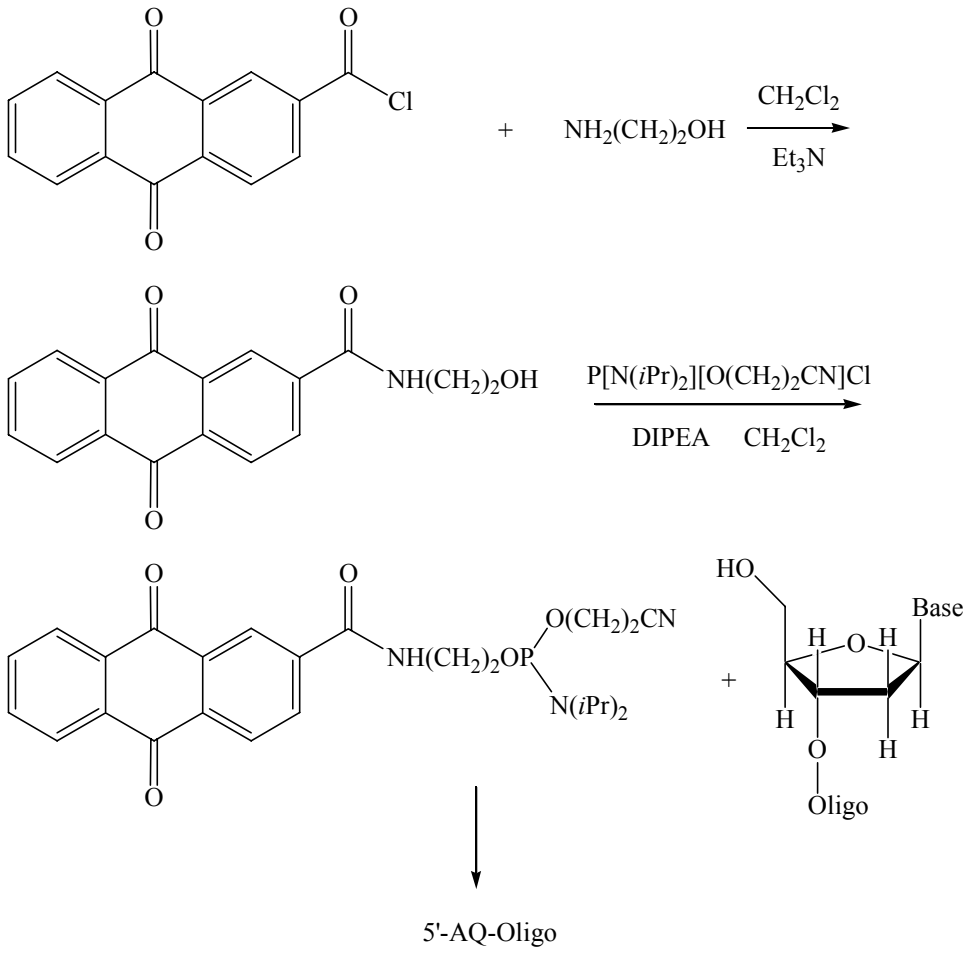

Figure 2.3. Synthetic Scheme for AQ.

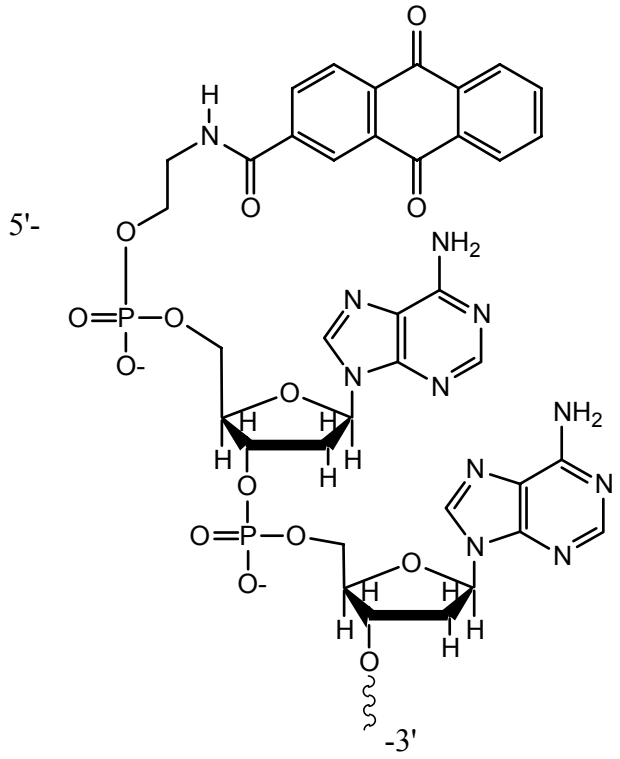

Figure 2.4. Schematic Representation of the Anthraquinone Moiety Attached to the 5'-Terminus of the Single-Stranded DNA. DNA sequence depicted is 5'-AQ-A-A…-3'.

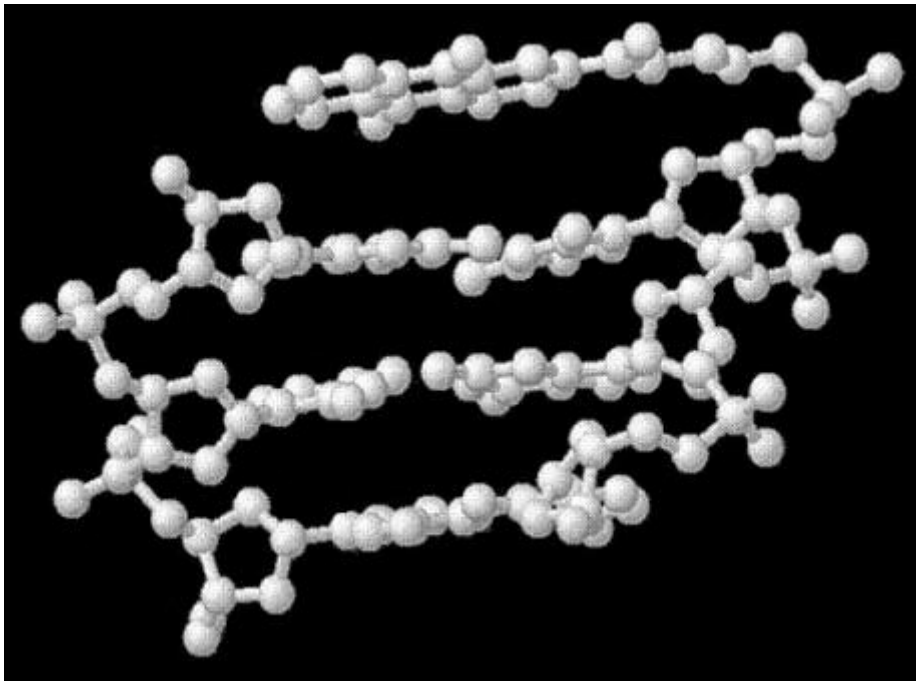

Figure 2.5.[24] Molecular Modeling Showing AQ End-Capping the DNA Duplex.

The absorption properties of the AQ molecule are ideal for charge injection into DNA. AQ readily absorbs at 350nm where the DNA molecule is transparent. Irradiation of the AQ at 350nm promotes it from the ground state to the singlet excited state. This singlet excited state has been shown to be energitcally capable of abstracting an electron from a neighboring base, however, the singlet radical ion pair has a relatively short life-time and affords a rapid back electron transfer. Fortunately, the singlet excited state efficiently intersystem crosses to the triplet excited state, which can then abstract an electron from the neighboring base creating a nucleobase radical cation. This triplet radical ion pair is relatively long-lived because spin conservation rules forbid back electron transfer. Subsequent reaction of the $AQ^{\cdot -}$ with O_2 gives superoxide and the

neutral AQ (Figure 2.6). This allows the radical cation to migrate through the DNA until it reacts predominantly at a guanine, the base with the lowest oxidation potential[25] (Table 2.1). The efficiency of charge injection by AQ has been shown to be highly sensitive to the bases nearest the AQ.[26] When a guanine is too close to the AQ, within three base pairs, charge injection is severely retarded. It was found that the sequence of bases that yields the highest charge injection efficiency is 5'-AQ-AAAT, where the AQ is covalently linked to the 5'-phosphate of the A at the 5'-terminus.

Table 2.1. Oxidation Potentials of the DNA Bases.[25]

Bases	E_{ox} (V)vs. NHE
Adenine	1.42
Thymine	1.7
Guanine	1.29
Cytosine	1.6

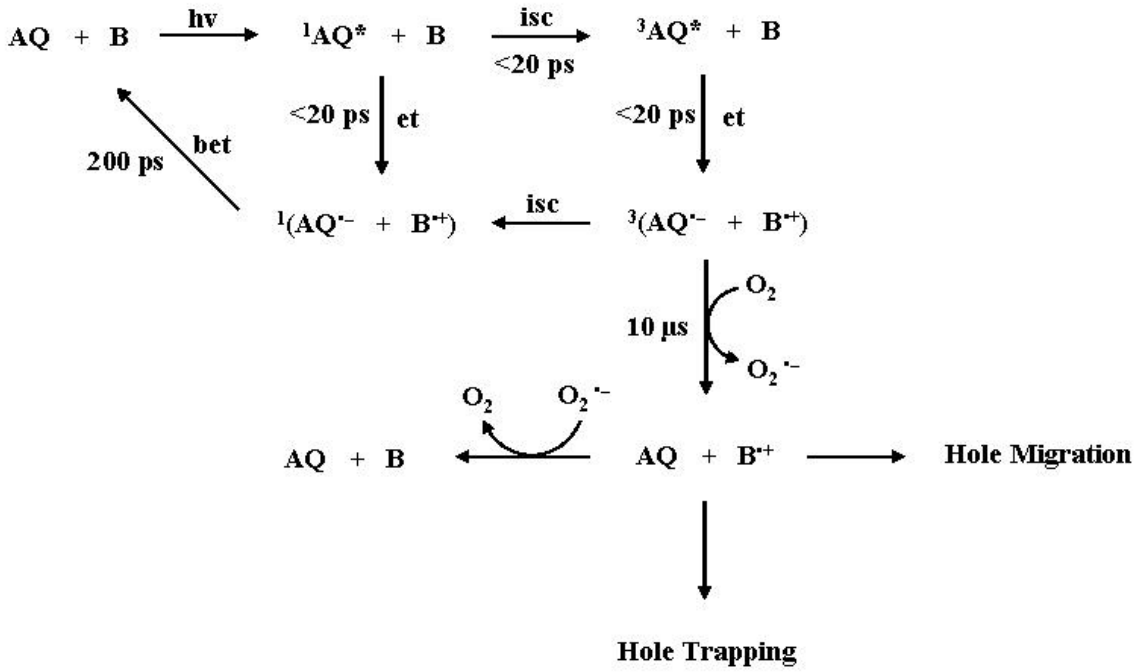

Figure 2.6. Charge Injection Schematic.

Charge Migration

One-electron oxidation of DNA, resulting in the migration of a radical cation through the DNA to sites up to 200 Å away, have been extensively studied. It has been shown that the efficiency of charge migration is drastically affected by the DNA base sequence.[21, 26-30] Oxidative damage to guanine yields a piperidine labile product. Treatment with hot piperidine yields strand scission of the DNA backbone, providing a basis for studying the mechanism of charge migration through DNA. While charge transport through DNA is well accepted experimentally, the mechanism for how charge migration through DNA proceeds is still not well established. Nearly 15 years a vigorous debate about the mechanism of charge migration has led to a few predominant theories.

Initial reports indicated a very fast electron transport from a donor to an acceptor mediated by the π-stacking of the DNA base pairs, referred to as a "π-way"[4]. This fast electron transfer was attributed to a coherent, rapid, single-step from the donor to the acceptor.

Subsequent investigation has afforded contradicting reports as to the mechanism of charge transfer through DNA, varying from superexchange and tunneling[28, 31-34] (Figure 2.7), to varying hopping mechanisms[29, 35], as well as a combination of mechanisms that vary based upon DNA sequence. Most notably, three mechanisms have been proposed to account for charge migration over long distances. The first is an incoherent random walk, multi-step hopping mechanism[31], where the radical cation resides on guanines and hopping between guanines is facilitated by superexchange through intervening A/T base pairs. The explanation of this theory is as follows: if the distance between donor and acceptor is short, the electron tunnels in a single-step reaction between the guanines, and the A/T base pairs do not act as charge carriers. However, if the distance is long, then the $G^{\cdot+}$ oxidizes the adjacent adenine where it very rapidly travels to the next G (Figure 2.8). This theory is postulated to occur if the lifetime of the $G^{\cdot+}$ is long enough to oxidize the adjacent A/T base pair. This theory recognizes that DNA is not a static molecule and continuous thermal motions of the DNA must influence the charge transfer efficiency, but it does not offer any explanation as to how these fluctuations are incorporated into their theory.

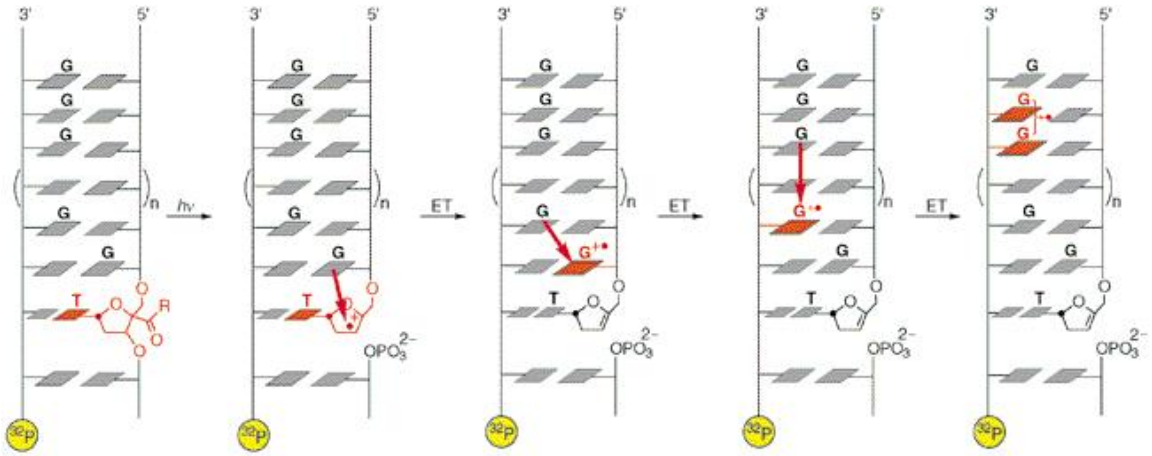

Figure 2.7.[31] Charge Transfer of the Radical Cation from Guanine to Guanine via a Single-Step Superexchange.

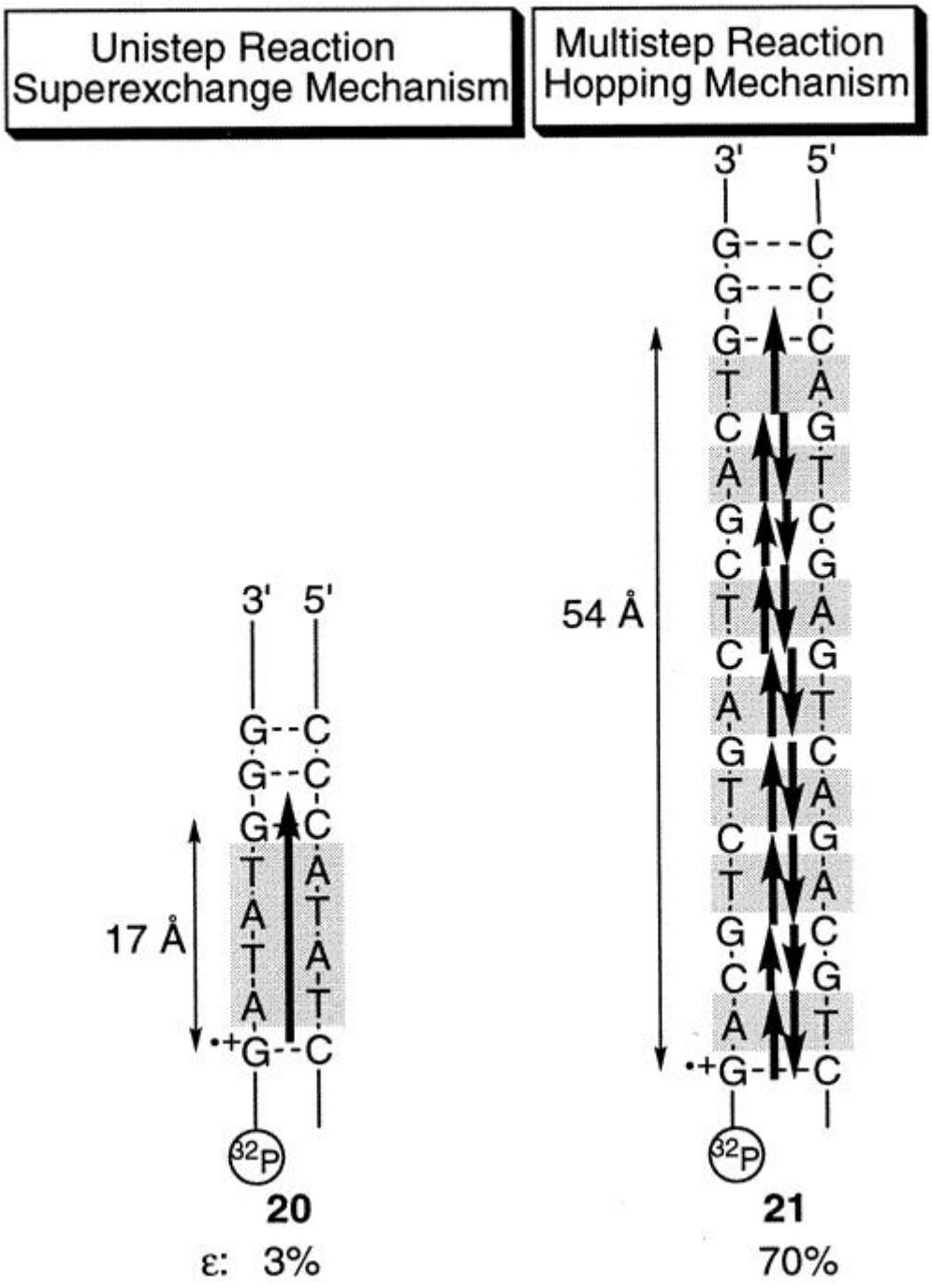

Figure 2.8.[31] Incoherent Random-Walk, Single-Step Hopping Model for CT.

In comparison to theories that involve superexchange, there are two theories that involve the delocalization of the radical cation over several bases centered on guanine. The charge transfer from one site to the other is postulated to be hopping propogated by thermal motions of the DNA and its environment, where the charge resides on the barrier or "bridge", while migrating from one guanine to the other. These two theories are dependent on thermal fluctuations of the DNA, and differ from the superexchange mechanism in that the charge is thought to reside on the intervening bases during the hopping process.

The first theory involving the hopping of the radical cation is described as conformationally gated hopping among stacked domains (Figure 2.9).[35] This conformationally gated hopping suggests that charge transfer occurs within DNA assemblies possessing specific, well-coupled conformations of the DNA bases, CT-active domains, accessed through base motion. Upon charge injection, the DNA bases are arranged in a random conformation, DNA assembly, which may or may not be an assembly that is conducive for CT. If not, the thermal motions of the DNA can adopt an assembly of well-coupled conformations of the bases that is conducive of CT. If this conformation is adopted within the lifetime of the radical cation, then the charge will migrate through the DNA. Otherwise the radical cation will be annihilated through other processes that aren't revealed as charge migration. The key to this proposed mechanism is the formation of these DNA assemblies that are required before charge migration can occur.

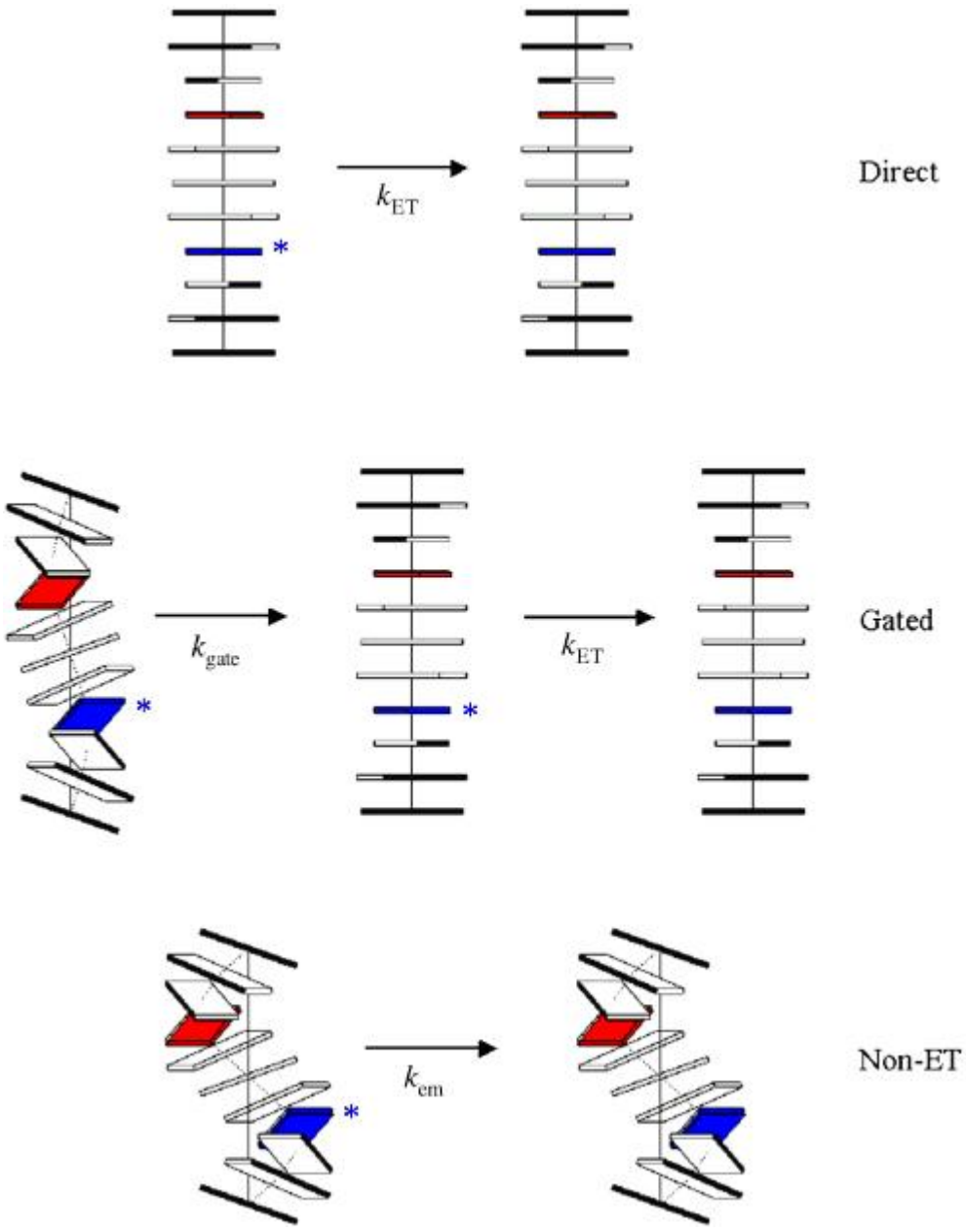

Figure 2.9.[36] Conformationally Gated Hopping Among Stacked Domains Model of Charge Transfer.

The second theory involving delocalization of the radical cation, followed by a hopping mechanism where the charge does reside on the bridge, is termed phonon-assisted polaron hopping.[37] After charge injection into the DNA, the bases around the radical cation distort themselves to accommodate the charge, as well as delocalize the charge over several bases, referred to as a polaron, again centered on guanines because of their low oxidation potential. This polaron formation theory is supported by quantum mechanical calculations that report the radical cation charge density is delocalized predominantly over the three G's with a small amount of the charge on the A of a GAGG sequence[38] (Figure 2.10). The extent of the delocalization is governed by the energy required to distort the DNA and the energy gained by delocalizing the radical cation, which is dependent on the sequence of the DNA. Thermal motions of the DNA and its environment, H_2O and cations, then assist in transferring the charge through the DNA over bridges to low energy sites, referred to as phonon-assisted hopping. Similar molecular dynamics simulations show that cations are not only very closely associated with the DNA backbone and the bases (Figure 2.11), but that motions of these cations has a drastic affect on the polaron's charge distribution. This change in charge distribution as a result of cation motions is believed to assist in polaron hopping through the DNA. Recent reports support the notion that fluctuations in the environment of DNA facilitate CT through the DNA.[39] These findings suggest that as the charge is migrating through the DNA, the structure of the DNA and its base pairs are distorting their conformation around the charge, essentially moving the polaron through the DNA (Figure 2.12).

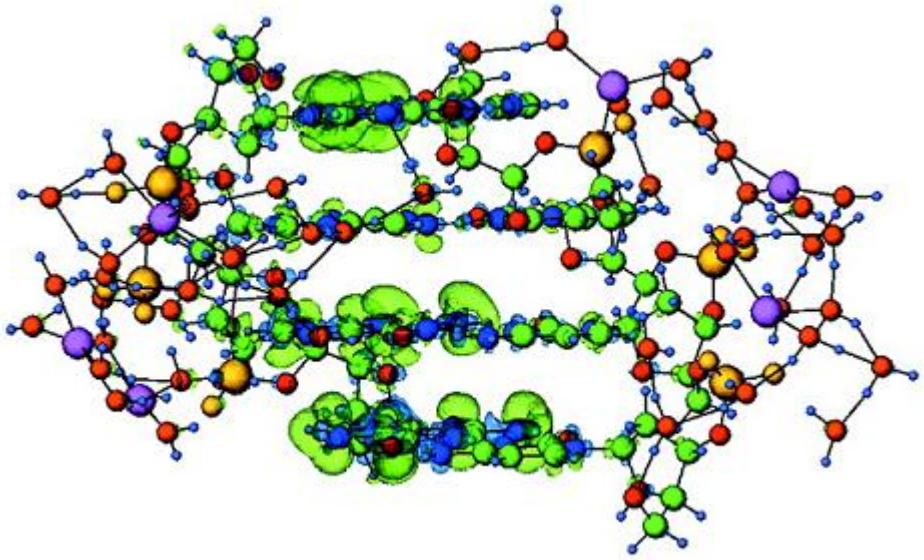

Figure 2.10.[38] Quantum Mechanical Calculations of the Radical Cation Charge Delocalization (green isosurface) for DNA $d(GAGG)^{\cdot+}$.

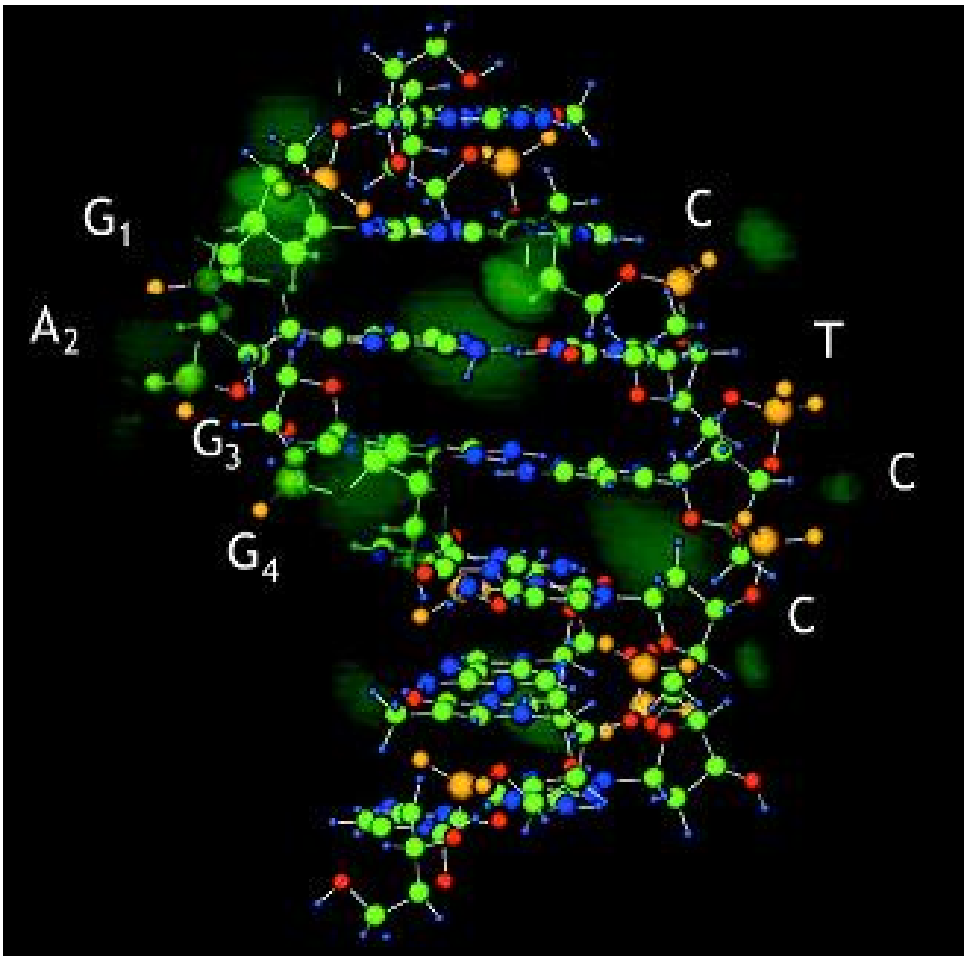

Figure 2.11.[38] Molecular Dynamics Simulation of Sodium Atom (green isosurface) Site Probabilities around DNA.

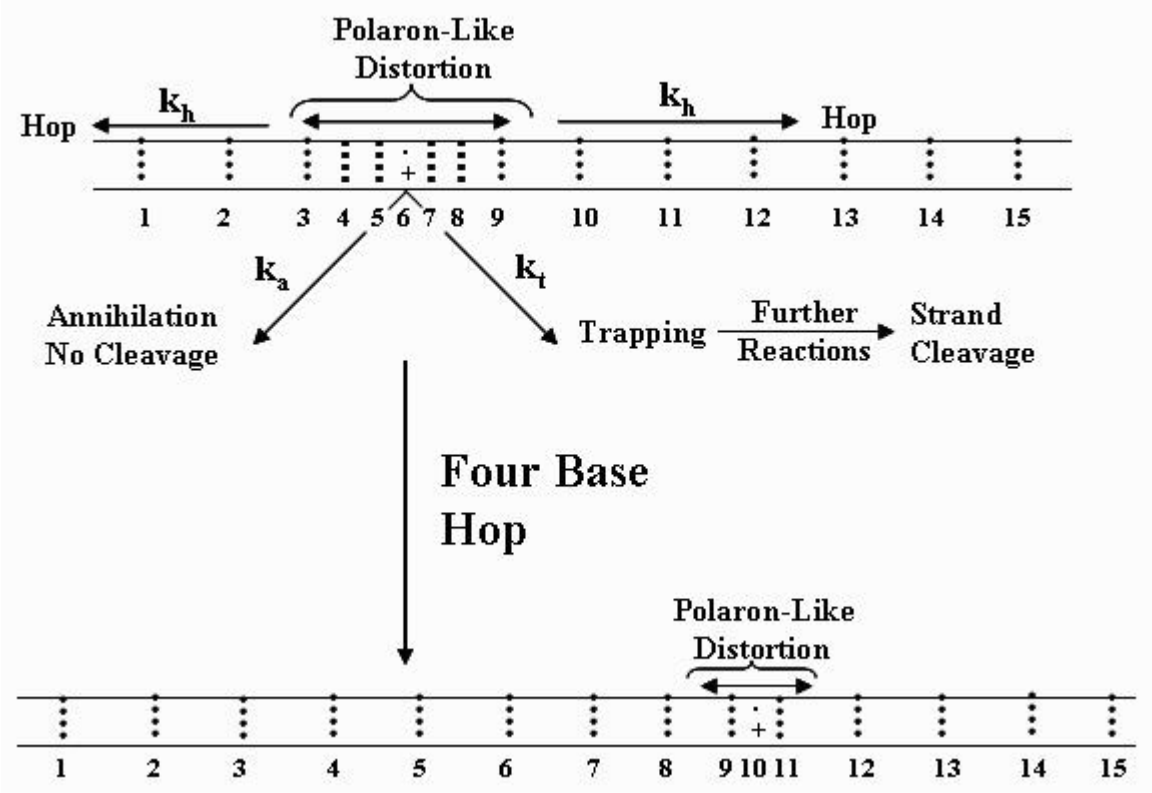

Figure 2.12. Phonon-Assisted Polaron Hopping Mechanism Charge Migration Schematic.

The major difference between the superexchange model and the polaron hopping model is the location of the radical cation as it is transferred from guanine to the nearest low energy site across the bridge. As mentioned before, the superexchange model suggests a tunneling phenomenon where the charge only exists virtually in the orbitals of the bridge bases. In contrast, the polaron hopping model requires that the radical cation exist as a detectable entity during migration through the bridge. Studies using 2'-deoxy-N^6-cyclopropyl-adenosine located between the charge injection site and a distal guanine site have been employed to determine if the bridge bases act as charge carriers (Figure 2.13).[40] The studies have shown that the radical cation does indeed react with the cyclopropyl moiety of the modified adenosine, indicating the charge resides on the bridge bases at least long enough for the ring opening reaction to occur. These findings are not possible if superexchange is the mechanism for charge transport over the bridges, however, they support the phonon-assisted polaron hopping model.

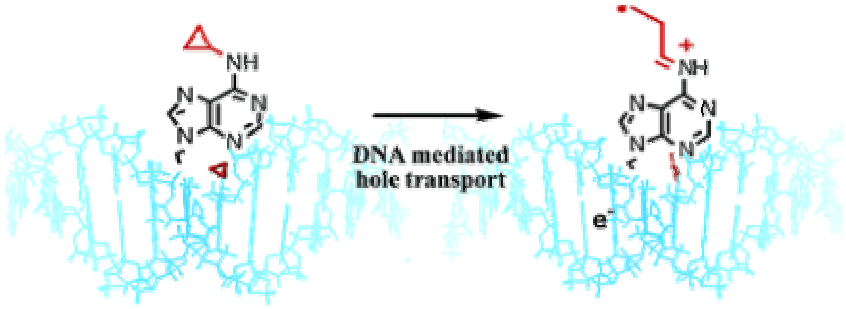

Figure 2.13.[40] Schematic Illustration of Ring-Opening of N^6-Cyclopropyladenosine by Charge Transfer.

Further studies involving the kinetic rate constants of CT have been revealed to support the phonon-assisted polaron hopping mechanism. It was reported, based on kinetic experiments and oxidation product yields, that the rate of trapping (k_t) is on the order of 6 x 10^4 s^{-1} at pH 7.[41] Using this value for k_t, and the reported ratios of k_h/ k_t in sequences containing multiple GG steps separated by $(A/T)_n$ bridges[29], Schuster deduced that the rate of hopping is on the order of 10^4 to 10^6 s^{-1} based upon the size of the bridge. Recently, the first experiments of the direct observation of long-distance (>100 Å) CT in DNA using time-resolved transient absorption measurements has been reported.[42] Attaching a donor (phenothiazine) to the 5'-terminus of a DNA single-strand and an acceptor (naphthalimide) to the 5'-terminus of the complementary strand allowed for the accurate determination of the rate of hopping. Transient absorption of the naphthalimide radical anion (after charge is injected into the DNA) at 400 nm, followed by transient absorption of the phenothiazine radical cation (hole transfer from the DNA indicating the charge has travel the entire length of the DNA) at 520 nm reveals a rate constant of 10^4 to 10^7 s^{-1}, based on the length of the DNA. These experiments are in direct correlation with the phonon-assisted polaron hopping mechanism.

Charge Trapping

In order to examine the properties that govern charge migration and oxidation through DNA, there first has to be a method for monitoring the CT efficiency. As previously mentioned, the radical cation prefers to be predominantly delocalized on guanine bases. The guanine radical cation, $G^{\cdot+}$, of a GG step (lower oxidation potential than single G's) is readily oxidized by H_2O or O_2 (Figure 2.14) to yield piperidine labile

products. Treatment of the oxidized DNA single-strands with hot piperidine leads to strand cleavage at sites of guanine oxidation. Gel electrophoresis allows for the separation of DNA molecules based on a size to charge ratio, effectively separating the cleaved DNA fragments from the parent DNA strands that were unaffected by the CT. This cleavage and separation technique allows for the accurate quantification of charge migration efficiency.

The efficiency of CT through DNA is dependent on two rates: rate of hopping (k_h) and the rate of trapping (k_t) as illustrated in Figure 2.12. If the rate of hopping is greater than the rate of trapping, CT will be highly efficient and oxidation at GG steps will be approximately equivalent throughout the DNA. If the rate of trapping is greater than the rate of hopping, CT will be highly inefficient and the majority of oxidation will occur closest to the AQ. And finally, if the rate of hopping is approximately equivalent to the rate of trapping, CT will decrease with distance from the AQ.

To adequately analyze the efficiency of charge migration the combination of efficient charge injection, charge migration, and charge trapping are required. Experiments have been set up to have multiple sites of oxidation, G_n steps where n = 2 or 3, throughout the DNA so that the efficiency of CT can be derived from the ratios of damage at each G_n step as a function of distance from the site of charge injection. Anthraquinone is an ideal charge injector for accurate analysis of CT efficiency as a function of distance because the site of injection is determined by the end-capping conformation. Therefore, experimental set-ups using AQ as charge injector, the phonon-

assisted polaron hopping model, and piperidine-labile strand cleavage analysis can be used to further elucidate the properties that effect CT and oxidation in DNA.

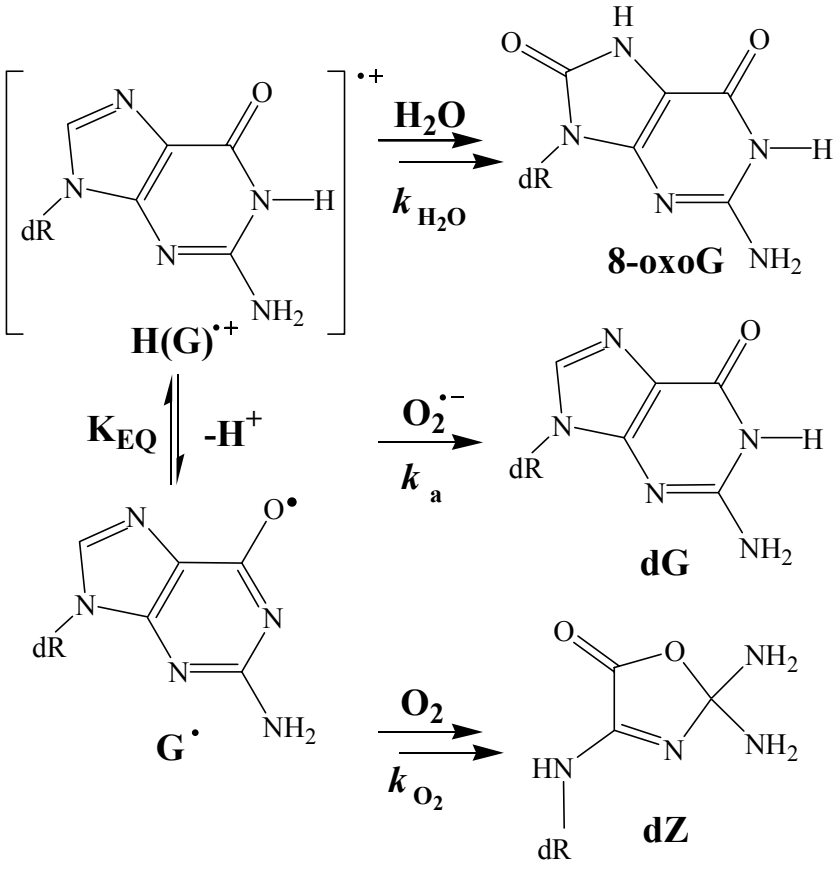

Figure 2.14. Schematic Representation for Oxidation of the Guanine Radical Cation.

REFERENCES

[1] Watson, James. D.; Crick, Francis H. C., Molecular Structure of Nucleic Acids: A Structure for Deoxyribose Nucleic Acid. *Nature* 1953, 171, 737-738.

[2] Eley, D. D., Organic Semiconductors. *Research* 1959, 12, 293.

[3] Eley, D. D.; Spivey, D. I., Semiconductivity of Organic Substances. Part 9.—Nucleic Acid in the Dry State. *Transactions of the Faraday Society* 1962, 58, 411-415.

[4] Murphy, C. J.; Arkin, M. R.; Jenkins, Y.; Ghatlia, N. D.; Bossmann, S. H.; Turro, N. J.; Barton, J. K., Long-Range Photoinduced Electron Transfer Through a DNA Helix. *Science* 1993, 262, (5136), 1025-1029.

[5] Armitage, B., Photocleavage of Nucleic Acids. *Chem. Rev.* 1998, 98, (3), 1171-1200.

[6] Burrows, C. J.; Muller, J. G., Oxidative Nucleobase Modifications Leading to Strand Scission. *Chem. Rev.* 1998, 98, (3), 1109-1152.

[7] Sancar, A., DNA Excision Repair. *Annual Review of Biochemistry* 1996, 65, (1), 43-81.

[8] Kow, Yoke W., Base Excision Repair in E. coli--an Overview. *Annals of the New York Academy of Sciences* 1994, 726, 178-180.

[9] Kanvah, S.; Schuster, G. B., One-Electron Oxidation of DNA: The Effect of Replacement of Cytosine with 5-Methylcytosine on Long-Distance Radical Cation Transport and Reaction. *J. Am. Chem. Soc.* 2004, 126, (23), 7341-7344.

[10] Demple, B.; Harrison, L., Repair of Oxidative Damage to DNA - Enzymology and Biology. *Annual Review of Biochemistry* 1994, 63, 915-948.

[11] Poulsen, H. E.; Prieme, H.; Loft, S., Role of Oxidative DNA Damage in Cancer Initiation and Promotion. *European Journal of Cancer Prevention* 1998, 7, (1), 9-16.

[12] Armitage, Bruce; Yu, Changjun; Devadoss, Chelladurai; Schuster, Gary B., Cationic Anthraquinone Derivatives as Catalytic DNA Photonucleases: Mechanisms for DNA Damage and Quinone Recycling. *Journal of the American Chemical Society* 1994, 116, (22), 9847-9859.

[13] Macgregor, Jr Robert B., Photogeneration of Hydroxyl Radicals for Footprinting. *Analytical Biochemistry* 1992, 204, (2), 324-327.

[14] Breslin, D. T.; Schuster, G. B., Anthraquinone Photonucleases: Mechanisms for GG-Selective and Nonselective Cleavage of Double-Stranded DNA. *J. Am. Chem. Soc.* 1996, 118, (10), 2311-2319.

[15] Hall, Daniel B.; Holmlin, R. Erik; Barton, Jacqueline K., Oxidative DNA damage through long-range electron transfer. *Nature* 1996, 382, (6593), 731-735.

[16] Murphy, C. J.; Arkin, M. R.; Ghatlia, N. D.; Bossmann, S.; Turro, N. J.; Barton, J. K., Fast Photoinduced Electron Transfer through DNA Intercalation. *PNAS* 1994, 91, (12), 5315-5319.

[17] Fahlman, R. P.; Sharma, R. D.; Sen, D., The Charge Conduction Properties of DNA Holliday Junctions Depend Critically on the Identity of the Tethered Photooxidant. *J. Am. Chem. Soc.* 2002, 124, (42), 12477-12485.

[18] Olson, E. J. C.; Hu, D.; Hormann, A.; Barbara, P. F., Quantitative Modeling of DNA-Mediated Electron Transfer between Metallointercalators. *J. Phys. Chem. B* 1997, 101, (3), 299-303.

[19] Lewis, F. D.; Letsinger, R. L.; Wasielewski, M. R., Dynamics of Photoinduced Charge Transfer and Hole Transport in Synthetic DNA Hairpins. *Acc. Chem. Res.* 2001, 34, (2), 159-170.

[20] Krebs, Frederik C.; Laursen, Bo W.; Johannsen, Ib; Faldt, Andre; Bechgaard, Klaus; Jacobsen, Claus S.; Thorup, Niels; Boubekeur, Kamal, The Geometry and Structural Properties of the 4,8,12-Trioxa-4,8,12,12c-tetrahydrodibenzo[cd,mn]pyrene System in the Cationic State. Structures of a

Planar Organic Cation with Various Monovalent and Divalent Anions. *Acta Crystallographica Section B* 1999, 55, (3), 410-423.

[21] Giese, Bernd, Long-Distance Electron Transport through DNA. *Annual Review of Biochemistry* 2002, 71, (1), 51-70.

[22] Moore, John N.; Phillips, David; Nakashima, Nobuaki; Yoshihara, Keitaro, Photophysics and Photochemistry of Sulphonated Derivatives of 9,10-Anthraquinone. Strong versus Weak Sensitisers. *Journal of the Chemical Society, Faraday Transactions 2: Molecular and Chemical Physics* 1987, 83, 1487-1508.

[23] Gasper, S. M.; Schuster, G. B., Intramolecular Photoinduced Electron Transfer to Anthraquinones Linked to Duplex DNA: The Effect of Gaps and Traps on Long-Range Radical Cation Migration. *J. Am. Chem. Soc.* 1997, 119, (52), 12762-12771.

[24] Schuster, G. B., Long-Range Charge Transfer in DNA: Transient Structural Distortions Control the Distance Dependence. *Acc. Chem. Res.* 2000, 33, (4), 253-260.

[25] Steenken, S.; Jovanovic, S. V., How Easily Oxidizable Is DNA? One-Electron Reduction Potentials of Adenosine and Guanosine Radicals in Aqueous Solution. *J. Am. Chem. Soc.* 1997, 119, (3), 617-618.

[26] Sanii, L.; Schuster, G. B., Long-Distance Charge Transport in DNA: Sequence-Dependent Radical Cation Injection Efficiency. *J. Am. Chem. Soc.* 2000, 122, (46), 11545-11546.

[27] Liu, C. S.; Schuster, G. B., Base Sequence Effects in Radical Cation Migration in Duplex DNA: Support for the Polaron-Like Hopping Model. *J. Am. Chem. Soc.* 2003, 125, (20), 6098-6102.

[28] Lewis, Frederick D.; Liu, Jianqin; Weigel, Wilfried; Rettig, Wolfgang; Kurnikov, Igor V.; Beratan, David N., Donor-Bridge-Acceptor Energetics Determine the Distance Dependence of Electron Tunneling in DNA. *PNAS* 2002, 99, (20), 12536-12541.

[29] Liu, C. S.; Hernandez, R.; Schuster, G. B., Mechanism for Radical Cation Transport in Duplex DNA Oligonucleotides. *J. Am. Chem. Soc.* 2004, 126, (9), 2877-2884.

[30] Shao, F.; Augustyn, K.; Barton, J. K., Sequence Dependence of Charge Transport through DNA Domains. *J. Am. Chem. Soc.* 2005, 127, (49), 17445-17452.

[31] Giese, B., Long-Distance Charge Transport in DNA: The Hopping Mechanism. *Acc. Chem. Res.* 2000, 33, (9), 631-636.

[32] Armitage, N. P.; Briman, M.; Grüner, G., Charge Transfer and Charge Transport on the Double Helix. *physica status solidi (b)* 2004, 241, (1), 69-75.

[33] Bixon, M.; Giese, Bernd; Wessely, Stephan; Langenbacher, Thomas; Michel-Beyerle, Maria E.; Jortner, Joshua, Long-Range Charge Hopping in DNA. *PNAS* 1999, 96, (21), 11713-11716.

[34] Berlin, Yuri A.; Burin, Alexander L.; Ratner, Mark A., Elementary Steps for Charge Transport in DNA: Thermal Activation vs. Tunneling. *Chemical Physics* 2002, 275, (1-3), 61-74.

[35] O'Neill, M. A.; Barton, J. K., DNA Charge Transport: Conformationally Gated Hopping through Stacked Domains. *J. Am. Chem. Soc.* 2004, 126, (37), 11471-11483.

[36] O'Neill, Melanie A.; Becker, Hans-Christian; Wan, Chaozhi; Barton, Jacqueline K.; Zewail, Ahmed H., Ultrafast Dynamics in DNA-Mediated Electron Transfer: Base Gating and the Role of Temperature. *Angewandte Chemie International Edition* 2003, 42, (47), 5896-5900.

[37] Henderson, Paul T.; Jones, Denise; Hampikian, Gregory; Kan, Yongzhi; Schuster, Gary B., Long-Distance Charge Transport in Duplex DNA: The Phonon-Assisted Polaron-Like Hopping Mechanism. *PNAS* 1999, 96, (15), 8353-8358.

[38] Barnett, Robert N.; Cleveland, Charles L.; Joy, Abraham; Landman, Uzi; Schuster, Gary B., Charge Migration in DNA: Ion-Gated Transport. *Science* 2001, 294, (5542), 567-571.

[39] Alexander A. Voityuk, Khatcharin Siriwong Notker Rösch, Environmental Fluctuations Facilitate Electron-Hole Transfer from Guanine to Adenine in DNA π Stacks. *Angewandte Chemie International Edition* 2004, 43, (5), 624-627.

[40] Dohno, C.; Ogawa, A.; Nakatani, K.; Saito, I., Hole Trapping at N^6-Cyclopropyldeoxyadenosine Suggests a Direct Contribution of Adenine Bases to Hole Transport through DNA. *J. Am. Chem. Soc.* 2003, 125, (34), 10154-10155.

[41] Giese, Bernd; Spichty, Martin, Long Distance Charge Transport through DNA: Quantification and Extension of the Hopping Model. *ChemPhysChem* 2000, 1, (4), 195-198.

[42] Takada, Tadao; Kawai, Kiyohiko; Fujitsuka, Mamoru; Majima, Tetsuro, Direct Observation of Hole Transfer through Double-Helical DNA over 100 A. *PNAS* 2004, 101, (39), 14002-14006.

CHAPTER 3

CHARGE MIGRATION THROUGH CONTIGUOUS A•A AND T•T MISMATCHES

Charge migration through duplex DNA has been extensively studied, and it has been shown that the efficiency of charge transfer is highly dependent on base sequence and length. Traditionally, the study of charge transfer has focused on fully complementary Watson-Crick base pairing while altering the sequence design and length. However, there have been some studies indicating single base pair mismatches reduce the efficiency of charge migration through DNA, indicating a potential sensor for base pair mismatches. Our research has focused on monitoring charge transfer through serial mispairs $(A•A)_n$ and $(T•T)_n$ and their effect on CT efficiency.

Mismatched Base Pairs in Duplex DNA

Mispaired DNA Bases

Watson-Crick base pairing is preserved in DNA through the use of repair enzymes that recognize and replace bases that result in non-canonical base pairing (i.e. A•T or G•C base pairs). DNA mismatches occur in vivo as a result of several factors: error in replication[1], heteroduplex formation during homologous recombination[2], mutagenic chemicals[3, 4], ionizing radiation[5], and spontaneous deamination.[6] Incomplete

repair of mismatch base pairs results in mutations during replication, possibly leading to mutagenesis or carcinogenesis.

Mismatch base pairs are incorporated into the DNA usually with little structural distortion to the secondary structure.[7, 8] Changes in base stacking, hydrogen bonding[9] and DNA secondary structure can effect charge migration through DNA, therefore, mismatches in dsDNA may have an effect on the charge migration efficiency. A few studies investigating the efficiency of charge transfer through mismatch base pairs or deletions have been studied[10-14], indicating C•A mismatches yield a reduction in efficiency[15, 16] and an A•A mismatch has effectively no change on the efficiency.[17] However, the reports indicating C•A mismatches yield a reduction in efficiency may be unreliable as the photosensitizer used, Ru intercalator, may cause aggregation complicating thier results.[18]

Zipper-like DNA Motif

Since the elucidation of the secondary structure of dsDNA[19], it has become increasingly clear that the double helix is not a rigid molecule. Rather, it has been extensively shown that dsDNA can adopt a wide array of secondary structures, in addition to the standard A, B, and Z forms (Figures 1.6-1.8), as a result of their sequence and environment. Among these varying secondary structures is included triple helical structures[20], a guanine-rich DNA quadruplex[21-26], a four-stranded intercalated cytosine-rich i-DNA motif[27-30], as well as many more[31-34] (Figure 3.1). Of particular interests are

those DNA sequences within cellular organisms that have an unusual or ill-defined structural motif.

At the replication origins of bacteriophages and parvoviruses there exist conserved ssDNA nucleotide sequences. These sequences have been proposed to adopt a hairpin conformation.[35-38] In particular, bacteriophage G4[39], consisting of circular ssDNA genome of 5577 nucleotides, contains an 8 base pair stem and the loop sequence d(GAAAGCC) at the initiation site of replication. Synthetic analogues containing the sequence (GAAA) have been shown to have extremely high melting temperatures[40], high gel mobility[41], and resistance to endonuclease activity[42], even with only two Watson-Crick base pairs on the stem region.

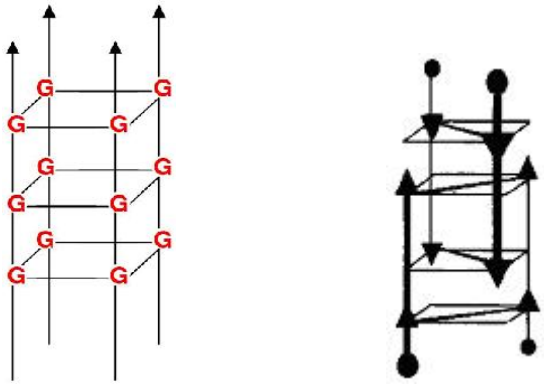

Figure 3.1.[26, 30] Schematic Illustration of the Unusual Secondary Structures of DNA, G-Quadruplex and i-DNA Motifs.

Similarly, human chromosomes have been shown to have tandem repeats of purine-rich sequences that can occupy up to 97% of the DNA content[43], although their structure and function are yet to be fully understood. These sequences are often found within the telomere and centromere, and have been postulated to adopt unusual secondary structures.[44-50] The centromere has been shown to have the highly conserved sequence $d(GGAAT)_n$, which is very similar to the d(GAAA) sequence of bacteriophage G4. Original reports indicated a dsDNA structure with mismatched G•A base pairs.[47] However, more recent reports of analogues of this sequence indicate a mixture of dsDNA and stem loop structures of the ssDNA.[45, 46, 51, 52] This ssDNA oligomer has been shown to exhibit melting temperatures that are comparable with its complementary dsDNA analogue[47] implying an unusually stable secondary structure.

To better understand the unusual behavior of the (GAAA) containing ssDNA oligomer, analogues containing complementary double-stranded regions on either side of this loop sequence were designed. Based upon preliminary NMR studies and molecular dynamics calculations, the hairpin sequence d(GCGAAAGC) was proposed to account for the unusual properties exhibited by bacteriophage G4.[53-55] The x-ray crystal structure of the dsDNA sequence $d(GCGAAAGCT)_2$ was determined to 2.1 Å (Figures 3.2 and 3.3).[56] The structural conformation of this dsDNA is very similar to the structures of dsDNA sequences 5'-d(GXA)/(AYG)-5' where the G•A sheared mismatches flank either side of an interdigitated X•Y stack (X•Y is any complementary base pair, A•A or G•G mismatch).[57] This secondary structure is referred to as a "zipper-like" conformation.

The "zipper-like" DNA duplex structure with the sequence d(GCGAAAGCT)$_2$ is remarkably stable considering there are only two base pairs on either side of the mismatch region. The duplex is found to have two Watson-Crick G•C base pairs at each end of the duplex that adopt a B-form conformation. The T at the 3'-terminus of the dsDNA was expected to have an intermolecular interaction with an upaired A as a means of crystal stabilization. However, it was found to freely move around at the end of the DNA, giving a very ill-defined position in the electron density map. The core of the duplex contains two sheared G•A mismatched base pairs encapsulating four unpaired A's that stack in a "zipper-like" motif (Figure 3.2b).

Characteristic of the adenine "zipper-like" core is the continuous base overlap through the unpaired region, allowing for base stacking through the entire length of the dsDNA. This unusual unpaired stacking of the DNA elongates and stretches the DNA as compared to standard B-DNA (Figure 3.3). Following the stacking of the DNA bases, the order of bases directly interacting with the neighboring bases is as follows: G-C-G-A-A*-A-A*-G*-C*-G*, where * indicates the bases of one of the ssDNA oligomers. This "zipper-like" motif is accommodated by elongation of the phosphodiester backbone linkages, maintaining B-DNA base stacking distances of ~3.3 Å throughout the DNA.

The "zipper-like" conformation occurs through severe buckling of the sheared G•A mismatch base pair, bringing the phosphodiester backbone considerably closer together than in B-DNA, 6.36 Å vs. 17.75 Å respectively. This structural distortion

allows the adenine bases to stack in a near linear alignment through the core of the DNA. The only variation in the sugar conformation occurs at the first unpaired A (d(GCG**A**AAGCT)$_2$ with the first upaired A in bold), where it adopts a C3'-*endo* conformation and packs against the A of the G•A mismatch. The following unpaired A reverts back to the standard B-DNA sugar pucker of C2'-*endo*.

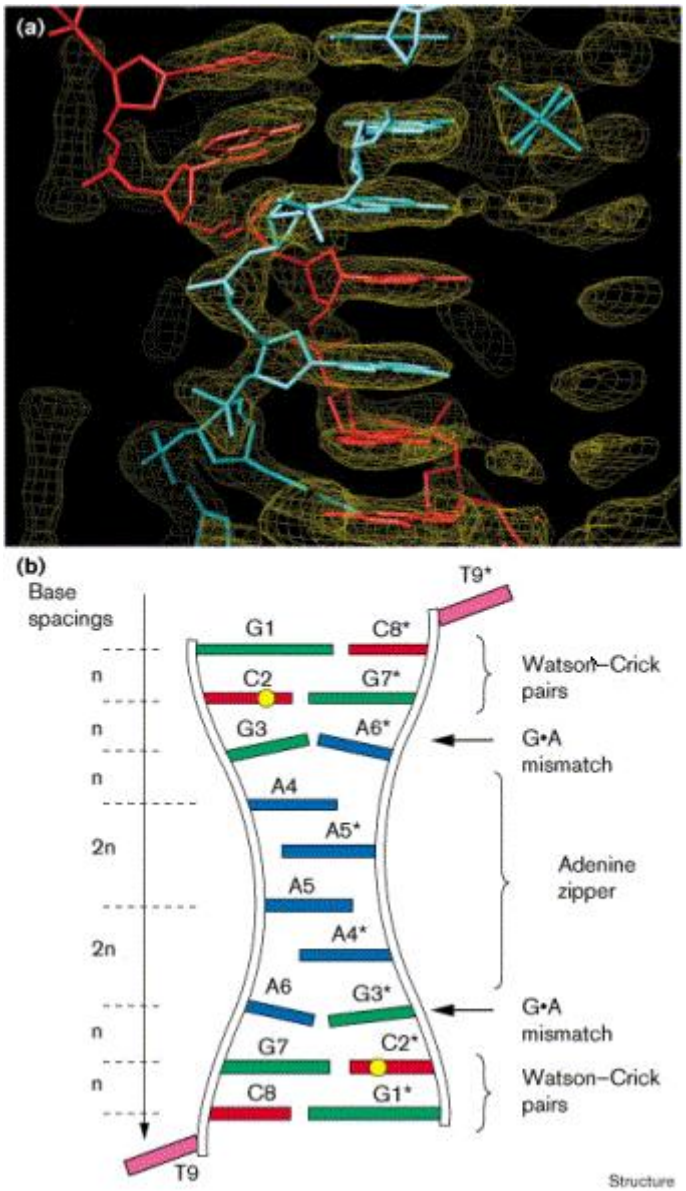

Figure 3.2.[56] Structure of the d(GAAA)$_2$ "Zipper-Like" Duplex. View (a) is the structure obtained from X-ray crystal data. View (b) is a schematic illustration of the base pairing and stacking of the DNA duplex.

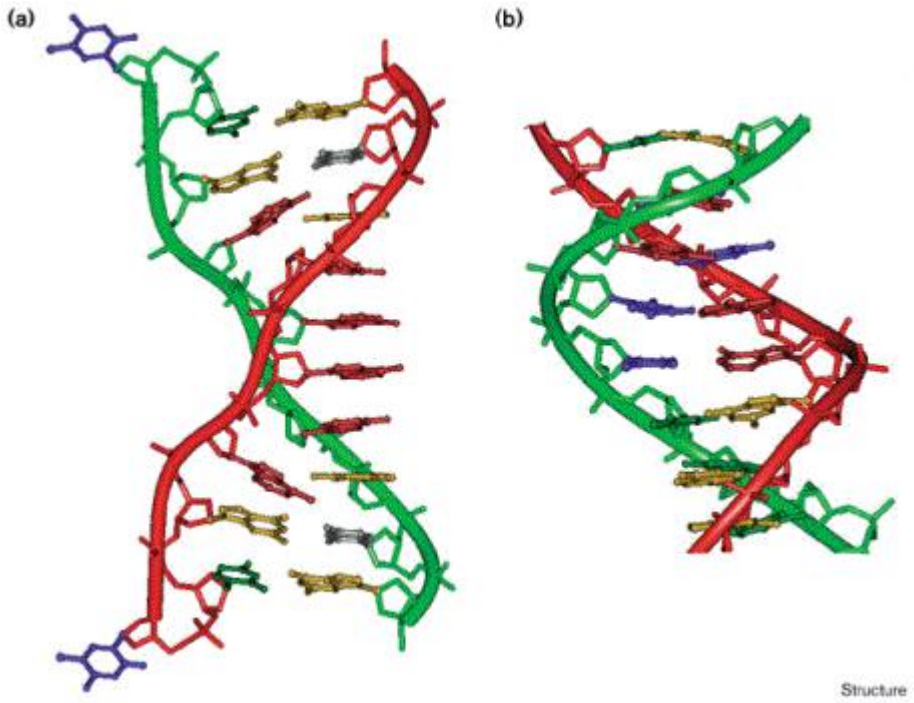

Figure 3.3.[56] Structural Distortion of "Zipper-Like" Duplex DNA. View (a) shows the elongation of the duplex, whereas view (b) illustrates standard B-DNA.

T•T Wobble Base Pair

In the late 70's it was determined that the T•T base pair mismatch was incorporated within the base stacking of duplex DNA[58, 59], however the structure of the mismatch was not fully understood. It was shown based upon NMR evidence that the T•T mismatched base pair was shielded by the neighboring bases, therefore it must be intercalated in the DNA with a "wobble" base pair (Figure 3.3). It was later confirmed that the T•T mismatch is indeed incorporated in the duplex DNA with little structural distortion of the B-DNA secondary conformation.[7, 60, 61]

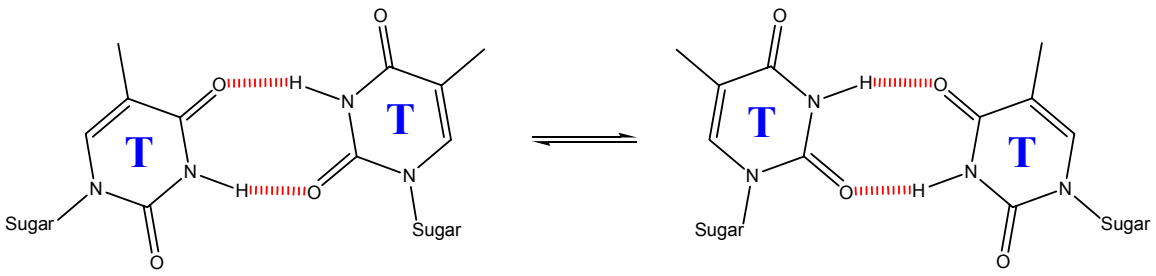

Figure 3.4. T•T Wobble Base Pair.

Incorporation of the T•T mismatch within dsDNA occurs without disruption of the B-DNA conformation; however the hydrogen bonding can adopt two conformations. This wobble base pair fluctuates on the time scale of NMR and yields a broadening of the peak. It is evident that the bases are stacked with the neighboring base pairs and also hydrogen bonding with each other, allowing for continuous overlap of the bases through the mismatch region. Even though the duplex conformation isn't altered by the incorporation of a T•T mismatch, there is a noticeable decrease in the thermal stability of the dsDNA molecule as compared to the Watson-Crick base paired analogue.

Design of DNA Double Helices

Charge migration through dsDNA with fully complementary Watson-Crick base pairing is monitored by oxidation at GG steps within the dsDNA. To study the unusual structural effects of A•A and T•T base pair mismatches on charge transfer through dsDNA, several sequences were designed to incorporate varying sizes of contiguous mismatches (Table 3.1). The fully complementary dsDNA contains two GG steps on

either side of the "variable" region (region of the dsDNA that may contain the contiguous mismatches) in order to monitor the efficiency of charge migration through this region. The variable region contains A•T, T•A, A•A, and T•T base pairing of increasing size to determine if a change in mismatch length also effects the efficiency of charge migration.

Table 3.1. DNA Sequences 1-16. AQ is the anthraquinone moiety tethered to the 5' terminus of the DNA single strand as shown in Figure 2.4. * = ^{32}P radiolabel.

5'- AQ A A A T G C C G G T A C X_n C A T G G C C G T A C G -3' 3'- T T T A C G G_1 C C A T G Y_n G T A C C G G_2 C A T G C* -5'			
DNA(1) $X_n=T_2$; $Y_n=A_2$	DNA(5) $X_n=T_4$; $Y_n=A_4$	DNA(9) $X_n=T_6$; $Y_n=A_6$	DNA(13) $X_n=T_8$; $Y_n=A_8$
DNA(2) $X_n=A_2$; $Y_n=A_2$	DNA(6) $X_n=A_4$; $Y_n=A_4$	DNA(10) $X_n=A_6$; $Y_n=A_6$	DNA(14) $X_n=A_8$; $Y_n=A_8$
DNA(3) $X_n=A_2$; $Y_n=T_2$	DNA(7) $X_n=A_4$; $Y_n=T_4$	DNA(11) $X_n=A_6$; $Y_n=T_6$	DNA(15) $X_n=A_8$; $Y_n=T_8$
DNA(4) $X_n=T_2$; $Y_n=T_2$	DNA(8) $X_n=T_4$; $Y_n=T_4$	DNA(12) $X_n=T_6$; $Y_n=T_6$	DNA(16) $X_n=T_8$; $Y_n=T_8$

The DNA sequence design is envisioned to study charge transfer through zipper-like protions of dsDNA (Figure 3.4), as well as fully complementary and non-purine containing wobble base pair regions. The T•T mismatch region is anticipated to have reduced, or no charge transfer characteristics because purines are believed to act as charge carriers in DNA. However, it has been recently reported that oxidative damage at T's occurs in the absence of G•C base pairs[62]. This evidence supports the polaron theory that the radical cation is delocalized over several bases, and it shows that the charge resides on the T's to a degree. Therefore, even in the T•T mismatch region of the DNA the charge can potentially occupy the T's and hop through the mismatch region. The extent of charge migration through these variable regions will help to understand the structural fluctuations and distortion effects on charge transfer.

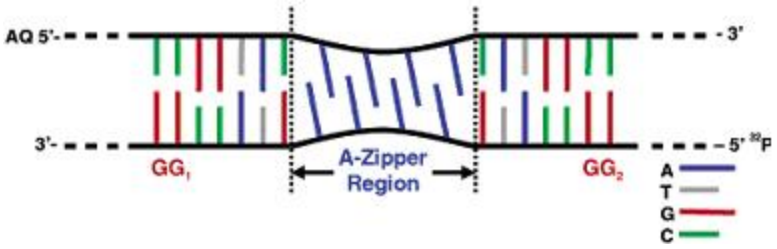

Figure 3.5.[63] Schematic Representation of the "Zipper-Like" Portion of DNA 6.

Experimental

Materials and Methods

All synthetic DNA oligonucleotides were either acquired commercially from Dr. Nadia Boguslavsky of Georgia Institute of Technology, or synthesized in our laboratory by Dr. Sriram Kanvah on an Applied Biosystems Inc. Expedite DNA Synthesizer. All DNA nucleotides and reagents for synthesis were purchased from Glen Research with standard phosphoramidite chemistry functional groups. These synthetic DNA oligonucleotides were purified by HPLC on a Hitachi 7000 HPLC system equipped with a Varian Dynamax 25x21.4 mm reverse-phase C-18 column using 5-20% Acetonitrile in 0.5 M Triethylammonium Acetate. UV/Vis studies on DNA oligonucleotides were conducted at 260 nm on a Hewlett-Packard Spectrophotometer, and the extinction coefficients were calculated using nearest-neighbor values (AQ replaced with A for calculation purposes). The mass of each oligonucleotide was determined by Matrix-Assisted Laser Desorption Ionization Time-of-Flight (MALDI-TOF) or Electrospray Ionization (ESI) mass spectrometry techniques. Radioactively labeled isotopes (α- and γ-

^{32}P) Adenosine triphosphate (ATP) were purchased from GE Healthcare, formerly Amersham Biosciences. The enzyme T4 polynucleotide kinase (T4PNK) and its buffer (PNK buffer) were purchased from New England Biolabs, whereas the enzyme terminal dinucleotide transferase (TdT) and its buffer were purchased from GE Healthcare, i.e. Amersham Biosciences, and all were stored at -20 °C. UV melting and cooling curves were performed an a Cary 1E Spectrophotometer equipped with a multi-cell block, temperature controller and sample transport accessory. Circular Dichroism (CD) measurements were conducted on a JASCO-720 instrument equipped with a temperature controller. Autoradiography was performed on a FUJI 2340 BAS-Image system. Kodak film was purchased from Aldrich. The buffer used for all experiments was 10 mM sodium phosphate (NaPi) at pH 7.0.

Synthesis and Purification of DNA Oligonucleotides

The DNA oligomers, with sequences shown in Table 3.1, were synthesized with standard phosphoramidite chemistry[64] on an ABI expedite DNA synthesizer, using nucleotides with dimethoxytrityl (DMT) and phosphoramidite protecting groups on the 5' and 3' OH's of the sugar, respectively. The oligomers were synthesized on a solid support column, and therefore a deprotection/cleavage reaction was first performed. The oligomers were treated with 1 M ammonium hydroxide (2x at room temperature for 45 minutes, which results in cleavage from the solid support, followed by treatment at 60 °C for up to 18 hours to remove the oligomer protecting groups, and finally concentrated *in vacuo*) followed by purification on HPLC. Prior to injection onto the HPLC, the oligomers were filtered through a micro-pore syringe filter to prevent any solid

particulate from entering the HPLC. Following isolation of the purified oligomers from the HPLC, the salts in solution were removed through filtration of a Sep-Pak desalting column.

The concentration of the purified oligomers was calculated using the equation:

$$Abs_{260} = \varepsilon \cdot b \cdot conc \qquad \text{Equation 3.1}$$

where Abs_{260} is the absorbance value at 260 nm (Figure 3.5), b is the path length of 1 cm, ε is the extinction coefficient calculated using nearest-neighbor values, and conc is the concentration of the DNA oligomer. Approximately 10 µl of 100 µM DNA were submitted for mass spectrometry analysis to determine the accuracy of the purification, as well as verification of the oligomer purity (Table 3.2).

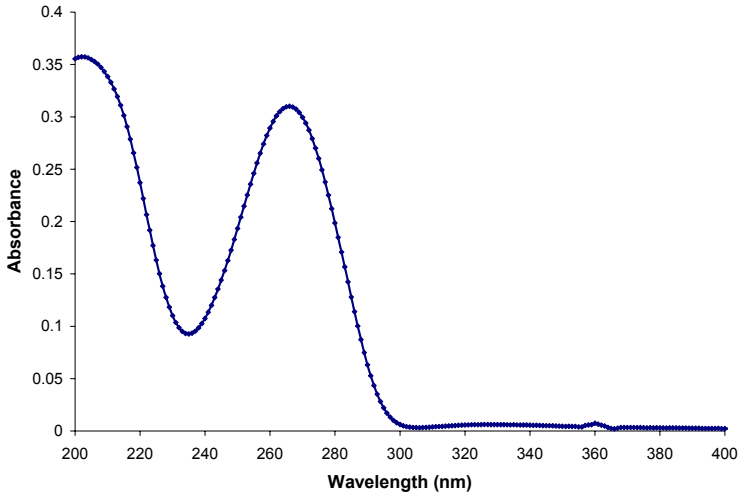

Figure 3.6. UV/Vis Absorption of Non-AQ Containing Single Strand of DNA 7.

Table 3.2. Electrospray Ionization Mass Spectrometry Results for Oligonucleotides Comprising DNA Duplexes 1-16. * Sample ID denotes the composition of the variable region of the AQ or non-AQ containing single-stranded oligomer.

Mass Spec Results		
Sample ID*	**Calc Mass**	**Found Mass**
A2	7971	7972
A4	8598	8597
A6	9224	9222
A8	9850	9848
T2	7954	7951
T4	8562	8562
T6	9170	9168
T8	9778	9781
AQ A2	8364	8346
AQ A4	8972	8975
AQ A6	9598	9597
AQ A8	10225	10221
AQ T2	8328	8328
AQ T4	8936	8935
AQ T6	9544	9544
AQ T8	10152	10151

Thermal Denaturation

The thermal stability of the DNA duplexes 1-16 (Table 3.1) is determined by monitoring the change in absorbance at 260 nm due to the hyperchromicity of the DNA duplexes.[65] As dsDNA is thermally denatured, i.e. melted into two separate single strands, the intensity of the absorbance at 260 nm is increased. This is due to the increase in rotational freedom of the nucleotides as the transition from dsDNA to ssDNA occurs

allowing the ssDNA to adopt more energy levels and absorb more of the UV light. Plotting this change in absorbance with time gives a curve with a change in inflection point, and plotting the first derivative of the curve gives the temperature at which the concentrations of ssDNA and dsDNA are equivalent. This temperature is considered the melting temperature, Tm, of the DNA.

The Tm's of DNA 1-16 were taken with 2.5 μM of each of the oligomers required to make the desired duplex, and 10 mM NaPi buffer at pH 7.0 (Figures 3.6-3.9). The samples were placed in 1 cm path length quartz cells and sealed, then placed in the Cary 1E Spectrophotometer. The samples were heated to 90 °C then cooled to 15 °C at a rate of 1 °C/min, followed by the subsequent heating back to 90 °C at the same rate. This cycle was repeated four times to ensure consistent results, and then the samples were slowly returned to 25 °C for further analysis.

Circular Dichroism

The secondary structures of DNA 1-16 were determined by CD experiments at room temperature with a scan rate of 200 nm/min over the range 200 to 400 nm. A total of 5 scans per sample were completed, and the scans are averaged to result in the CD spectrum for each DNA duplex (Figures 3.10-3.13). The spectral resolution and the bandwidth were 0.2 nm and 1 nm, respectively. The samples were taken directly from the Tm experiments to the CD instrument, and therefore have the same DNA and salt concentrations (described above).

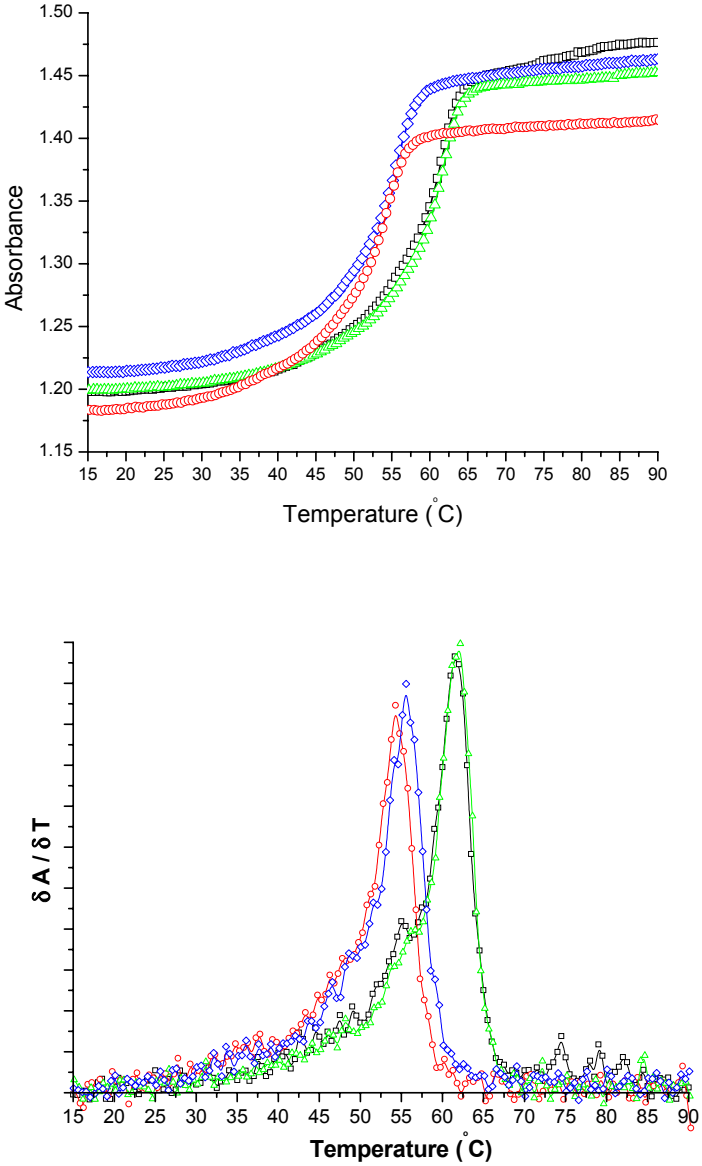

Figure 3.7. Thermal Denaturation Curves of DNA Duplexes 1-4. DNA 1 is black, DNA 2 is red, DNA 3 is green, and DNA 4 is blue.

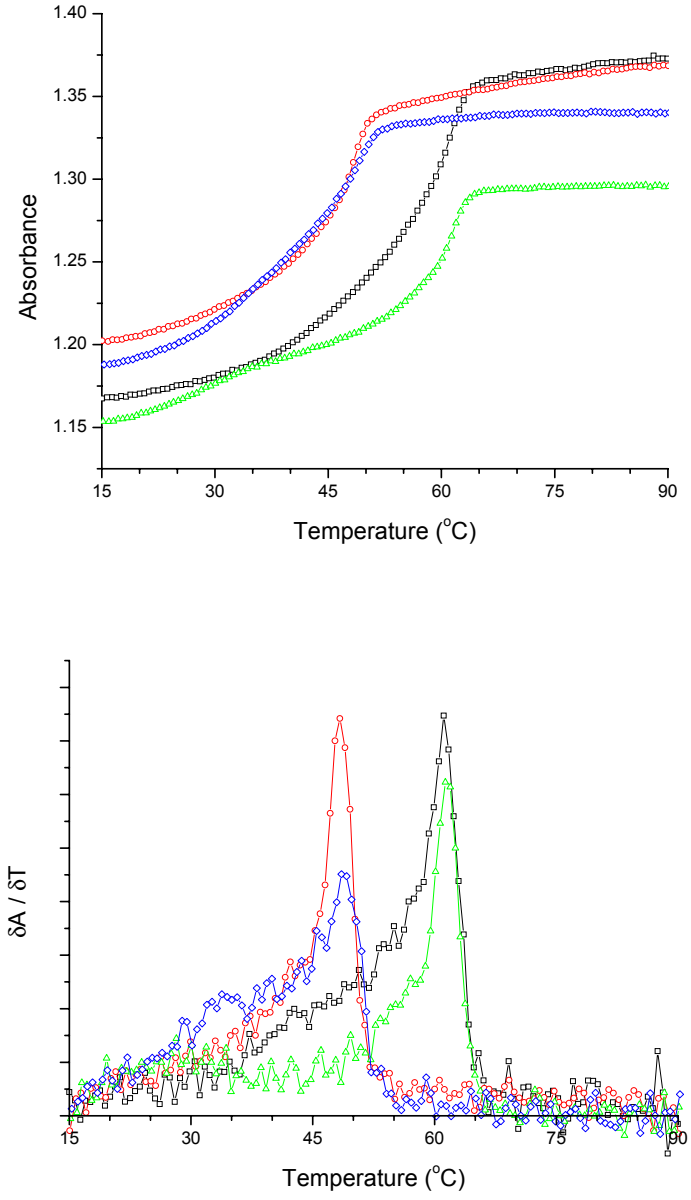

Figure 3.8. Thermal Denaturation Curves of DNA Duplexes 5-8. DNA 5 is black, DNA 6 is red, DNA 7 is green, and DNA 8 is blue.

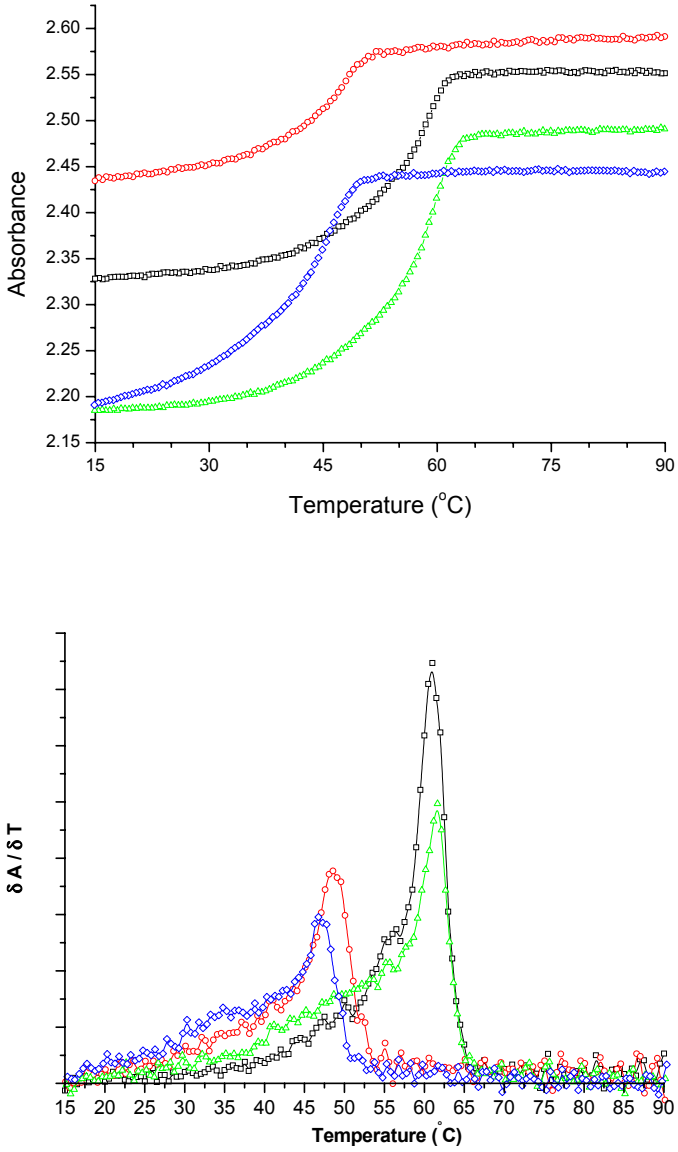

Figure 3.9. Thermal Denaturation Curves of DNA Duplexes 9-12. DNA 9 is black, DNA 10 is red, DNA 11 is green, and DNA 12 is blue.

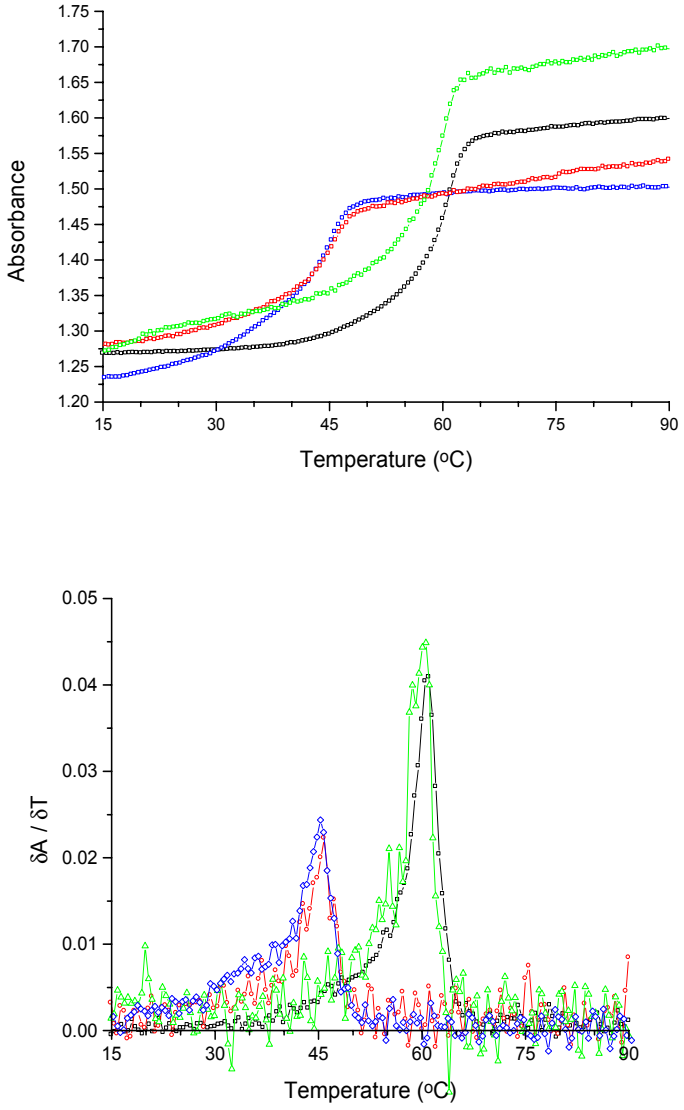

Figure 3.10. Thermal Denaturation Curves of DNA Duplexes 13-16. DNA 13 is black, DNA 14 is red, DNA 15 is green, and DNA 16 is blue.

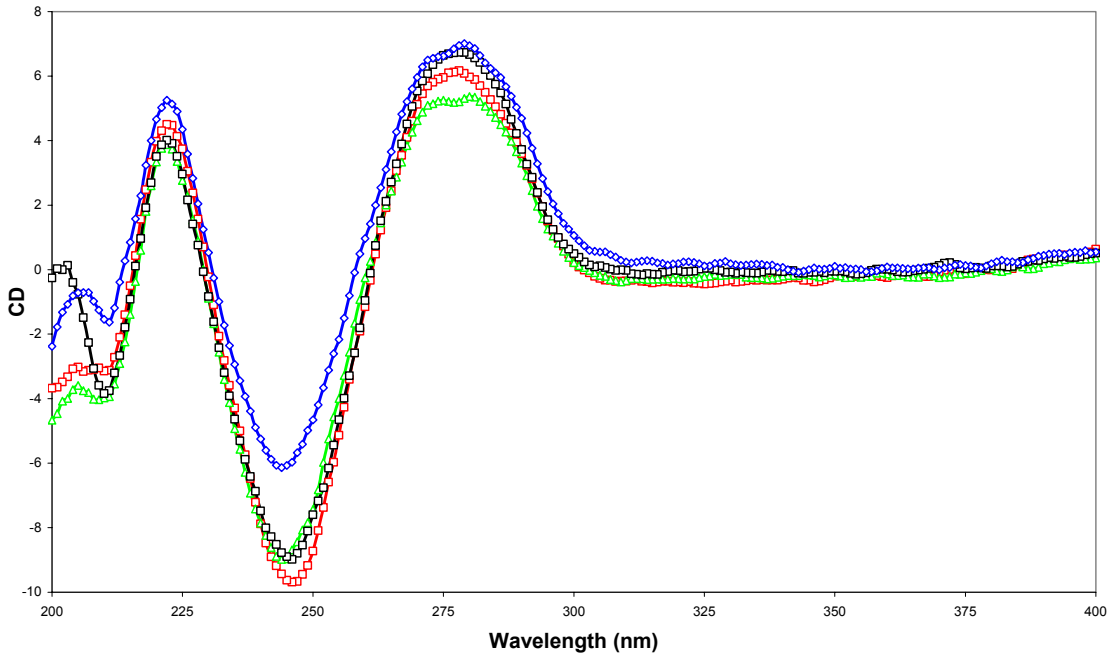

Figure 3.11. Circular Dichroism of DNA Duplexes 1-4. DNA 1 (□), DNA 2 (□), DNA 3 (□), DNA 4 (□).

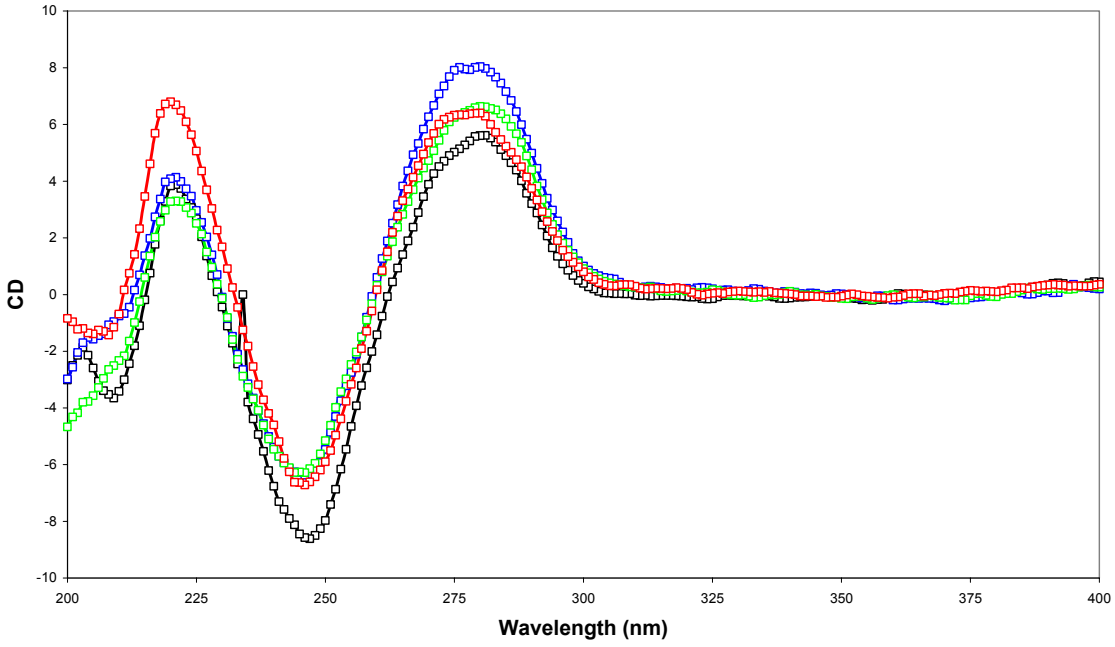

Figure 3.12. Circular Dichroism of DNA Duplexes 5-8. DNA 5 (□), DNA 6 (□), DNA 7 (□), DNA 8 (□).

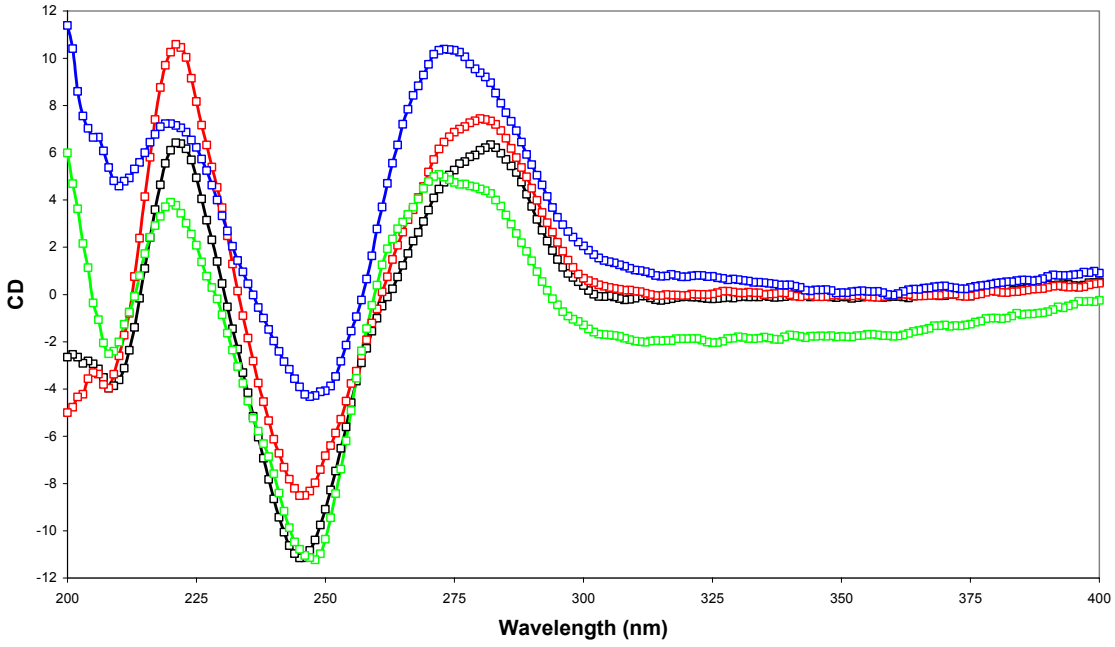

Figure 3.13. Circular Dichroism of DNA Duplexes 9-12. DNA 9 (□), DNA 10 (□), DNA 11 (□), DNA 12 (□).

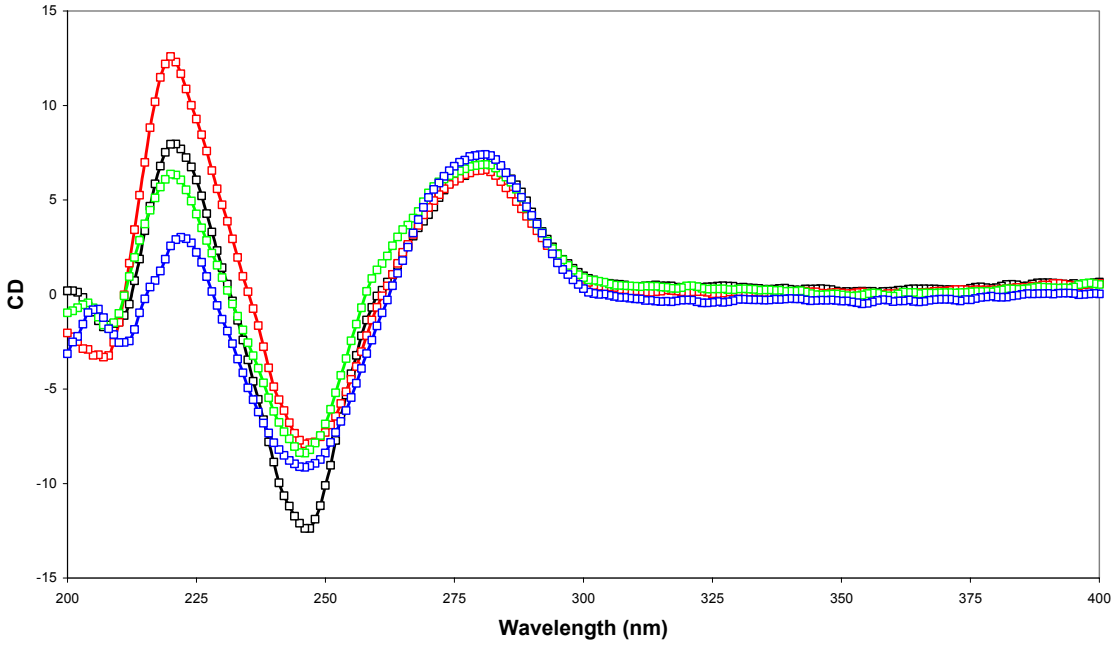

Figure 3.14. Circular Dichroism of DNA Duplexes 13-16. DNA 13 (□), DNA 14 (□), DNA 15 (□), DNA 16 (□).

Radiolabeling

Visualization of the amount of damage at GG steps in the DNA is essential for determining the efficiency of charge migration. End-labeling the ssDNA oligomer containing the GG steps with α or γ-^{32}P-radiolabeled phosphate (α is placed at the 3'-end of the ssDNA, whereas γ is placed on the 5'-end) allows for quantitative measurements of the ratio of damage occurring at the GG steps within the dsDNA.

Approximately 25 μM of the ssDNA oligomer (17 μl) containing the GG steps (non-AQ ssDNA) was incubated at 37 °C with 1μl PNK buffer, 1 μl γ-^{32}P-ATP, and 1 μl PNK enzyme for 45 min. After incubation, 10 μl of a tetrabromophenolsulfonphthalein (bromophenol blue) glycerol solution was added to the DNA mixture. This DNA mixture was loaded onto a 19:1 acrylamide/bisacrylamide gel and electrophoresis separated the enzyme and unreacted ATP from the newly radiolabeled DNA. This DNA was eluted from the acrylamide/bisacrylamide gel overnight, followed by precipitation in 100% ethyl alcohol at -78 °C for 1h. The supernatant was removed and the resulting purified and radiolabeled ssDNA was washed 2x with 80% ethyl alcohol then dried *in vacuo*.

Irradiation and Piperidine Treatment

Prior to inducing the charge injection into the dsDNA, the radiolabeled ssDNA and its complementary ssDNA strand are annealed. The radiolabeled ssDNA (non-AQ ssDNA*) was diluted to 10,000 counts per minute (cpm) per μl of solution with nanopure H_2O. A total volume of 20 μl per sample was constructed with 5 μM AQ ssDNA and 5

μM non-AQ ssDNA in 10 mM NaPi buffer with 2 μl non-AQ ssDNA*. The ssDNA mixture was hybridized to dsDNA by heating to 90 °C and slowly cooling to room temperature overnight.

The 20 μl solution of DNA containing the radiolabel was then irradiated at 350 nm for varying amounts of time ranging from 0 to 20 min. There is always one sample for each dsDNA that is not irradiated because it is used as the control experiment. In these experiments, the extent of reaction is controlled so that the dsDNA is reacted only once or not at all. This was demonstrated by showing that the results of irradiation are independent of the irradiation time at the relevant extent of reaction. Varying irradiation times and showing that the ratio of damage at the GG steps for the desired irradiation time is equivalent for all times of irradiation is an indication that the dsDNA is, on average, reacted only once or not at all. The dsDNA samples are then precipitated in 100% ethyl alcohol at -78 °C for 1 h. The resulting supernatant was removed and the precipitate was washed 2x with 80% ethyl alcohol then dried *in vacuo*. The precipitate was suspended in 20 μl of 1 M piperidine and heated to 90 °C for 30 min. The hot piperidine cleaves the alkaline-labile lesions in the dsDNA that were caused by charge transfer to the GG steps followed by oxidation with H_2O or O_2. The dsDNA solutions are dried *in vacuo* followed by two repeated steps of adding 20 μl nanopure H_2O and drying *in vacuo*.

PAGE Analysis

In order to accurately quantify the efficiency of charge migration, the DNA mixture after piperidine treatment is separated by polyacrylamide gel electrophoresis (PAGE) using a gel containing urea to denature the DNA. Electrophoresis of the DNA mixture separates the different fragments based on a charge to size ratio. The smaller fragments of DNA will migrate at a faster rate affording adequate separation of all DNA fragments.

The piperidine treated and dried DNA oligomers are first diluted with the bromophenol blue and a 4:1 formamide to H_2O solution to 1,000 cpm per µl solution. The samples are then heated to 90 °C for 5 min then immediately plunged into ice. The samples were then loaded onto the polyacrylamide gel, with 3000 cpm per lane (3 µl solution). Concluding electrophoresis, the gel was separated from the glass plates and placed on a sheet of blotting paper and covered with cellophane. The gel was then dried *in vacuo* at 80 ºC for 2 h on a gel dryer. The dried gel was then placed in a closed casket with a sheet of Kodak film for 18 h. The Kodak film was removed from the casket and developed to give the image of the gel. The gel images for DNA 1-16 are shown in Figures 3.14-3.17

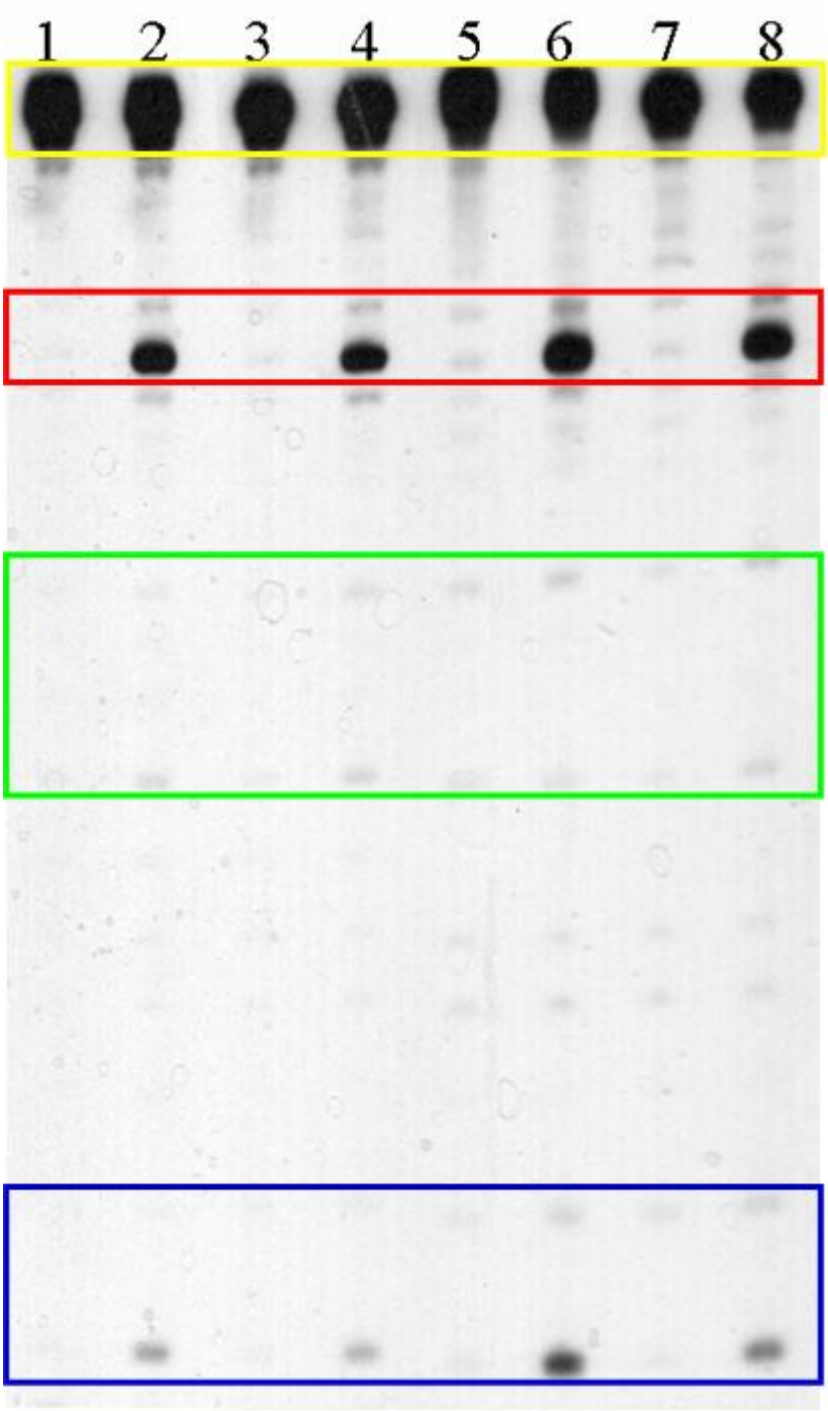

Figure 3.15. Autoradiogram Showing Strand Cleavage of DNA Samples 1-4 Following Irradiation and Piperidine Treatment. Lanes 1(2), 3(4), 5(6), 7(8) correspond to 0(3) min irradiations of DNA (1), (2), (3), and (4), respectively. Yellow box is uncut DNA, red box is GG_1, green box is the variable region, and blue box is GG_2.

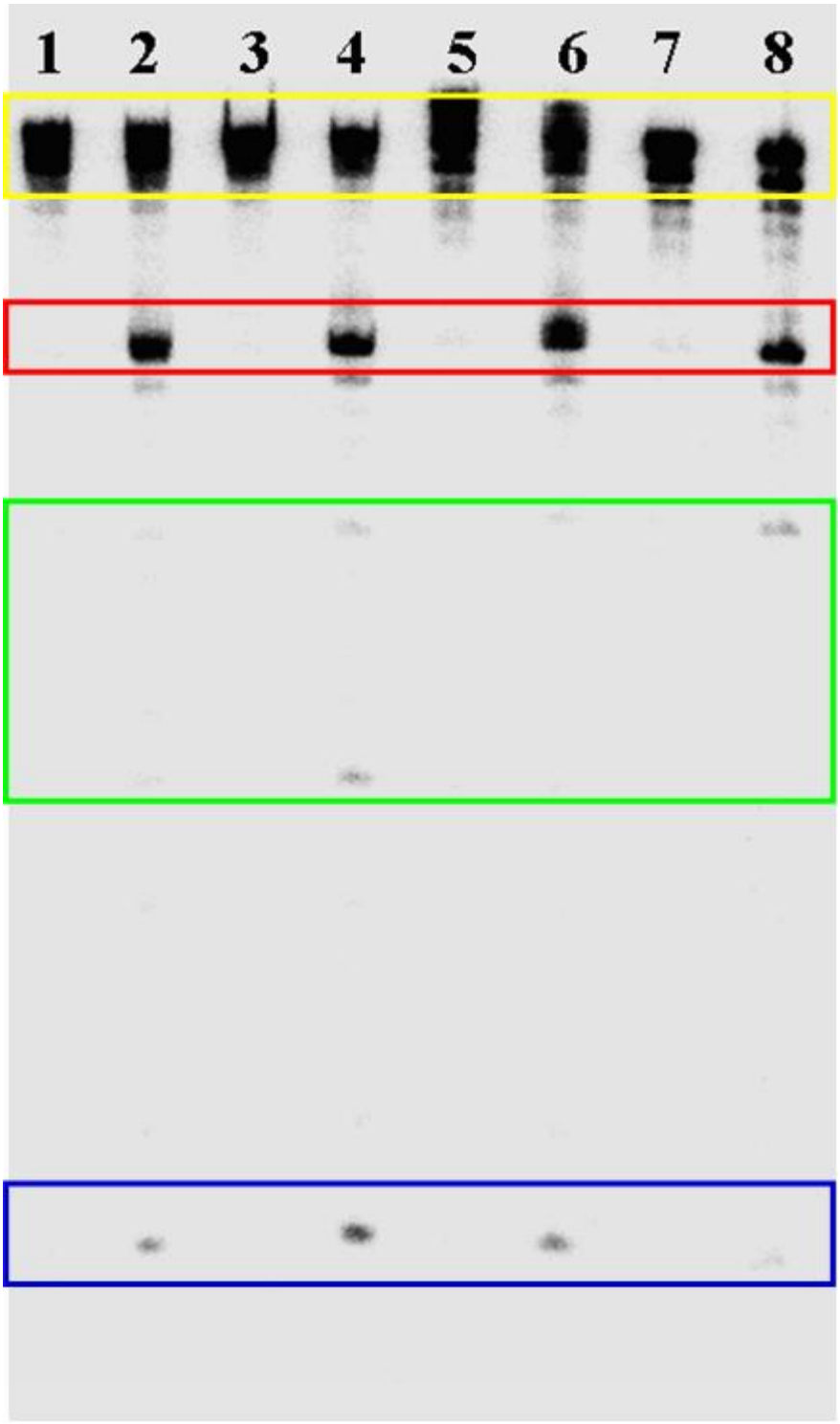

Figure 3.16. Autoradiogram Showing Strand Cleavage of DNA Samples 5-8 Following Irradiation and Piperidine Treatment. Lanes 1(2), 3(4), 5(6), 7(8) correspond to 0(3) min irradiations of DNA (5), (6), (7), and (8), respectively. Yellow box is uncut DNA, red box is GG_1, green box is the variable region, and blue box is GG_2.

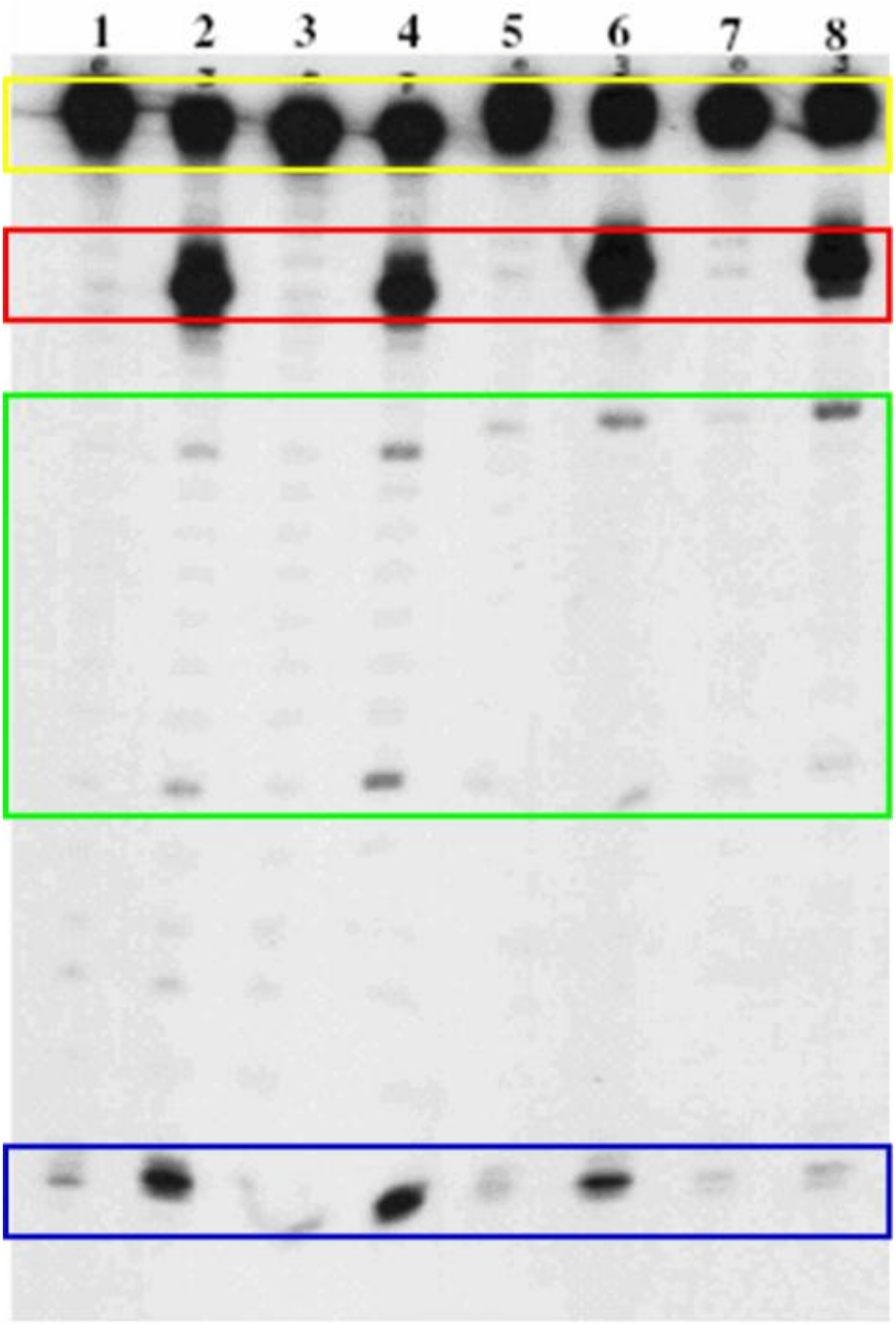

Figure 3.17. Autoradiogram Showing Strand Cleavage of DNA Samples 9-12 Following Irradiation and Piperidine Treatment. Lanes 1(2), 3(4), 5(6), 7(8) correspond to 0(3) min irradiations of DNA(9), (10), (11), and (12), respectively. Yellow box is uncut DNA, red box is GG_1, green box is the variable region, and blue box is GG_2.

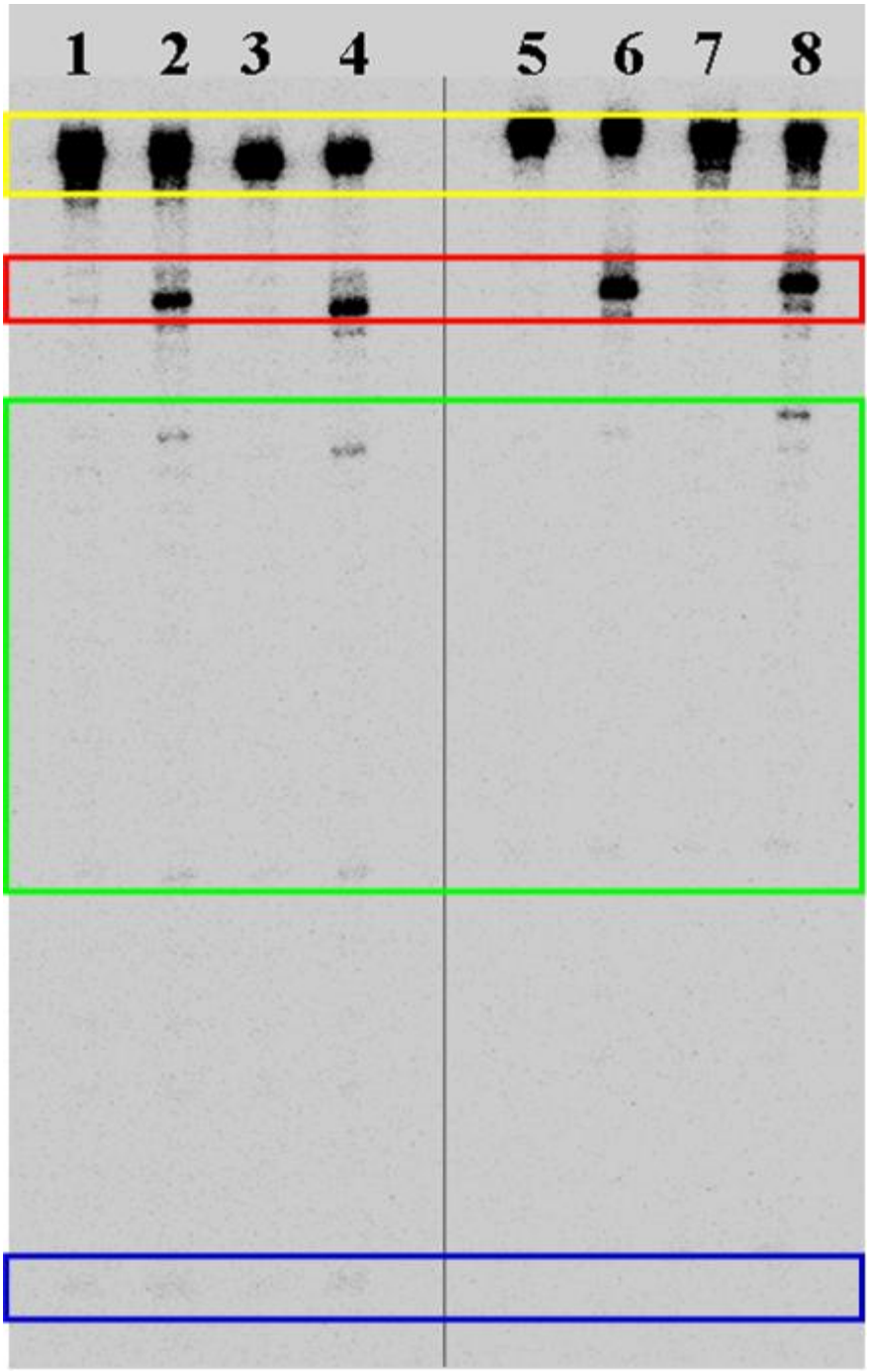

Figure 3.18. Autoradiogram Showing Strand Cleavage of DNA Samples 13-16 Following Irradiation and Piperidine Treatment. Lanes 1(2), 3(4), 5(6), 7(8) correspond to 0(3) min irradiations of DNA(13), (14), (15), and (16), respectively. Yellow box is uncut DNA, red box is GG_1, green box is the variable region, and blue box is GG_2.

Phosphorimagery

To quantify the relative amount of DNA at each GG step, the gels are "counted" on a FUJI 2340 BAS-Image system. The gels are placed within a FUJI casket for 4 to 6 h then removed. The imaging plate is then removed from the casket and recorded by the FUJI image system. The image looks essentially identical to the image on the Kodak film, however, this image can now be counted using ImageGuage software. Each of the dark spots in the image represents the ^{32}P-radiolabel attached to the 5'-end of a DNA fragment. The intensity of each spot is counted and the appropriate ratios can be determined. Assuming the rate of reaction at each GG step is equivalent, then the ratio of the amount of DNA at each GG step is equivalent to the efficiency of charge transfer through the DNA.

Results

Structural Conformation and Thermal Integrity

Charge transfer through DNA duplexes containing contiguous A:A and T:T mismatches has been studied. Table 3.1 shows the sequences of the DNA duplexes analyzed to examine the effects that mismatch base sequence and mismatch length have on radical cation transport in DNA. Examination of the overall secondary structure of Normal Watson-Crick base paired B-DNA results in a CD curve with a positive peak at ~275 nm and a negative peak at ~245 nm.[66, 67] The customary curve of B-DNA is a result of the bases of the DNA absorbing right- and left-handed polarized UV light to varying degrees dependent on their overall secondary structure. The secondary structure of contiguous A•A mismatches was shown to form a zipper-like conformation with the

Watson-Crick base pairs flanking the interdigitated region adopting a B-DNA structure.[56] This secondary structure conformation change at the central region of the DNA isn't obvious from the CD experiments, where the overall secondary structure was unaffected by the A•A mismatch length (Figures 3.10-3.13).

The T•T mismatch has been reported to have essentially no effect on the B-DNA base stacking, however, local distortion in base arrangements occurs via a wobble base pair.[7] Similar to the experiments with A•A mismatch DNA, the circular dichroism experiments (Figures 3.10-3.13) don't reveal any structural fluctuations. The overall secondary structure of the dsDNA is unperturbed regardless of the T•T mismatch size. It is observed that even the largest contiguous mismatches, $(A•A)_8$ and $(T•T)_8$, yield a CD that indicates an overall B-DNA conformation of the dsDNA molecule, as revealed by the position of the positive and negative peaks of the CD curves, despite the larger percentage of overall content in the DNA. However, the CD is roughly an average of the molecules overall secondary structure and minor local distortions are difficult to analyze under these experimental conditions.

Thermal stability of duplex DNA has been reported to decrease with the introduction of mismatched base pairs. Presumably, the larger the number of mismatches within the dsDNA molecule, the lower the melting temperature of that molecule. This trend holds true for the A•A and T•T contiguous mismatch DNA duplexes analyzed. As the melting temperature of the fully complementary DNA is essentially unchanged with increasing DNA length, the Tm of the mismatch DNA duplexes decreases as the size of

the mismatch region increases (Table 3.3). The decrease in Tm of the mismatch DNA is consistent with expected melting behavior based on empirical correlation with structure.[61] The overall secondary structure of the mismatched dsDNA along with the thermal stabilities indicates both structures adopt a predominantly intrahelical conformation.

Table 3.3. Melting Temperatures of DNA 1-16.

dsDNA	Tm (°C)	dsDNA	Tm (°C)	dsDNA	Tm (°C)	dsDNA	Tm (°C)
DNA (1)	62	DNA (5)	60	DNA (9)	61	DNA (13)	61
DNA (2)	56	DNA (6)	50	DNA (10)	49	DNA (14)	45
DNA (3)	62	DNA (7)	60	DNA (11)	62	DNA (15)	62
DNA (4)	56	DNA (8)	48	DNA (12)	47	DNA (16)	44

Charge Migration Efficiency

The effect of A•A and T•T contiguous mismatches on charge transfer was examined by irradiation of the AQ-linked dsDNA at 350nm, followed by treatment with hot piperidine. The DNA fragments were separated by gel electrophoresis and analyzed by phosphorimagery (Figures 3.14-3.17). It was revealed that the charge migration through the variable region was highly sequence dependent, and in most cases length dependent as well (Table 3.4). It is obvious from the gel images that the DNA samples with 8 base pairs in the variable region create a sufficient barrier to charge migration that prohibits a significant amount of detectable damage at the distal GG steps. Therefore, only the DNA samples with detectable damage at the distal GG steps were quantified.

The fully complementary DNA (DNA 1, 3, 5, 7, 9, and 11) revealed an expected distance dependence on charge transfer, that was only mildly dependent on the orientation of the base pairs, A•T vs. T•A, in the duplex. However, the A•A and T•T mismatch DNA exhibited completely differing results of charge transfer.

Table 3.4. Charge Migration Efficiency Results for DNA 1-12. [a]Proximal (GG_1) to distal (GG_2) ratios of the GG steps in the DNA indicates the efficiency of charge migration through the DNA.

Sample	GG_1/GG_2[a]	Sample	GG_1/GG_2[a]	Sample	GG_1/GG_2[a]
DNA(1)	9	DNA(5)	14	DNA(9)	16
DNA(2)	10	DNA(6)	7	DNA(10)	8
DNA(3)	5	DNA(7)	9	DNA(11)	23
DNA(4)	8	DNA(8)	25	DNA(12)	>40

The contiguous A•A mismatch DNA (DNA 2, 6, and 10) is at least as efficient as the complementary DNA, and showed essentially no change in charge transfer efficiency as a function of length. The T•T mismatch DNA (DNA 4, 8, and 12), on the other hand, showed a drastic dependence on length, with the $(T•T)_4$ DNA creating a sufficient barrier to almost completely inhibit charge transfer.

Conclusions

Charge migration efficiency through contiguous A•A and T•T mismatches has been examined. The mismatch DNA molecules appear to exhibit an overall B-DNA conformation, with minor perturbations in the secondary structure not being analyzed in these experiments. The samples decrease in Tm as the size of the mismatch increases, as expected. The reduction in damage at the distal GG steps (GG_2) indicates the varying mismatch duplexes have drastically differing effects on the efficiency of charge transfer. These differences can be contributed to the differing secondary structures of the mismatched dsDNA.

The T•T mismatch, although it has little effect on the B-DNA conformation, does not contain any purines. Purines are believed to be the major carriers of charge during migration through the DNA, and the loss of purines in the variable region would be expected to diminish the ability of a radical cation to hop beyond this barrier. This is shown by the fact that more than two consecutive T•T mismatches essentially creates a barrier that stops charge transfer. It is clear that the efficiency of charge injection is unaffected by the amount of damage that occurs before the T•T mismatch region at the proximal GG step (GG_1). Quantum mechanical calculations indicate the delocalized radical cation during polaron formation resides on the T to a small degree.[68] Recent evidence supports this claim by showing that in DNA containing only A•T base pairs, the T's are oxidatively damaged as opposed to the A's.[68] These finding prove that the radical cation resides on the T's long enough to react with either H_2O or O_2, therefore it is

possible that the radical cation could be delocalized over a small T•T mismatch barrier. However, when the barrier size is increased beyond two T•T mismatches, the radical cation cannot delocalize across the mismatch region and therefore the charge migration is diminished.

The A•A mismatch DNA duplexes studied appear to have little effect on the overall structure of the DNA. However, charge migration through the mismatched DNA duplexes is essentially unaffected by the length of the mismatch. Although studies have indicated A•A mismatches can form wobble base pairs, this requires significant structural distortion of the DNA helix.[67] More recently, it has been reported that $(A•A)_2$ mismatches form an interdigitated "zipper-like" double helical structure with well-aligned base stacking throughout the DNA helix.[56] We envision the contiguous A•A mismatches reported here to adopt the zipper-like conformation.

The zipper-like A's are not restricted in motion by base pairing with a complementary base. Therefore, during polaron formation and phonon-assisted hopping of the radical cation through the A•A mismatch region, the unrestricted motion of the A's could assist in the charge transfer. This is consistent with our findings that the charge migration through A•A mismatched DNA has no affect on charge migration efficiency. Therefore, charge migration through contiguous A•A and T•T mismatch base pairs is consistent with the phonon-assisted polaron-like hopping mechanism.

REFERENCES

[1] Goodman, M. F.; Creighton, S.; Bloom, L. B.; Petruska, J., Biochemical Basis of DNA Replication Fidelity. *Crit Rev Biochem Mol Biol* 1993, 28, (2), 83-126.

[2] Bhattacharyya, Anamitra; M.J. Lilley, David, Single Base Mismatches in DNA Long- and Short-range Structure Probed by Analysis of Axis Trajectory and Local Chemical Reactivity. *Journal of Molecular Biology* 1989, 209, (4), 583-597.

[3] Leonard, Gordon A.; Booth, Ewan D.; Brown, Tom, Structural and Thermodynamic Studies on the Adenine·Guanine Mismatch in B-DNA. *Nucl. Acids Res.* 1990, 18, (19), 5617-5623.

[4] Plum, G. Eric; Grollman, Arthur P.; Johnson, Francis; Breslauer, Kenneth J., Influence of the Oxidatively Damaged Adduct 8-Oxodeoxyguanosine on the Conformation, Energetics, and Thermodynamic Stability of a DNA Duplex. *Biochemistry* 1995, 34, (49), 16148-16160.

[5] Brown, T., *Aldrichimica Acta* 1995, 28, 15-20.

[6] Lindahl, Tomas, Instability and Decay of the Primary Structure of DNA. *Nature* 1993, 362, (6422), 709-715.

[7] Gervais, V.; Cognet, J. A.; Le Bret, M.; Sowers, L. C.; Fazakerley, G. V., Solution Structure of Two Mismatches A·A and T·T in the K-ras Gene Context by Nuclear Magnetic Resonance and Molecular Dynamics. *Eur J Biochem* 1995, 228, (2), 279-290.

[8] Lilley, David M. J., The Formation of Alternative Structures in DNA. In *Bioorganic Chemistry: Nucleic Acids*, Hecht, S. M., Ed. Oxford University Press: New York, 1996; pp 186-215.

[9] Patel, D. J.; Kozlowski, S. A.; Ikuta, S.; Itakura, K., Dynamics of DNA Duplexes Containing Internal G·T, G·A, A·C, and T·C Pairs: Hydrogen Exchange at and Adjacent to Mismatch Sites. *Federation Proceedings* 1984, 43, (11), 2663-2670.

[10] Gasper, S. M.; Schuster, G. B., Intramolecular Photoinduced Electron Transfer to Anthraquinones Linked to Duplex DNA: The Effect of Gaps and Traps on Long-Range Radical Cation Migration. *J. Am. Chem. Soc.* 1997, 119, (52), 12762-12771.

[11] Kelley, S. O.; Holmlin, R. E.; Stemp, E. D. A.; Barton, J. K., Photoinduced Electron Transfer in Ethidium-Modified DNA Duplexes: Dependence on Distance and Base Stacking. *J. Am. Chem. Soc.* 1997, 119, (41), 9861-9870.

[12] Boone, Edna; Schuster, Gary B., Long-range Oxidative Damage in Duplex DNA: the Effect of Bulged G in a G-C Tract and Tandem G/A Mispairs. *Nucl. Acids Res.* 2002, 30, (3), 830-837.

[13] Paul T. Henderson, Edna Boone Gary B Schuster, Bulged Guanine is Uniquely Sensitive to Damage Caused by Visible-Light Irradiation of Ethidium Bound to DNA: A Possible Role in Mutagenesis. *Helvetica Chimica Acta* 2002, 85, (1), 135-151.

[14] Giese, Bernd; Wessely, Stephan, The Significance of Proton Migration during Hole Hopping through DNA. *Chemical Communications* 2001, (20), 2108-2109.

[15] Kelley, S. O.; Boon, E. M.; Barton, J. K.; Jackson, N. M.; Hill, M. G., Single-base Mismatch Detection based on Charge Transduction through DNA. *Nucl. Acids Res.* 1999, 27, (24), 4830-4837.

[16] Kelley, Shana O.; Jackson, Nicole M.; Hill, Michael G.; Barton, Jacqueline K., Long-Range Electron Transfer through DNA Films. *Angewandte Chemie International Edition* 1999, 38, (7), 941-945.

[17] Bernd Giese, Stefan Wessely, The Influence of Mismatches on Long-Distance Charge Transport through DNA. *Angewandte Chemie* 2000, 39, (19), 3490-3491.

[18] Fahlman, R. P.; Sharma, R. D.; Sen, D., The Charge Conduction Properties of DNA Holliday Junctions Depend Critically on the Identity of the Tethered Photooxidant. *J. Am. Chem. Soc.* 2002, 124, (42), 12477-12485.

[19] Watson, James. D.; Crick, Francis H. C., Molecular Structure of Nucleic Acids: A Structure for Deoxyribose Nucleic Acid. *Nature* 1953, 171, 737-738.

[20] Moser, H. E.; Dervan, P. B., Sequence-specific Cleavage of Double Helical DNA by Triple Helix Formation. *Science* 1987, 238, (4827), 645-650.

[21] Han, F. X.; Wheelhouse, R. T.; Hurley, L. H., Interactions of TMPyP4 and TMPyP2 with Quadruplex DNA. Structural Basis for the Differential Effects on Telomerase Inhibition. *J. Am. Chem. Soc.* 1999, 121, (15), 3561-3570.

[22] Laughlan, G.; Murchie, A. I.; Norman, D. G.; Moore, M. H.; Moody, P. C.; Lilley, D. M.; Luisi, B., The High-Resolution Crystal Structure of a Parallel-Stranded Guanine Tetraplex. *Science* 1994, 265, (5171), 520-524.

[23] Mergny, Jean-Louis; Mailliet, Patrick; Lavelle, Francois; Riou, Jean-Francois; Laoui, Abdelazize; Helene, Claude, The Development of Telomerase Inhibitors: the G-Quartet Approach. *Anti-Cancer Drug Design* 1999, 14, 327-339.

[24] Sundquist, Wesley I.; Klug, Aaron, Telomeric DNA Dimerizes by Formation of Guanine Tetrads Between Hairpin Loops. *Nature* 1989, 342, (6251), 825-829.

[25] Williamson, James R.; Raghuraman, M. K.; Cech, Thomas R., Monovalent Cation-Induced Structure of Telomeric DNA: The G-Quartet Model. *Cell* 1989, 59, (5), 871-880.

[26] Nelson, Stephanie M; Ferguson, Lynnette R; Denny, William A, DNA and the Chromosome – Varied Targets for Chemotherapy. *Cell & Chromosome* 2004, 3, (2), 1-26.

[27] Gehring, Kalle; Leroy, Jean-Louis; Gueron, Maurice, A Tetrameric DNA Structure with Protonated Cytosine-Cytosine Base Pairs. *Nature* 1993, 363, (6429), 561-565.

[28] Kang, C.; Berger, I.; Lockshin, C.; Ratliff, R.; Moyzis, R.; Rich, A., Crystal Structure of Intercalated Four-Stranded d(C_3T) at 1.4 A Resolution. *PNAS* 1994, 91, (24), 11636-11640.

[29] Nonin, Sylvie; Leroy, Jean-Louis, Structure and Conversion Kinetics of a Bi-stable DNA i-motif: Broken Symmetry in the $[d(5mCCTCC)]_4$ Tetramer. *Journal of Molecular Biology* 1996, 261, (3), 399-414.

[30] Mergny, Jean-Louis; Lacroix, Laurent; Han, Xiaogang; Leroy, Jean-Louis; Helene, Claude, Intramolecular Folding of Pyrimidine Oligodeoxynucleotides into an i-DNA Motif. *J. Am. Chem. Soc.* 1995, 117, (35), 8887-8907.

[31] Bouaziz, Serge; Kettani, Abdelali; Patel, Dinshaw J., A K Cation-Induced Conformational Switch within a Loop Spanning Segment of a DNA Quadruplex Containing G-G-G-C Repeats. *Journal of Molecular Biology* 1998, 282, (3), 637-652.

[32] Chaput, John C.; Switzer, Christopher, A DNA Pentaplex Incorporating Nucleobase Quintets. *PNAS* 1999, 96, (19), 10614-10619.

[33] Kettani, Abdelali; Bouaziz, Serge; Skripkin, Eugene; Majumdar, Ananya; Wang, Weimin; Jones, Roger A.; Patel, Dinshaw J., Interlocked Mismatch-Aligned Arrowhead DNA Motifs. *Structure* 1999, 7, (7), 803-815.

[34] Lin, Chin H.; Wang, Weimin; Jones, Roger A.; Patel, Dinshaw J., Formation of an Amino-Acid-Binding Pocket through Adaptive Zippering-up of a Large DNA Hairpin Loop. *Chemistry & Biology* 1998, 5, (10), 555-572.

[35] Fiddes, John C.; Barrell, B. G.; Godson, G. Nigel, Nucleotide Sequences of the Separate Origins of Synthesis of Bacteriophage G4 Viral and Complementary DNA Strands. *PNAS* 1978, 75, (3), 1081-1085.

[36] Sims, John; Dressler, David, Site-Specific Initiation of a DNA Fragment: Nucleotide Sequence of the Bacteriophage G4 Negative-Strand Initiation Site. *PNAS* 1978, 75, (7), 3094-3098.

[37] Sims, J.; Capon, D.; Dressler, D., dnaG (Primase)-dependent Origins of DNA Replication. Nucleotide Sequences of the Negative Strand Initiation Sites of Bacteriophages St-1, ΦK, and α3. *J. Biol. Chem.* 1979, 254, (24), 12615-12628.

[38] Astell, Caroline R.; Smith, Michael; Chow, Marie B.; Ward, David C., Structure of the 3' Hairpin Termini of Four Rodent Parvovirus Genomes: Nucleotide Sequence Homology at Origins of DNA Replication. *Cell* 1979, 17, (3), 691-703.

[39] McKenna, Robert; Bowman, Brian R.; Ilag, Leodevico L.; Rossmann, Michael G.; Fane, Bentley A., Atomic Structure of the Degraded Procapsid Particle of the Bacteriophage G4: Induced Structural Changes in the Presence of Calcium Ions

and Functional Implications. *Journal of Molecular Biology* 1996, 256, (4), 736-750.

[40] Hirao, Ichiro; Ishida, Miki; Watanabe, Kimitsuna; Miura, Kin-ichiro, Unique Hairpin Structures Occurring at the Replication Origin of Phage G4 DNA. *Biochimica et Biophysica Acta (BBA) - Gene Structure and Expression* 1990, 1087, (2), 199-204.

[41] Hirao, I.; Naraoka, T.; Kanamori, S.; Nakamura, M.; Miura, K., Synthetic Oligodeoxyribonucleotides Showing Abnormal Mobilities on Polyacrylamide Gel Electrophoresis. *Biochem. Int.* 1988, 16, 157-162.

[42] Yoshizawa, Satoko; Ueda, Takuya; Ishido, Yoshiharu; Miura, Kin-ichiro; Watanabe, Kimitsuna; Hirao, Ichiro, Nuclease Resistance of an Extraordinarily Thermostable Mini-Hairpin DNA Fragment, d(GCGAAGC) and its Application to in vitro Protein Synthesis. *Nucl. Acids Res.* 1994, 22, (12), 2217-2221.

[43] Nowak, R, Mining Treasures from 'Junk DNA'. *Science* 1994, 263, (5147), 608-610.

[44] Blackburn, Elizabeth H., Structure and Function of Telomeres. *Nature* 1991, 350, (6319), 569-573.

[45] Catasti, Paolo; Gupta, Goutam; Garcia, Angel E.; Ratliff, Robert; Hong, Lin; Yau, Peter; Moyzis, Robert K.; Bradbury, E. Morton, Unusual Structures of the Tandem Repetitive DNA Sequences Located at Human Centromeres. *Biochemistry* 1994, 33, (13), 3819-3830.

[46] Chou, Shan-Ho; Zhu, Leiming; Reid, Brian R., The Unusual Structure of the Human Centromere (GGA)2 Motif : Unpaired Guanosine Residues Stacked Between Sheared G[middle dot]A Pairs. *Journal of Molecular Biology* 1994, 244, (3), 259-268.

[47] Grady, D. L.; Ratliff, R. L.; Robinson, D. L.; McCanlies, E. C.; Meyne, J.; Moyzis, R. K., Highly Conserved Repetitive DNA Sequences are Present at Human Centromeres. *PNAS* 1992, 89, (5), 1695-1699.

[48] Henderson, Eric; Hardin, Charles C.; Walk, Steven K.; Tinoco, Jr Ignacio; Blackburn, Elizabeth H., Telomeric DNA Oligonucleotides Form Novel

Intramolecular Structures Containing Guanine[middle dot]Guanine Base Pairs. *Cell* 1987, 51, (6), 899-908.

[49] Huang, Chih-Hung; Lin, Yi-Shing; Yang, Ya-Ling; Huang, Shu-wen; Chen, Carton W., The Telomeres of Streptomyces Chromosomes Contain Conserved Palindromic Sequences with Potential to Form Complex Secondary Structures. *Molecular Microbiology* 1998, 28, (5), 905-916.

[50] Huertas, D.; Azorin, F., Structural Polymorphism of Homopurine DNA Sequences. $d(GGA)_n$ and $d(GGGA)_n$ Repeats Form Intramolecular Hairpins Stabilized by Different Base-Pairing Interactions. *Biochemistry* 1996, 35, (40), 13125-13135.

[51] Chou, Shan-Ho; Zhu, Leiming; Reid, Brian R., On the Relative Ability of Centromeric GNA Triplets to Form HairpinsversusSelf-paired Duplexes. *Journal of Molecular Biology* 1996, 259, (3), 445-457.

[52] Zhu, Leiming; Chou, Shan-Ho; Reid, Brian R., The Structure of a Novel DNA Duplex Formed by Human Centromere d(TGGAA) Repeats with Possible Implications for Chromosome Attachment during Mitosis. *Journal of Molecular Biology* 1995, 254, (4), 623-637.

[53] Hirao, Ichiro; Nishimura, Yoshifumi; Naraoka, Tetsushi; Watanabe, Kimutsuna; Arata, Yoji; Miura, Kin-ichiro, Extraordinary Stable Structure of Short Single-stranded DNA Fragments Containing a Specific Base Sequence: d(GCGAAAGC). *Nucl. Acids Res.* 1989, 17, (6), 2223-2231.

[54] Hirao, Ichiro; Nishimura, Yoshifumi; Tagawa, Yon-ichi; Watanabe, Kimitsuna; Miura, Kin-ichiro, Extraordinarily Stable Mini-hairpins: Electrophoretical and Thermal Properties of the Various Sequence Variants of d(GCFAAAGC)and their Effect on DNA Sequencing. *Nucl. Acids Res.* 1992, 20, (15), 3891-3896.

[55] Tanikawa, J.; Nishimura, Y.; Hirao, I.; Miura, K., NMR Spectroscopic Study of Single-stranded DNA Fragments of d(CGGCGAAAGCCG) and d(CGGCAAAAGCCG). *Nucleic Acids Symp. Ser.* 1991, 25, 47-48.

[56] Shepard, William; Cruse, William B. T.; Fourme, Roger; de la Fortelle, Eric; Prange, Thierry, A Zipper-Like Duplex in DNA: the Crystal Structure of d(GCGAAAGCT) at 2.1 A Resolution. *Structure* 1998, 6, (7), 849-861.

[57] Chou, Shan-Ho; Chin, Ko-Hsin, Zipper-like Watson-Crick base-pairs. *Journal of Molecular Biology* 2001, 312, (4), 753-768.

[58] Aboul-ela, Fareed; Koh, David; Tinoco, Ignacio, Jr.; Martin, Francis H., Base-Base Mismatches. Thermodynamics of Double Helix Formation for dCA3XA3G + dCT3YT3G (X, Y = A,C,G,T). *Nucl. Acids Res.* 1985, 13, (13), 4811-4824.

[59] Cornelis, A. G.; Haasnoot, Jeroen H. J.; den Hartog, Jan F.; de Rooij, M.; Boom, Jacques H. van; Cornelis, Altona, Local Destabilisation of a DNA Double Helix by a T⁻T Wobble Pair. *Nature* 1979, 281, (5728), 235-236.

[60] Arnold, Frances H.; Wolk, Steven; Cruz, Phillip; Ignacio Tinoco, Jr., Structure, Dynamics, and Thermodynamics of Mismatched DNA Oligonucleotide Duplexes $d(CCCAGGG)_2$ and $d(CCCTGGG)_2$. *Biochemistry* 1987, 26, 4068-4075.

[61] Peyret, N.; Seneviratne, P. A.; Allawi, H. T.; SantaLucia, J., Nearest-Neighbor Thermodynamics and NMR of DNA Sequences with Internal A·A, C·C, G·G, and T·T Mismatches. *Biochemistry* 1999, 38, (12), 3468-3477.

[62] Joy, A.; Ghosh, A. K.; Schuster, G. B., One-Electron Oxidation of DNA Oligomers That Lack Guanine: Reaction and Strand Cleavage at Remote Thymines by Long-Distance Radical Cation Hopping. *J. Am. Chem. Soc.* 2006, 128, (16), 5346-5347.

[63] Schlientz, N. W.; Schuster, G. B., Long-Distance Radical Cation Migration in Duplex DNA: The Effect of Contiguous A•A and T•T Mismatches on Efficiency and Mechanism. *J. Am. Chem. Soc.* 2003, 125, (51), 15732-15733.

[64] Beaucage, S. L.; Caruthers, M. H., Deoxynucleoside Phosphoramidites--A New Class of Key Intermediates for Deoxypolynucleotide Synthesis. *Tetrahedron Letters* 1981, 22, (20), 1859-1862.

[65] Michelson, A. M., Hyperchromicity and Nucleic Acids. *Nature* 1958, 182, 1502-1503.

[66] Baase, Walter A.; Johnson, W. Curtis, Jr., Circular Dichroism and DNA Secondary Structure. *Nucl. Acids Res.* 1979, 6, (2), 797-814.

[67] Bloomfield, Victor A.; Crothers, Donald M.; Ignacio Tinoco, Jr., *Nucleic Acids: Structure, Properties, and Function* University Science Books: Sausalito, CA, 2000; p 800.

[68] Barnett, Robert N.; Cleveland, Charles L.; Joy, Abraham; Landman, Uzi; Schuster, Gary B., Charge Migration in DNA: Ion-Gated Transport. *Science* 2001, 294, (5542), 567-571.

CHAPTER 4

A PROBE INTO THE MECHANISM OF OXIDATIVE DAMAGE

Loss of an electron from a DNA base leads to hopping of a radical cation ("hole") through the DNA bases where it finally reacts irreversibly with H_2O or O_2. Reaction of the radical cation traditionally occurs at the guanines of G_n ($n > 1$) steps because guanines have the lowest oxidation potential of the four natural bases (Table 2.1).[1] Incomplete repair of oxidative damage has been shown to lead to mutations, carcinogenesis, and degenerative diseases.[2-4] Therefore, several studies have focused on understanding the mechanism of oxidative damage, especially elucidating the role of the N1 imino proton of G.[5-16]

Oxidation of Guanine

The G•C Base Pair

The DNA double helix consists of two sugar-phosphate backbones wrapped around a central helical axis with heterocyclic base pairs in the middle of the axis (Figure 1.9). Two base pairs, A•T and G•C, form the complementary duplex, being held together in part by hydrogen bonds (H-bonds). This hyrdrogen bonding affords the recognition of the bases that leads to the complementarity that is essential for DNA replication and genetic proliferation. The two base pairs differ in the number of H-bonds as well as the

orientation of the functional groups involved in the H-bonds. The A•T base pair only has two H-bonds where the G•C base pair has three. This increase in H-bonds increases the stability of DNA with a higher G/C content.

The G•C base pair is characterized by three hydrogen bonds between the C6-O, N1-H, and C2-NH_2 of G paired with the C4-NH_2, N3, and C2-O of C, respectively (Figure 1.5). The average hydrogen bond length from H to the acceptor in solution has been shown to be about 1.86 Å, as determined by NMR studies.[17] Crystal structure data is traditionally shorter by approximately 1 Å. The difference is most likely due to the calculation of distance in the NMR studies being dependent on the H-bond distance being linear. The crystal structure data is able to determine with a fairly high degree of certainty the distance between the N donor and N or O acceptor but not the H to acceptor distance. However, the DNA molecule is constantly in motion and the H-bond distances will continuously fluctuate with motions of the DNA and environment.

The G•C base pair is considerably solvated on both the minor and major grooves sides of the base pair. Exposed N and O atoms of the G•C base pair in the major groove (N7 and C6-O of G, and C4-NH_2 of C) are uniformly solvated in a non-geometrically regular manner. However, the minor groove exposed atoms of G and C (C2-NH_2 of G and C2-O of C) bind to H_2O to a lesser degree of specificity, slightly disrupting the spine of hydration found in the minor groove of B-DNA.[18] However, water molecules as well as cations are known to bind the DNA bases, and the extent of binding may be related to DNA sequence and structure.[19]

Guanine Oxidation

Charge transfer through DNA terminates with the oxidation of guanine within a G_n step (n > 1) and subsequent reaction of the radical cation with H_2O or O_2 (Figure 4.1). The reaction of $G^{\bullet+}$ with H_2O and O_2 has been studied extensively. Solution studies indicate different reaction pathways depending on the structure of the oxidized guanine, where the N1 proton of G plays the critical role.[5, 6, 11, 13] It is proposed that the $G^{\bullet+}$ reacts by hydration followed by one electron oxidation forming 8-oxoguanine (Figure 4.1). However, loss of a proton to yield the neutral radical doesn't react with H_2O, rather it reacts with O_2 through a multistep reaction process to yield oxazolone and imidazole products.

Several studies investigating the role of the N1 proton of G on charge migration and trapping reactions have resulted in conflicting reports. The loss of an electron from G to yield the radical cation significantly reduces the pKa from 9.4 for G to 3.9 for $G^{\bullet+}$.[7] Therefore, it was concluded that at pH 7.0, the N1-H of $G^{\bullet+}$ spontaneously transfers to N3 of the base paired C.[15] Gervasio[8, 9] supports these findings with first-principles molecular dynamics simulations, indicating proton transfer is favored for oxidized G. These calculations are supported by experiments with D_2O that reveal a kinetic isotope effect associated with charge transfer and oxidation of G.[14, 16] In contrast, density functional theory (DFT) calculations indicate the proton transfer product ($G^{\bullet}$-H/C^{+}+H) is unfavorable compared to the $G^{\bullet+}$/C base pair.[12] This is consistent with recent experimental evidence by Schuster[10] that reveals inhibition of proton transfer by base pairing G with 5-fluorocytidine (F_5C) has no significant affect on charge transfer

efficiency. Therefore the proton transfer from G to C is not coupled with charge migration. However, under the same conditions it was shown that proton transfer from G to C plays an important role in the reaction of the $G^{\bullet+}$ with H_2O or O_2, as revealed by a decrease in damage at GG steps opposite F_5C.

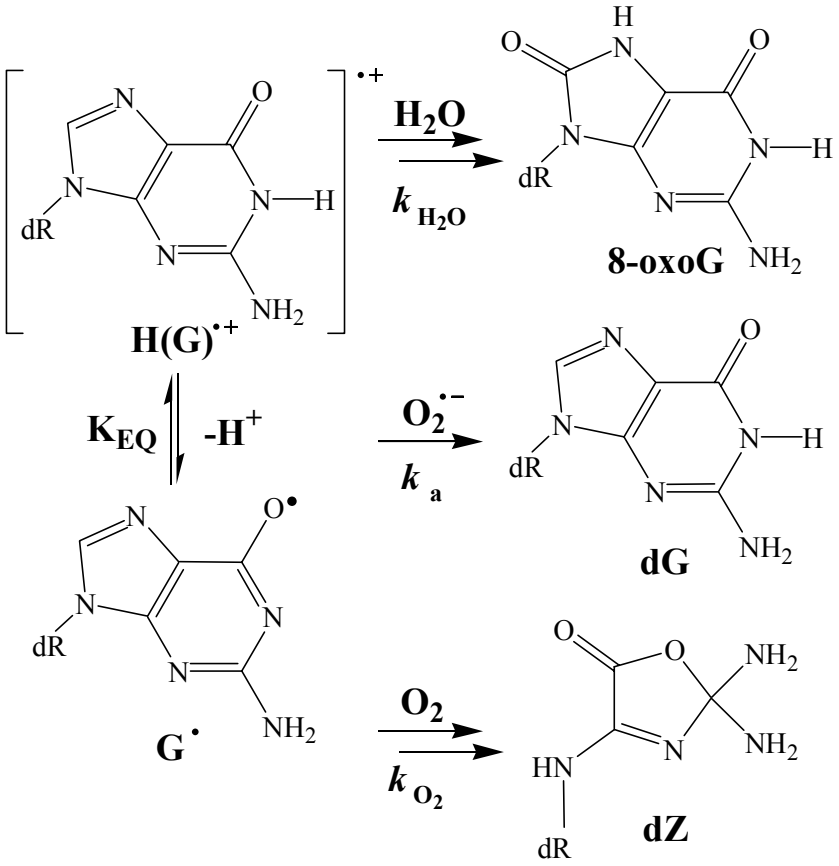

Figure 4.1. Reaction of Guanine Radical Cation with H_2O, O_2, and O_2^-.

Modified Cytidine: 3-Deazacytidine

The pyrimidine analogues, 3-deazapyrimidine, have been shown to have significant biological, biochemical and medicinal applications.[20, 21] Recently the cytidine analogue 3-deazacytidine (c_3C) was synthesized and incorporated into DNA for studies on effects of DNA replication.[22] Elimination of the central hydrogen bond of the G•C base pair was used to study the importance of hydrogen bonding on DNA polymerase activity. Studies using shape mimics have implied that hydrogen bonding is unnecessary for polymerase activity, only accurate size is required.[23] DNA polymerase activity in the presence of 3-deazacytidine is consistent with those reports, and polymerase activity was uninhibited with the incorporation of G opposite the c_3C just as found in the natural DNA. Interestingly, the structural analogue was found to have a drastic effect on the stability of the DNA, reducing its Tm by 17 ºC with the incorporation of just one c_3C.

Structural Effects

Incorporation of the DNA base analogue, 3-deazacytidine (c_3C), eliminates the central hydrogen bond present in the G•C base pair (Figure 4.2). Removal of the hydrogen bond would be expected to destabilize the DNA duplex, just as A•T base pairs are not as stable as G•C base pairs. In addition, the structural analogue introduces steric hindrance with the introduction of the C3-H of C when base paired with G. This additional destabilization is realized by the significant decrease (-17 ºC) of the Tm of a 15mer DNA duplex with only one c_3C analogue.

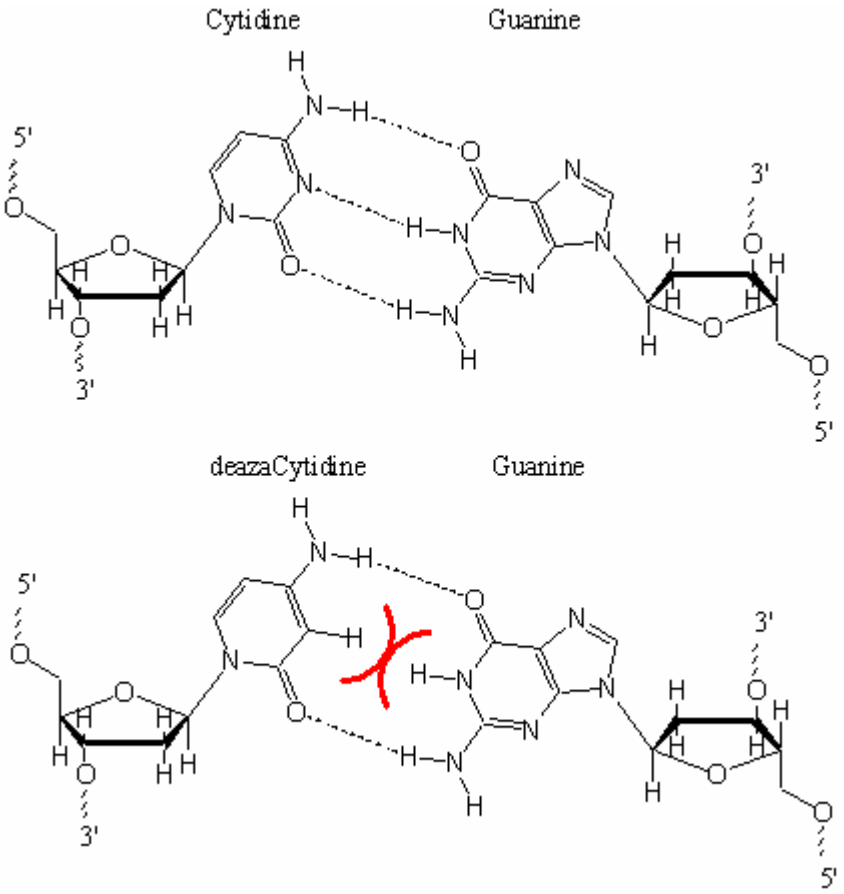

Figure 4.2. Hydrogen Bonding of G•C and G•3-Deazacytidine (c_3C) Base Pairs.

Elimination of the central hydrogen bond of the G•C base pair in duplex DNA, followed by charge migration experiments would examine further the role the N1 proton of G plays in the charge migration and trapping efficiency. Incorporation of the cytidine analogue (**3**) into DNA (Figure 4.3), as well as the 2'-methoxycytidine control, would afford DNA duplexes adequate for charge migration analysis.

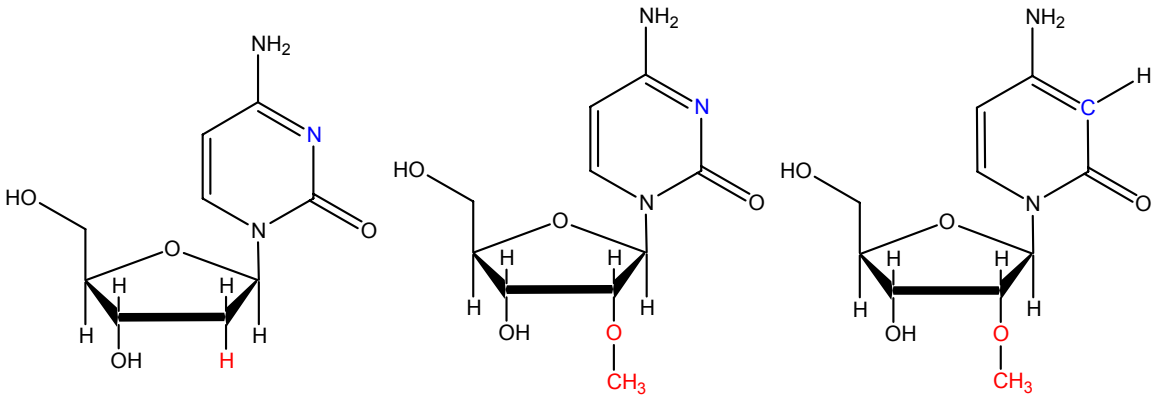

Cytidine (**1**) 2'-Methoxycytidine (**2**) 3-Deaza-2'-methoxycytidine (**3**)

Figure 4.3. Structure of Cytidine, 2'-Methoxycytidine, and 3-Deaza-2'-methoxycytidine.

As mentioned, the introduction of the 3-deazacytidine analogue distorts the secondary structure of B-DNA as a result of the steric interactions between the N1-H of G and C3-H of c_3C. Molecular modeling studies on the DNA duplex d(AACCAARRAACCAA)/d(TTGGTTGGTTGGTT), where R is cytidine (**1**), 2'-methoxycytidine (**2**), or 3-deaza-2'-methoxycytidine (**3**), reveal no effect on secondary structure with the incorporation of a 2'-methoxy group (Figure 4.4). However, the introduction of the 3-deazacytidine analogue bends the G•c_3C base pair out of plane and

stretches the remaining two hydrogen bonds. The average hydrogen bond distance of the Watson-Crick G•C base pairs in the HyperChem model are 1.83 Å from H to proton acceptor. Base pairing of c_3C with G increases this hydrogen bond distance to an average of 1.90 Å. The distortion has a minor effect on the base pairs directly flanking the G•c_3C base pairs, bending the A•T base pairs slightly out of plane as well. The bases two base pairs from the G•c_3C do not appear to be significantly affected by the structural distortion. These structural distortions, as well as the loss of the central hydrogen bond will have to be considered in analyzing the properties of charge migration through DNA containing the c_3C base analogue.

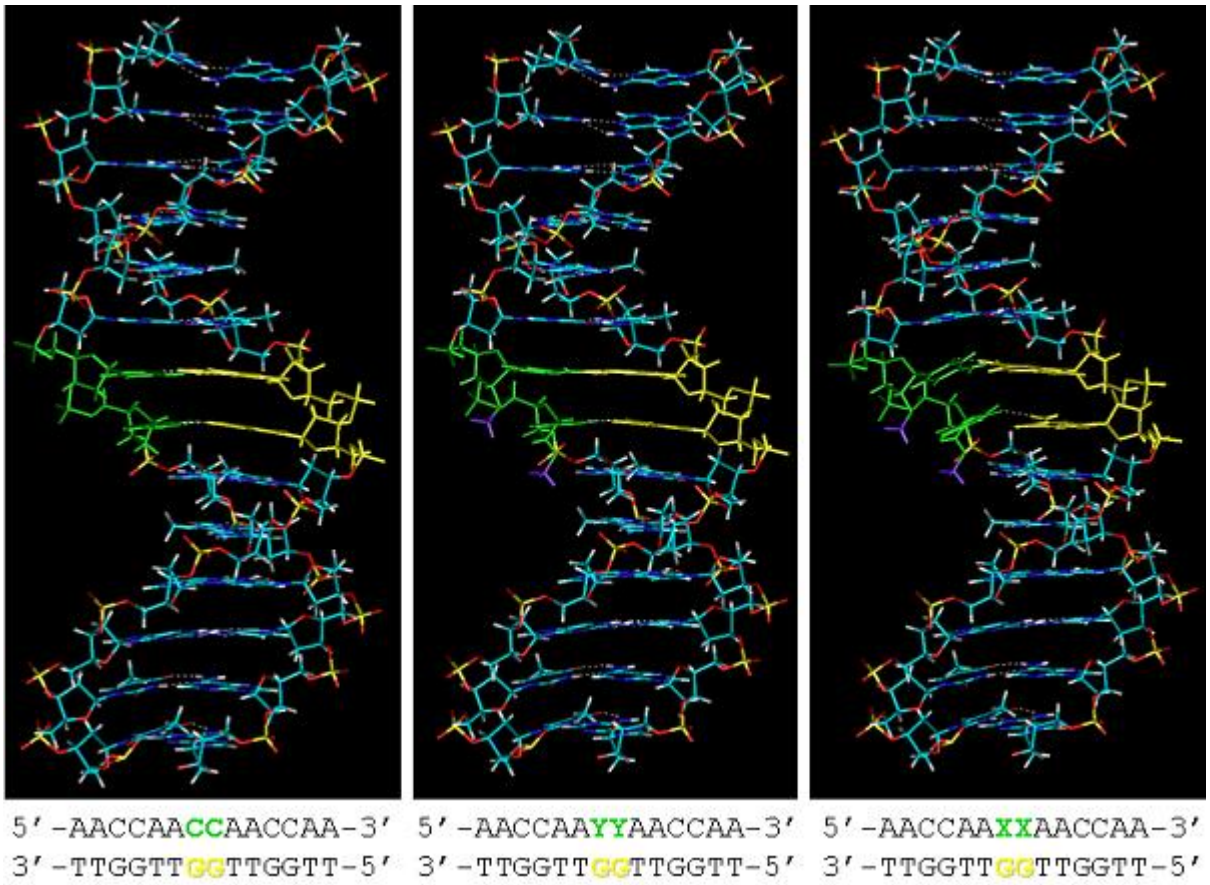

Figure 4.4. HyperChem Model of Duplex DNA Containing the Modification 3-Deaza-2'-methoxy-cytidine. Y = 2'-methoxy-cytidine and X = 3-deaza-2'-methoxy-cytidine nucleotide analogues (c3C).

3-Deazacytidine Oxidation Potential

Introduction of 3-deazacytidine within duplex DNA has been shown to cause minor local structural distortion to the B-DNA structure at the site of base modification. However, the effect of changing base pairing from G•C to G•c_3C on the reactivity of guanine is unknown. In completely complementary Watson-Crick base pairing, guanine has the lowest oxidation potential of the four natural bases.[1] During charge migration through DNA, the G bases act as charge carriers and react irreversibly with H_2O or O_2. Incorporation of a base analogue with a lower oxidation potential than G could potentially change the reactivity of the DNA, altering the ability to efficiently monitor charge migration and reaction. Cyclic voltammetry is used to determine the oxidation potential of the 3-deazacytidine nucleoside analogue **10** (Figure 4.5). The oxidation potential of the nucleoside analogue was shown to be 1.41 V vs. NHE after corrections for the reference electrode. This reveals that the 3-deazacytidine analogue has a lower oxidation potential than cytidine, however, it is still higher than guanine. Therefore, the radical cation migration through DNA will reside mostly on G in the presence of 3-deazacytidine, and reaction with H_2O or O_2 is expected to predominantly occur at the $G^{\bullet+}$ as opposed to the 3-deazacytidine.

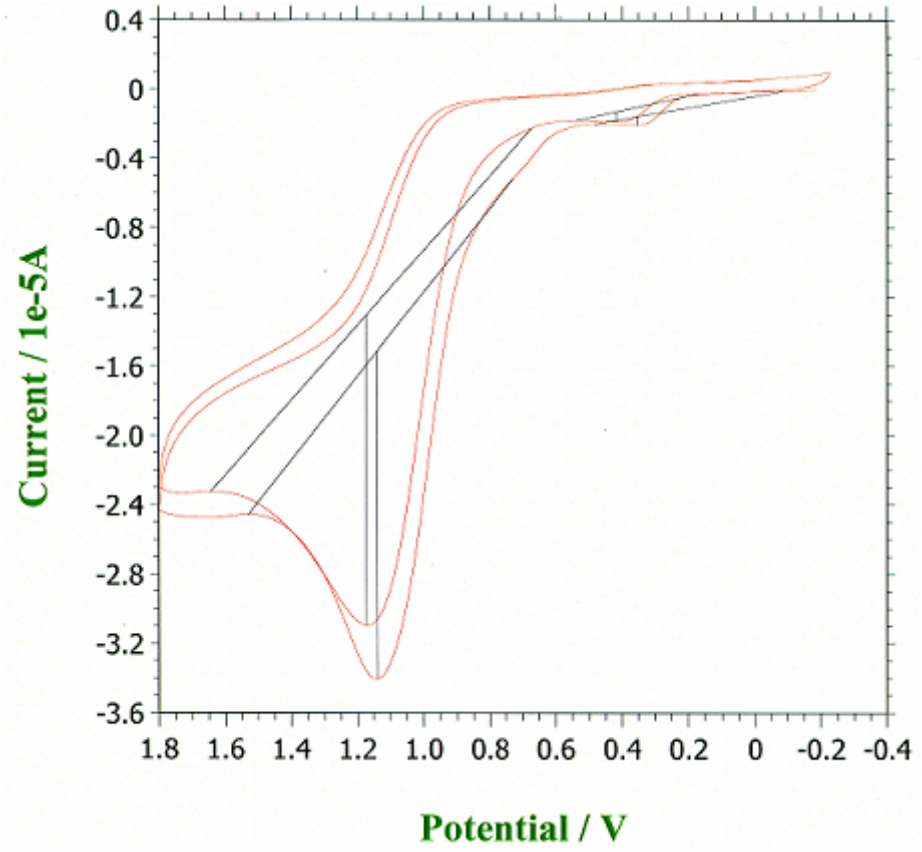

Figure 4.5. Oxidation Potential of 3',5'-di-O-p-toluyl-3-deaza-cytidine (**10**) as Measured by Cyclic Voltammetry (CV).

Base Analogue: 3-Deaza-2'-deoxy-4-N-diphenylacetyl-cytidine

Synthesis and Purification

The synthesis of the 3-deazacytidine moiety was first reported by Currie and coworkers in 1970.[24] The synthetic route was a many stepped process with considerably low yields. An improved synthetic route was later reported by Cook, Day, and Robins[25], although this strategy involves the use of the explosive alkyne starting material 1-methoxy-1-butene-3-yne, which is no longer available in the United States. It wasn't until 1999 that a synthetic strategy was reported that produced sufficient yields (Figures 4.5 and 4.6), and involved the use of safe and readily available starting materials.[22] Initial synthesis of the base analogue, 4-amino-2-pyridone (**8**), involved a four step synthetic strategy that resulted in a 60% overall yield. This base analogue was silylated then coupled to the chloro-sugar moiety (**9**). Subsequent protection and deprotection steps yielded the 3-deazacytidine analogue (**15**), which was incorporated into a ssDNA oligomer.

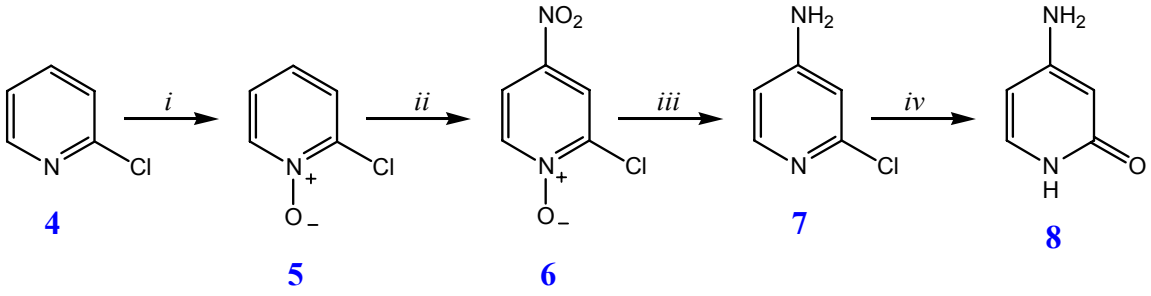

Figure 4.6. Synthetic Route for 4-Amino-2-pyridone (**8**). (*i*) H_2O_2, (*ii*) HNO_3/H_2SO_4, (*iii*) Zn/CH_3COOH, (*iv*) $NaOH/CH_3OH$.

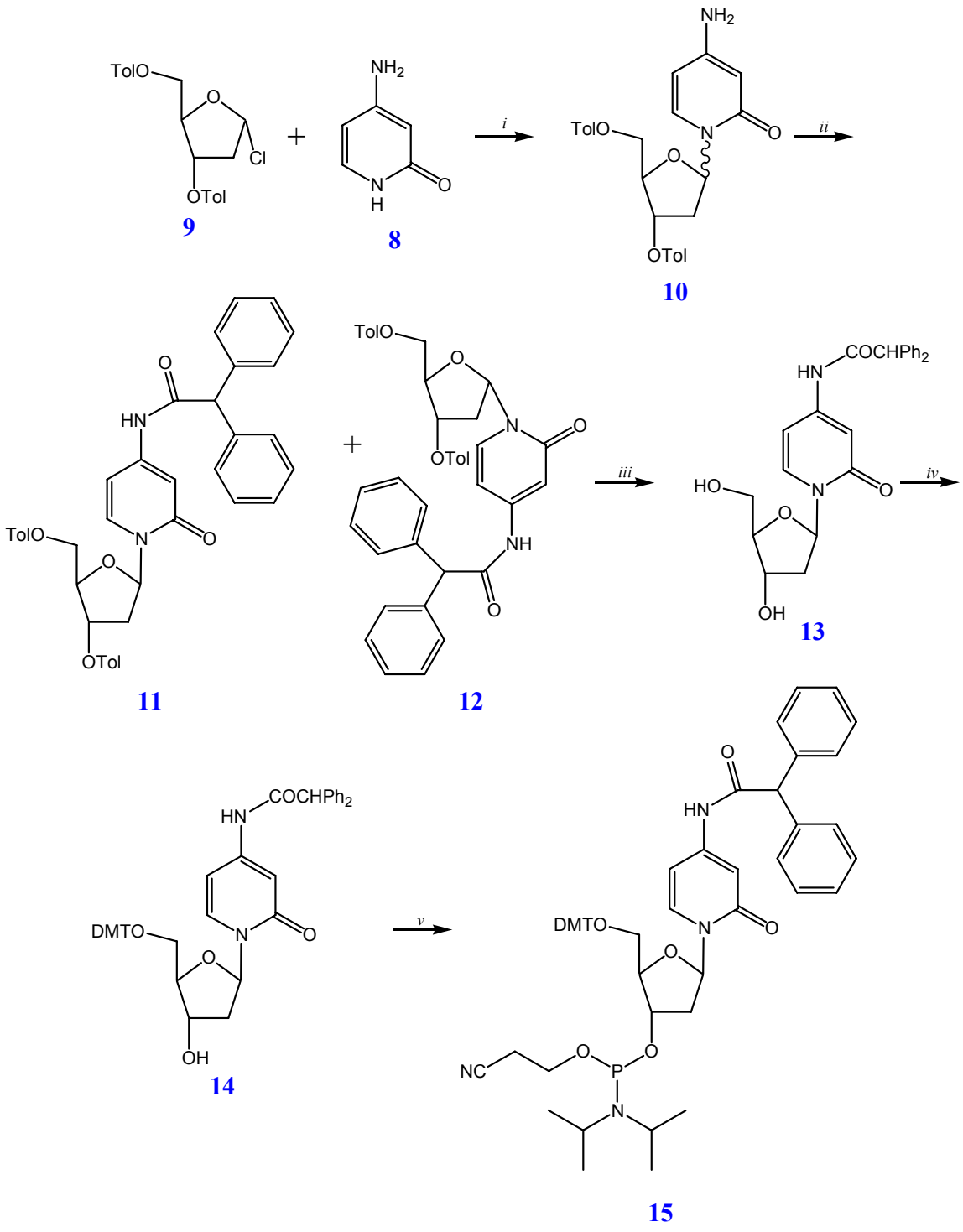

Figure 4.7. Synthetic Route for 3-Deazacytidine Analogue **15**. (*i*) BSA, $SnCl_4$, (*ii*) $Ph_2CHCOCl$/pyridine, (*iii*) $NaOCH_3/CH_3OH$, (*iv*) DMT-Cl/pyridine, (*v*) $CNCH_2CH_2OP(Cl)N(iPr)_2$/DIEA.

Incorporation into DNA

The 3-deazacytidine analogue (**15**) was added to the ABI DNA synthesizer, and incorporated into a ssDNA oligomer. Treatment of the ssDNA oligomer with 1 M ammonium hydroxide at 60 ºC for 18 hr has been reported to cleave the oligomer from the solid support, as well as remove the base protecting groups[22]. Purification of the ssDNA oligomer by HPLC, and mass spectrometry analysis on the purity of the ssDNA oligomer indicated inadequate deprotection of the diphenylacetyl protecting group on the 3-deazacytidine. Attempts to deprotect in 1 M ammonium hydroxide for up to seven days, as well as the use of the stronger base, methylamine, resulted in no observable cleavage of the protecting group. Therefore it was concluded that the diphenylacetyl protecting could not be removed in our laboratory, and an alternate 3-deazacytidine analogue would be required.

Base Analogue: 4-N-Acetyl-3-deaza-2'-methoxy-cytidine

Synthesis and Purification

The acetyl protecting group is the most commonly used amine-protecting group for standard phosphoramidite DNA synthesis. Therefore, a proposed synthetic route using the acetyl protecting group, as opposed to the diphenylacetyl group, was employed (Figure 4.7). This strategy employs known chemistry for other DNA base analogues, however, to the best of our knowledge it has never been used for the synthesis of a 3-deazacytidine analogue.

This route relies on the ability to synthesize the pyrimidine nucleoside lacking the N3. This pyrimidine moiety was accomplished through the nitration and reduction of the pyridine molecule (**4**). The 4-amino-2-pyridone (**8**) molecule is synthesized the same as above (Figure 4.5). Oxidation of 2-chloropyridine (**4**) through reaction with hydrogen peroxide and trifluoroacetic acid resulted in 2-chloropyridine-N-oxide (**5**), followed by nitration by reaction with nitric acid and sulfuric acid to yield 2-chloro-4-nitropyridine-N-oxide (**6**). Reduction of the nitro group to 4-amino-2-chloropyridine (**7**) was accomplished through reaction with iron powder and hydrogen chloride. Hydrolysis of the chloro substituent under high pressure and temperature with methyl alcohol and sodium hydroxide gave 4-amino-2-pyridone (**8**).

The sugar moiety was commercially, and coupling with the heterocyclic nucleoside was accomplished by first silylating the nucleoside. Reaction of 4-amino-2-pyridone (**8**) with N,O-bis-trimethylsilylacetamide afforded 2-O-trimethylsilyl-4-(N,N-bis(trimethylsilyl))-pyridine. Addition of trimethylsilyltriflate to the benzoyl-protected sugar (**16**) followed by the addition of the silyl-protected pyridine moiety afforded the benzoyl-protected 3-deazacytidine analogue (**17**). This step yields the β-anomer only, which requires no further separation steps to remove undesired α–anomer. Deprotection by reaction with methanolic ammonia (**18**), followed by acetylation gave compound (**19**). Selective deacetylation through reaction with sodium methoxide afforded near quantitative yields of compound **20**. Controlled silylation of the 3' and 5' OH groups through ring formation with 1,3-dichloro-(1,1,3,3-tetraisopropyl)-disilazane (**21**) allowed for the methylation of the 2'-OH with methyl iodide (**22**). Desilylation (**23**) followed by

5’-OH protection with 4,4’-dimethoxytrityl chloride (**24**) and 3’-OH protection with phosphoramidite afforded compound **25**. Compound **25** was purified through precipitation and verified through proton NMR. This compound was immediately dissolved in anhydrous acetonitrile for incorporation into the DNA synthesizer.

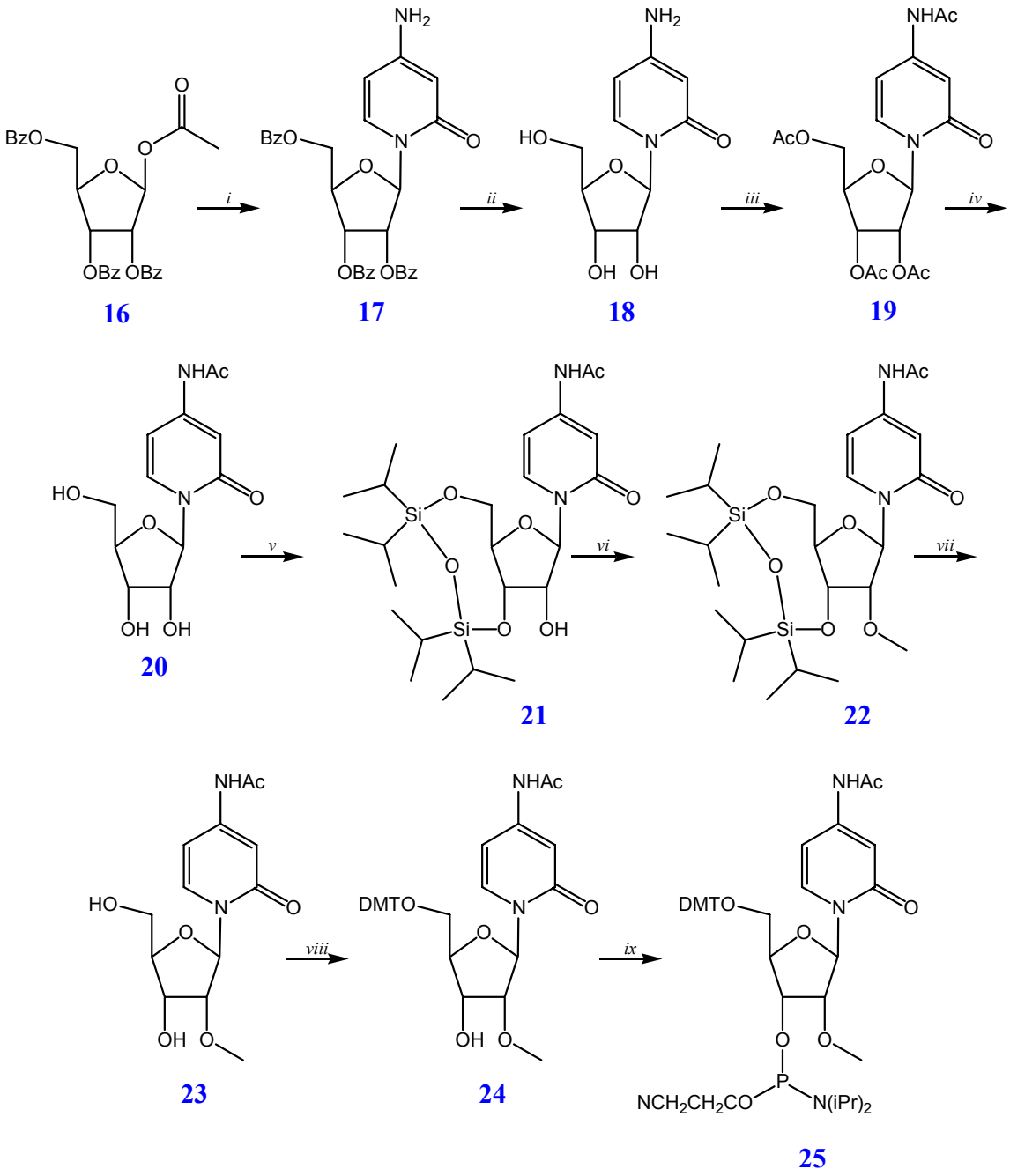

Figure 4.8. Synthetic Route for 3-Deazacytidine Analogue **25**. (*i*) TMOTf, **8**/BSA, (*ii*) $NaOCH_3/CH_3OH$, (*iii*) CH_3COCl/DMAP, (*iv*) $NaOCH_3/CH_3OH$, (*v*) $TIPDSCl_2$, (*vi*) CH_3I/Ag_2O, (*vii*) TBAF, (*viii*) DMT-Cl/pyridine, (*ix*) $CNCH_2CH_2OP(Cl)N(iPr)_2$.

Design of Oligomers

Charge migration through DNA has been extensively studied, and patterns of oxidative damage at GG steps have been determined. It has been observed experimentally that oxidation at the 5'-G of most GG steps is preferentially oxidized by radical cation transfer through DNA. The mechanism of reaction at $G^{\bullet+}$ with H_2O or O_2 has been investigated. Several reports indicate that charge migration as well as reaction at G is coupled to proton transfer from $G^{\bullet+}$ to C. However, recent evidence by Schuster[10] indicates the proton predominantly resides on the G during charge migration, but is donated to C during reaction. Incorporation of a F^5dC base opposite the GG_2 step (exactly as we have done for 3-deazacytidine in these experiments), and other GG steps, lowers the pKa of the analogue compared to cytidine. The weaker base makes proton transfer from G less favorable. This modification was shown to have no affect on the rate of charge migration, i.e. hopping, although it decreased the rate of trapping at the GG paired with the modified C.

Our studies have been designed to further assist in elucidating the mechanism of reaction at the $G^{\bullet+}$ by eliminating the possibility of proton transfer from N1-H of G to N3 of C. We have chosen to use the same sequence as previously reported by Schuster[10] (Table 4.1), as the charge transfer studies on these DNA sequences have been well characterized. The repeating $(TTGG)_n$ sequence has been shown to have a distance-dependent charge transfer efficiency, with observable oxidative reaction at the GG_6 step approximately 85 Å from the site of injection. Modification of the C bases opposite GG_2

allows for the determination of charge migration efficiency through the G•c_3C base pair, as well as the effect on trapping at GG_2.

Table 4.1. DNA Sequences 1-3. **2** is 2'-methoxycytidine and **3** is 2'-methoxy-3-deazacytidine.

5'- AQ A A T T G G T T G G T T G G T T G G T T G G T T G G A T A T -3'
3'- T T A A C C A A X X_2 A A C C A A C C A A C C A A C C T A T A -5'
DNA(1): X X_2 = CC	DNA(2): X X_2 = **2 2**	DNA(3): X X_2 = **3 3**

Incorporation into DNA

The deazacytidine base analogue **25** was added to the DNA synthesizer and the DNA sequences shown in Table 4.1 were synthesized. Deprotection of the DNA oligomers containing the base analogues required methyl amine at 60 ºC for 24 hr to fully deprotect the modified base. The oligomers were purified by HPLC, and the deprotection efficiency was monitored by mass spectrometry (Table 4.2). Accurate mass determinations verified the complete detprotection of the DNA oligomers, and further experiments on these ssDNA strands could be conducted.

Table 4.2. Electrospray Ionization Mass Spectrometry Results for Oligonucleotides Comprising DNA Duplexes 1-3. Y = 2'-methoxy-cytidine and X = 3-deaza-2'-methoxy-cytidine nucleotide analogues (c_3C).

Mass Spec Results		
Sample ID	**Calc'd Mass**	**Found Mass**
AQ(TTGG)	9757	9758
(AACC)	9011	9010
$(AAYY)_2$	9070	9069
$(AAXX)_2$	9068	9067

Experimental

Materials and Methods

All synthetic DNA oligonucleotides were synthesized in our laboratory by Dr. Sriram Kanvah on an Applied Biosystems Inc. Expedite DNA Synthesizer. All DNA nucleotides and reagents for synthesis were purchased from Glen Research with standard phosphoramidite chemistry functional groups. These synthetic DNA oligonucleotides were purified by HPLC on a Hitachi 7000 HPLC system equipped with a Varian Dynamax 25x21.4 mm reverse-phase C-18 column using 5-20% Acetonitrile in 0.5 M Triethylammonium Acetate. UV/Vis studies on DNA oligonucleotides were conducted at 260 nm on a Hewlett-Packard Spectrophotometer, and the extinction coefficients were calculated using nearest-neighbor values (AQ replaced with A for calculation purposes). The mass of each oligonucleotide was determined by Matrix-Assisted Laser Desorption Ionization Time-of-Flight (MALDI-TOF) or Electrospray Ionization (ESI) mass

spectrometry techniques. Radioactively labeled isotope (α-^{32}P) Adenosine triphosphate (ATP) was purchased from GE Healthcare, formerly Amersham Biosciences. The enzyme terminal dinucleotide transferase (TdT) and its buffer were purchased from GE Healthcare, i.e. Amersham Biosciences, and stored at -20 °C. UV melting and cooling curves were performed an a Cary 1E Spectrophotometer equipped with a multi-cell block, temperature controller and sample transport accessory. Circular Dichroism (CD) measurements were conducted on a JASCO-720 instrument equipped with a temperature controller. Autoradiography was performed on a FUJI 2340 BAS-Image system. Kodak film was purchased from Aldrich. The buffer used for all experiments was 10 mM sodium phosphate (NaPi) and 2 mM $MgCl_2$ at pH 7.0. Cyclic Voltammetry (CV) experiments were performed on a CH Instruments model 660 Electrochemical Workstation with a platinum electrode, $Ag/AgCl_2$ reference electrode, and 0.1 M tetrabutylammonium tetrafluoroborate electrolyte solution.

Synthesis of 3-Deaza-2'-methoxy-cytidine

4-Amino-1-(2',3',5'-tri-O-benzoyl-β-D-*erythro*-pentofuranosyl)-2-pyridone (17). To 1.0 g (9.08 mmol) of 4-amino-2-pyridone (**8**), coevaporated three times from anhydrous pyridine, was added 25 ml anhydrous acetonitrile. Compound **8** was allowed to dissolve completely, then 3.051 g (3.72 ml, 15.0 mmol, ~1.6 eq) N,O-Bis(trimethylsilyl)acetamide was added. The reaction was allowed to stir under nitrogen gas at room temperature for 18 hours. The solvents were removed *in vacuo* then the product/s were dissolved in 20 ml anhydrous dichloroethane. 2.2226 g (1.93 ml, 10.0

mmol) TMSOTf was added to the reaction mixture and allowed to stir under nitrogen gas at room temperature for 1 hour. A mixture of 4.010 g (7.95 mmol) β-D-Ribofuranose 1-acetate 2,3,5-tribenzoate (**16**) and 2.2226 g (1.93 ml, 10.0 mmol) TMSOTf in 20 ml anhydrous dichloroethane were added to the previous reaction mixture and stirred at 60 ˚C for 4 hours under nitrogen gas. The solvents were removed *in vacuo* and using silica gel column chromatography (0-5% CH_3OH in CH_2Cl_2) 2.5 g product **17** was recovered (50% yield).

Rf (methanol/dichloromethane, 1/19): 0.3.

^{1}H NMR ($CDCl_3$): δ = 4.611-4.708 (m, 2H, H5'), 4.809 (dd, 1H, H4', J = 2.4, 11.5), 5.545 (d, 1H, H3, J = 2.4), 5.607 (dd, 1H, H5, J = 2.4, 7.6), 5.782 (dd, 1H, H2', J = 4.6, 5.9), 5.889 (t, 1H, H3', J = 5.7), 6.502 (d, 1H, H1', J = 4.5), 7.227-7.567 (m, 10H, H6 and m,p-Ar-H), 7.891 (d, 2H, o-Ar-H, J = 7.3), 7.934 (d, 2H, o-Ar-H, J = 7.3), 8.065 (d, 2H, o-Ar-H, J = 7.2) ppm.

MS: calcd for $C_{28}H_{26}N_20_8$ ($M+H^+$), 554.6, found 555.3.

4-Amino-1-(β-D-*erythro*-pentofuranosyl)-2-pyridone (18). To 1.5 g (2.7 mmol) compound **17** was added 50 ml Ammonia 7 N in absolute methanol and allowed to stir at room temperature for 24 hours. TLC indicated near to complete reaction with the disappearance of starting material. The solvents were removed *in vacuo*. The resulting product **18** was extracted into the aqueous phase from CH_2Cl_2/H_2O mixture. The resulting solution was concentrated to yield 0.6 g (2.5 mmol, 90% yield) product **18**. No further purification of this compound was required.

Rf (methanol/dichloromethane, 1/19): 0.05.

^{1}H NMR (D_2O): δ = 3.645-3.807 (m, 2H, H5'), 3.974-4.017 (m, 1H, H4'), 4.090 (dd, 1H, H3', J = 5.5, 5.6), 4.174 (dd, 1H, H2', J = 4.5, 5.6), 5.520 (d, 1H, H3, J = 2.5), 5.946 (d, 1H, H1', J = 4.5), 5.993 (dd, 1H, H5, J = 2.5, 7.7), 7.455 (d, 1H, H6, J = 7.7) ppm.

MS: calcd for $C_{10}H_{14}N_20_5$ ($M+H^+$), 242.2, found 242.9.

4-Acetylamino-1-(2',3',5'-tri-O-acetyl-β-D-*erythro*-pentofuranosyl)-2-pyridone (19). To 1.1 g (4.54 mmol) compound **18**, coevaporated from anhydrous pyridine three times, was added 50 ml anhydrous pyridine. Next, a catalytic amount of DMAP was added to the solution, followed by 0.18 g (0.16 ml, 23 mmol, 5 eq.) acetyl chloride. The reaction mixture was allowed to stir at room temperature for 24 hours under nitrogen gas. TLC indicated the reaction had gone to completion with the absence of starting material. The solvents were removed *in vacuo* and the product extracted from CH_2Cl_2/H_2O into the organic phase. The product was concentrated then purified by silica gel column chromatography (0-5% CH_3OH in CH_2Cl_2). The product **19** was concentrated and recovered at 74% yield (1.37 g, 3.3 mmol).

^{1}HNMR ($CDCl_3$): δ = 2.066 (s, 6H, 2'-Ac-CH_3 and 3'-Ac-CH_3), 2.119 (s, 3H, 5'-Ac-CH_3), 2.138 (s, 3H, N-Ac-CH_3), 4.314-4.403 (m, 3H, H4' and H5'), 5.296 (dd, 1H, H3', J = 5.6, 5.8), 5.398 (dd, 1H, H2', J = 4.0, 5.6), 6.218 (d, 1H, H1', J = 3.9), 6.641 (d, 1H, H3, J = 2.2), 6.874 (dd, 1H, H5, J = 2.2, 7.8), 7.479 (d, 1H, H6, J = 7.8), 9.385 (s, 1H, N-H) ppm.

MS: calcd for $C_{18}H_{22}N_20_9$ ($M+H^+$), 410.4, found 411.1.

4-Acetylamino-1-(β-D-*erythro*-pentofuranosyl)-2-pyridone (20). A 0.07 M solution of sodium methoxide was created by dissolving 0.08 g Na in 50 ml anhydrous CH_3OH. To .25 g (0.61 mmol) compound **19** was added 2 ml anhydrous CH_3OH followed by the addition of 10 ml of the sodium methoxide solution. After 5 minutes at room temperature TLC indicated complete reaction of the starting material to product, therefore the reaction was quenched with H_2O. Removal of the solvents *in vacuo* and extraction of the product into the aqueous phase of CH_2Cl_2/H_2O followed by concentration of the product resulted in quantitative yields of slightly wet product **20** (0.019 g, 0.67 mmol).

Rf (methanol/dichloromethane, 1/19): 0.05.

^{1}H NMR (DMSO-d_6): δ = 2.055 (s, 3H, CH_3), 3.532-3.722 (m, 2H, H5'), 3.833-3.870 (m, 1H, H4'), 3.918-3.959 (m, 2H, H2' and H3'), 5.094-5.130 (m, 2H, 2'-OH and 3'-OH), 5.399-5.417 (m, 1H, 5'-OH), 5.959 (d, 1H, H1', J = 3.4), 6.328 (dd, 1H, H5, J = 2.3, 7.6), 6.766 (d, 1H, H3, J = 2.3), 7.855 (d, 1H, H6, J = 7.6), 10.137 (s, 1H, NH) ppm.

MS: calcd for $C_{12}H_{16}N_20_6$ ($M+H^+$), 284.3, found 285.0.

4-Acetylamino-1-(3',5'-(1,1,3,3-tetraisopropyl)-disilazane-β-D-*erythro*-pentofuranosyl)-2-pyridone (21). Compound **20** (0.60 g, 2.11 mmol) was coevaporated three times from anhydrous pyridine then brought up in 50 ml anhydrous pyridine. To this solution was added 0.67 g (2.12 mmol, 0.67 ml, 1 eq.) TIPDS-Cl_2. The reaction was allowed to stir under nitrogen gas at room temperature for 3 hours at which point the TLC indicated sufficient conversion of starting material to product. To the solution was added 10 ml CH_3OH and the solvent was removed *in vacuo*. The product **21** was extracted into

the organic phase of CH_2Cl_2/H_2O then concentrated. Purification by silica gel column chromatography (0-100% ethyl acetate in hexane) led to a recovery of 0.490 g (0.93 mmol, 44% yield).

Rf (ethyl acetate 100%): 0.5.

^{1}H NMR ($CDCl_3$): δ = 0.901-1.075 (m, 28H, iPr-H), 2.186 (s, 3H, N-Ac-CH_3) 3.962-4.272 (m, 5H, H2', H3', H4', and H5'), 5.970 (s, 1H, H1'), 6.593 (d, 1H, H3, J = 2.0), 7.141 (dd, 1H, H5, J = 2.0, 7.8), 7.814 (d, 1H, H6, J = 7.8), 9.794 (s, 1H, NH) ppm.

MS: calcd for $C_{24}H_{42}N_20_7Si_2$ ($M+H^+$), 526.8, found 527.3.

4-Acetylamino-1-(3',5'-(1,1,3,3-tetraisopropyl)-disilazane-2'-methoxy-β-D-*erythro*-pentofuranosyl)-2-pyridone (22). 0.490 g (0.93 mmol) compound **21** was coevaporated from anhydrous toluene three times then dissolved in 10 ml anhydrous toluene. To the solution was added 0.65 g (2.8 mmol, 3 eq.) silver (I) oxide followed by 2.64 g (18.60 mmol, 1.2 ml, 20 eq.) methyl iodide. The reaction was monitored by TLC, and too long of reaction allows for the formation of undesired side products. Therefore, even though the TLC indicated incomplete reaction of the starting material, the solvents were removed *in vacuo* and the mixture purified by silica gel column chromatography (0-100% ethyl acetate in hexane then 0-5% methanol in ethyl acetate). The product **22** was recovered and concentrated to give 0.110 g (0.20 mmol, 22% yield).

Rf (methanol/dichloromethane, 1/19): 0.5.

^{1}H NMR ($CDCl_3$): δ = 0.953-1.091 (m, 28H, iPr-H), 2.168 (s, 3H, N-Ac-CH_3) 3.673 (s, 3H, O-CH_3), 3.944-4.289 (m, 5H, H2', H3', H4' and H5'), 5.975 (s, 1H, H1'), 6.614 (d,

1H, H3, J = 2.2), 6.821 (dd, 1H, H5, J = 2.2, 7.8), 7.904 (d, 1H, H6, J = 7.8), 9.101 (s, 1H, NH) ppm.

MS: calcd for $C_{25}H_{44}N_20_7Si_2$ ($M+H^+$), 540.8, found 541.2.

4-Acetylamino-1-(2'-methoxy-β-D-*erythro*-pentofuranosyl)-2-pyridone (23). To .110 g (0.209 mmol) compound **22** dissolved in 10 ml THF was added 0.131 g (0.5 mmol, 0.15 ml) TBAF. The reaction was allowed to stir at room temperature under nitrogen gas while monitoring the progress by TLC. After 4 hours the TLC indicated the reaction had gone to completion by the depletion of starting material. The solvents were removed *in vacuo* and product purified by silica gel column chromatography (5-25% CH_3OH in CH_2Cl_2). Concentration of the product gave 56 mg (0.19 mmol, 90% yield) compound **23**.

Rf (methanol/dichloromethane, 1/19): 0.05.

^1H NMR (CD_3OD-d_4): δ = 2.129 (s, 3H, N-CH_3), 3.588 (s, 3H, O-CH_3), 3.730-4.218 (m, 5H, H2', H3', H4' and H5'), 6.126 (d, 1H, H1', J = 2.1), 6.580 (dd, 1H, H5, J = 2.3, 7.7), 6.953 (d, 1H, H3, J = 2.3), 8.128 (d, 1H, H6, J = 7.7) ppm.

HRMS: calcd for $C_{13}H_{18}N_20_6$ ($M+H^+$), 298.11649, found 298.11905.

4-Acetylamino-1-(5'-O-(4,4'-dimethoxytrityl)-2'-methoxy-β-D-*erythro*-pentofuranosyl)-2-pyridone (24). To 0.10 g (0.335 mmol) compound **23** coevaporated three times from anhydrous pyridine was added 5 ml anhydrous pyridine. To this solution was added 0.0576 g (0.170 mmol, 0.5 eq.) DMT-Cl and a catalytic amount of DMAP. The reaction was stirred at room temperature under nitrogen gas and monitored

by TLC. After 4 hours the reaction was not complete and 0.25 eq. DMT-Cl was added. Again after 12 hours the reaction was still not yet complete so another 0.25 eq. DMT-Cl was added. After a total reaction time of 36 hours the reaction appeared to have gone to completion and 10 ml CH_3OH was added. TLC of the product (**24**) showed a characteristic orange spot that charred when dipped in 10% H_2SO_4:H_2O solution and heat dried. The solvents were removed *in vacuo* and the product purified by silica gel column chromatography (1-10% CH_3OH in CH_2Cl_2). Concentration of the desired product gave 0.120 g (0.20 mmol, 60% yield) compound **24**.

Rf (methanol/dichloromethane, 1/19): 0.3.

^{1}H NMR ($CDCl_3$): δ = 2.164 (s, 3H, N-CH_3), 2.565-2.648 (m, 1H, H2'), 3.469-3.619 (m, 2H, H5'), 3.717 (s, 3H, C2'-OCH_3), 3.804 (s, 6H, 4,4'-DMT-OCH_3), 4.002-4.029 (m, 1H, H4'), 4.391-4.432 (m, 1H, H3'), 6.195 (s, 1H, H1'), 6.377 (d, 1H, H5, J = 7.5), 6.617 (s, 1H, H3), 6.854 (d, 4H, 3,3,3',3'-DMT-Ar-H, J = 8.6), 7.242-7.640 (m, 9H, Ar-H), 8.090 (d, 1H, H6, J = 7.6) ppm.

4-Acetylamino-1-(5'-O-(4,4'-dimethoxytrityl)-3'-cyanoethyl-N,N-diisopropylphosporamidite-2'-methoxy-β-D-*erythro*-pentofuranosyl)-2-pyridone (25). To 0.120 g (0.20 mmol) of compound **24** dissolved in 2 ml anhydrous CH_2Cl_2 was added 1.03 g (8.0 mmol, 1.32 ml, 4 eq.) N,N-diisopropylethylamine. The mixture was allowed to dissolve completely, followed by the addition of 0.096 g (0.40 mmol, 0.089 ml, 2 eq.) phosphoramidite. The reaction was stirred at room temperature under nitrogen gas and monitored by TLC. After 1 hour 5 ml CH_3OH was added to quench the reaction, followed by 50 ml CH_2Cl_2. The compound was extracted from 5% $NaHCO_3$/H_2O then

dried over $MgSO_4$. The solvents were removed *in vacuo* and then the product was dissolved in 2 ml CH_2Cl_2. The addition of 40 ml hexane caused the product **25** to crash out of solution. The precipitate was filtered and no further purification was required. Yield of **25** was 150 mg (0.19 mmol, 94% yield).

Rf (methanol/dichloromethane, 1/19): 0.5.

Thermal Denaturation

The thermal denaturation properties of DNA duplexes 1-3 were characterized by UV absorption at 260 nm. Plotting the first derivative of the absorbance vs. temperature curve gives the melting temperature of the DNA duplex. The DNA samples are placed in a UV transparent quartz cell with a 1 cm path length and placed inside the Cary 1E Spectrophotometer. Several temperature ramps from 15 to 90 ºC were taken to verify the reversibility of the thermal transitions.

The melting temperatures were first determined with 5 μM DNA and 10 mM NaPi at pH 7.0(Figure 4.8). However, the melting temperature of DNA (3) was right at about 45 ºC with a broad melting transition overlapping 35 ºC which is too low to study charge migration because the irradiation chamber is approximately 35 ºC. Therefore, the melting temperature was determined with 5 μM DNA, 10 mM NaPi and 2 mM $MgCl_2$ at pH 7.0 (Figure 4.9). The addition of divalent metal ions has been shown to increase the melting temperature of dsDNA.[26] This is shown in the increase of the melting temperature of all duplexes by more than 15 ºC. Thus, all experiments conducted are with 5 μM DNA, 10 mM NaPi and 2 mM $MgCl_2$.

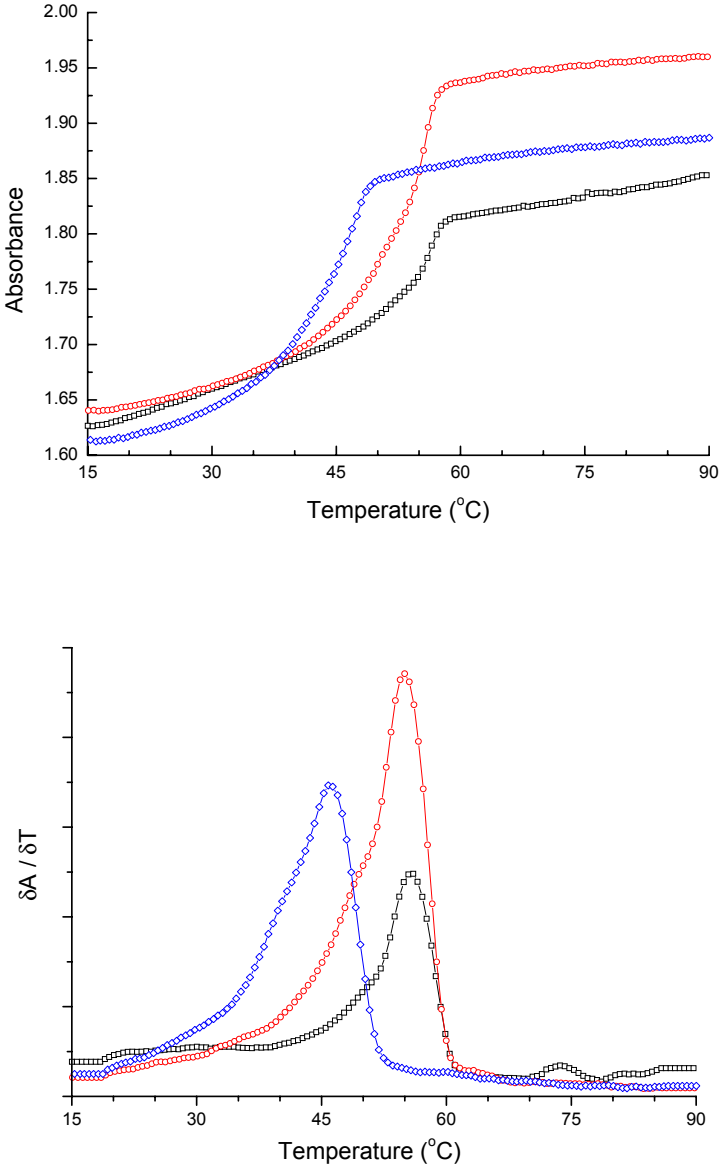

Figure 4.9. Thermal Denaturation Curves of DNA 1-3 with 5 μM DNA and 10 mM NaPi. Top view: Thermal denaturation curve. Bottom view: First derivative of the thermal denaturation curve. Black line is DNA 1, red line is DNA 2, and blue line is DNA 3.

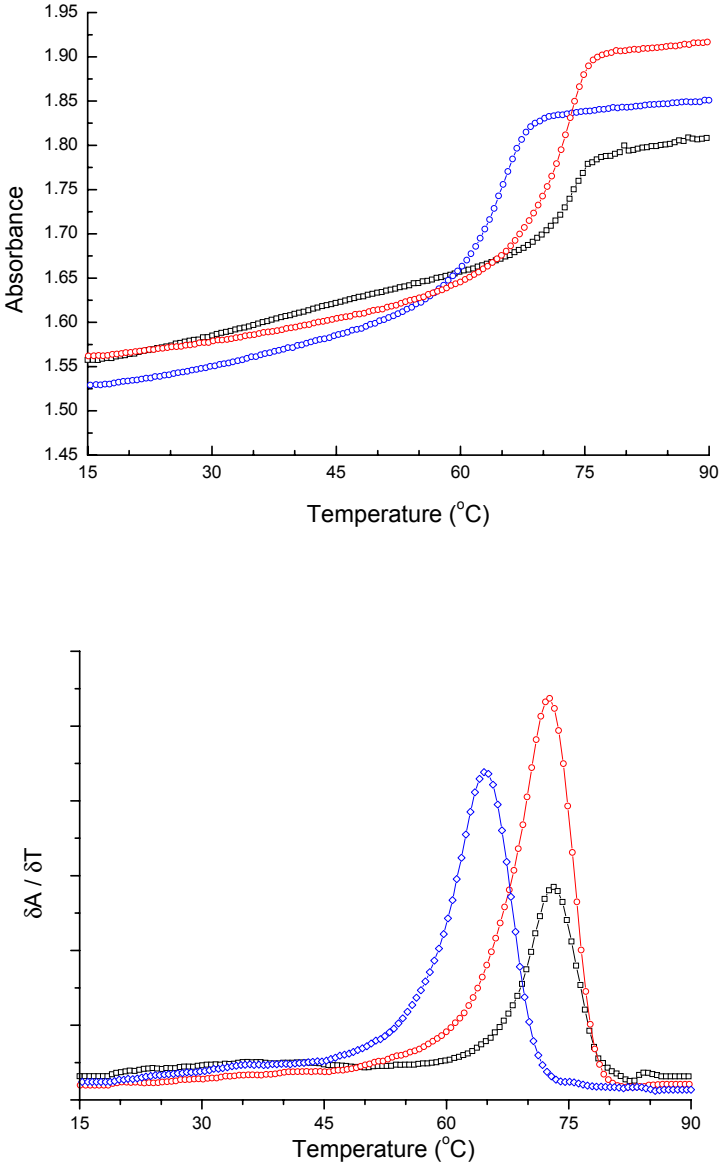

Figure 4.10. Thermal Denaturation Curves of DNA 1-3 with 5 μM DNA, 10 mM NaPi and 2 mM $MgCl_2$. Top view: Thermal denaturation curve. Bottom view: First derivative of the thermal denaturation curve. Black line is DNA 1, red line is DNA 2, and blue line is DNA 3.

Circular Dichroism

The secondary structure of DNA (1-3) was determined with 2 mM $MgCl_2$ at room temperature. The exact samples used for the thermal denaturation experiments discussed above were used for the CD experiements. The DNA duplexes examined are fully complementary Watson-Crick base pair sequences, with the exception of DNA (3) that has two modifications opposite GG_1. The DNA oligomers are 30 bases in length, not including the AQ, therefore two modifications are not expected to affect the overall secondary conformation of the DNA duplexes. Similarly, introduction of a methoxy functional group at the 2'-position of the sugar, which would more closely resemble RNA, for only two bases within the oligomer is expected to have a negligible affect on the overall observed CD. This is indeed the case for DNA (1-3), where under our experimental conditions each DNA molecule resembles B-DNA with no significant structural distortions (Figure 4.10).

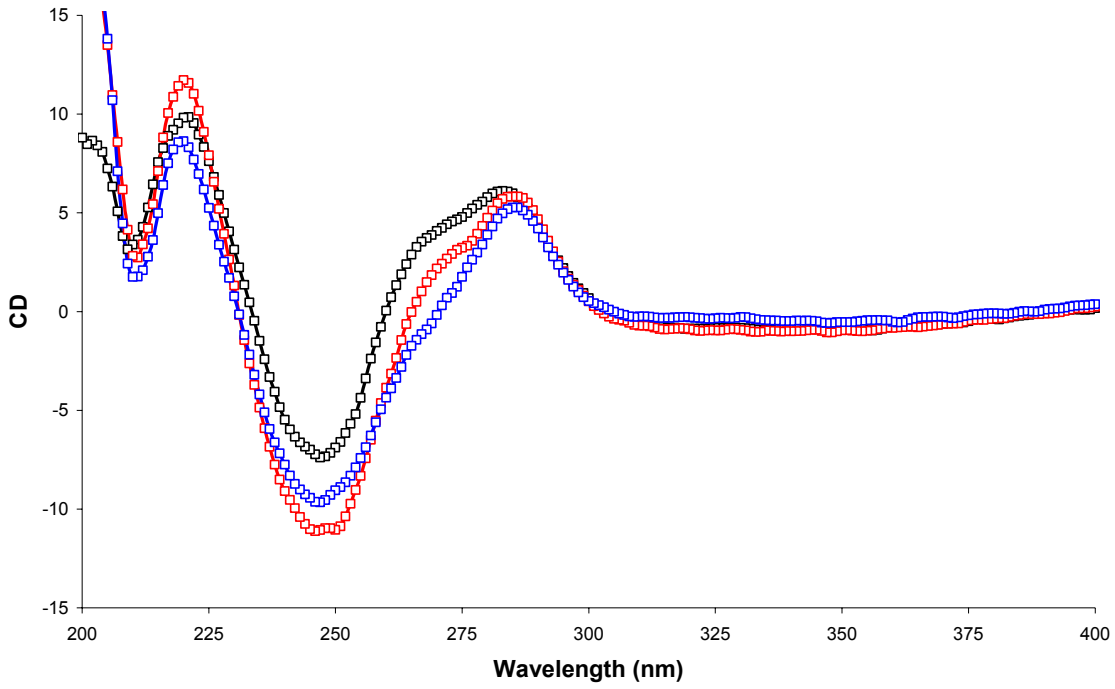

Figure 4.11. Circular Dichroism of DNA 1-3. Black line is DNA 1, red line is DNA 2, and blue line is DNA 3.

Labeling, Irradiation and PAGE Analysis

Approximately 25 μM of the ssDNA oligomer (17 μl) containing the GG steps (AQ linked oligomer for DNA 1-3) was incubated at 37 °C with 1μl terminal dinucleotide transferase (TdT) buffer, 1 μl α-^{32}P-ATP, and 1 μl TdT enzyme for 45 min. After incubation, 10 μl of a tetrabromophenolsulfonphthalein (bromophenol blue) glycerol solution was added to the DNA mixture. This DNA mixture was loaded onto a 19:1 acrylamide/bisacrylamide gel and electrophoresis separated the enzyme and unreacted ATP from the newly radiolabeled DNA, as well as verifying one final purification step by separating DNA fragments from the full length oligomer. This DNA was eluted from the acrylamide/bisacrylamide gel overnight, followed by precipitation in 100% ethyl alcohol at -78 °C for 1h. The supernatant was removed and the resulting purified and radiolabeled ssDNA was washed 2x with 80% ethyl alcohol then dried *in vacuo*.

The purified and ^{32}P-radiolabeled DNA oligomer was suspending in nanopure H_2O to get 10,000 cpm per μl. A 20 μl solution per experiment of 5 μM of each ssDNA oligomer (AQ and non-AQ containing strands without ^{32}P-radiolabel), 10 mM NaPi, 2 mM $MgCl_2$ and 2 μl 32P-radiolabeled oligomer were annealed by heating to 90 ºC for 5 min followed by slow cooling to room temperature. The samples were then irradiated at 350 nm for 0 or 10 min (amount of time was previously determined to result in single-hit oxidative conditions[10]) followed by ethanol precipitation. The DNA samples were then treated with piperidine at 90 ºC for 30 min to cleave the DNA at sites of oxidative

damage. The piperidine was removed *in vacuo* followed by two washes with H_2O and removal of the H_2O *in vacuo*.

The piperidine-treated DNA samples were then brought up in the bromophenol solution to 1000 cpm per µl. The DNA solution was heated to 90 ºC for 5 min followed by immediate transfer to 0 ºC. The DNA samples, 3 µl at 1000 cpm/µl, were loaded per lane on a polyacrylamide gel and electrophoresis separated the DNA fragments based on a charge to size ratio. The polyacrylamide gels were then dried *in vacuo* between blotting paper and cellophane, and subsequently exposed to Kodak film for 18 hr. The film was then developed to give the image in Figure 4.11.

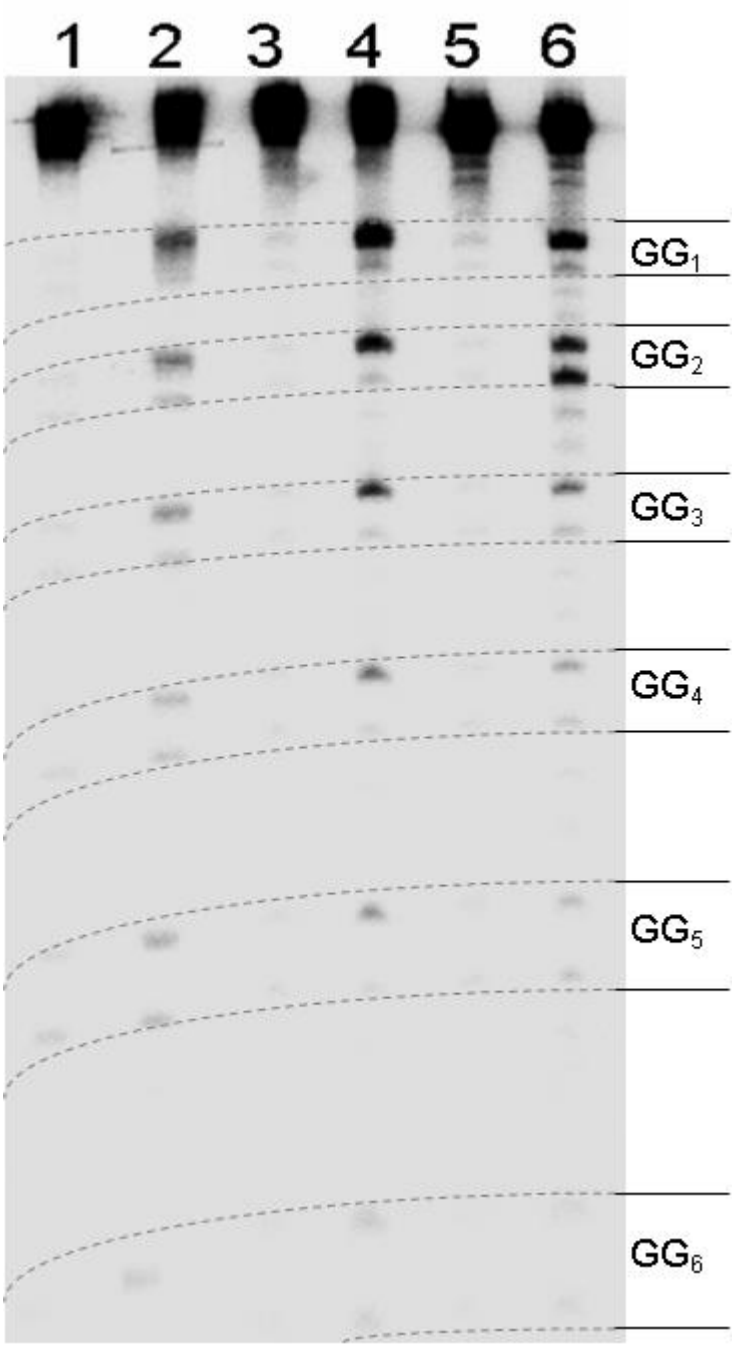

Figure 4.12. Autoradiogram Showing Strand Cleavage of DNA Samples 1-3 Following Irradiation and Piperidine Treatment. Lanes 1, 3, and 5 are dark controls and lanes 2, 4, and 6 are 10 minutes irradiation for DNA 1, 2, and 3 respectively.

Quantitative Analysis through Phosphorimagery

Quantification of the amount of DNA damage at each GG step, which is relative to the efficiency of charge transfer through DNA, is accomplished by reading the gel image in a FUJI phosphorimager. The gel is exposed to a FUJI imaging plate, and read in the FUJI 2340 BAS-Image system. ImageGuage software is then used to determine the relative intensity of radiolabel at each GG step, revealed as dark spots in the Kodak image. This relative intensity is directly related to the amount of DNA oligomer at the position on the gel, and sequencing allows for the exact determination of the site of oxidative damage on the oligomer.

Results

Structural Conformation and Thermal Integrity

The affect of eliminating the central hydrogen bond between G and C (N1-H of G H-bond to N3 of C) on charge transfer as well as oxidative damage to G has been studied. Incorporation of the cytidine analogue, 3-deaza-2'-methoxycytidine (**3**), base paired to each G of the GG_2 step slightly reduced the Tm of the modified duplex when compared to the unmodified DNA. The introduction of a C-H bond in place of an N introduces steric strain on the base pair, but it doesn't appear to have any noticeable affect on the neighboring base pairs (Figure 4.4). However, there appeared to be no structural affect on the B-DNA conformation of the dsDNA, as seen in the CD experiments (Table 4.3).

Table 4.3. Tm and CD Experimental Results.

	Tm (°C)	B-form
DNA (1)	73	YES
DNA (2)	73	YES
DNA (3)	65	YES

The thermal stability of dsDNA has been linked to the G/C content of the DNA, with the higher G/C content the higher the Tm. This has been studied in depth, and the larger number of H-bonds in G•C compared to A•T is responsible for the increased stability of dsDNA with a higher G/C content.[27, 28] More importantly, the steric effects of **3** base paired with G influence the melting temperature by destabilizing the DNA.

The affects of incorporating a cytidine analogue, 3-deazacytidine, on charge migration efficiency and oxidative damage at base-analogue paired guanines was studied. Irradiation of the end-capped AQ at 350 nm efficiently injects a radical cation into the duplex DNA. The radical cation has been shown to migrate through duplex DNA where it then typically oxidizes the 5'-G of GG steps, with migration efficiency depending on DNA length. Cleavage of the oxidation sites by treatment with piperidine yields strand breaks that are then separated by PAGE, followed by autoradiography for quantitative analysis.

It was revealed that the charge migration efficiency was unperturbed by the introduction of 3-deazacytidine, as seen by plotting $\ln(GG_n/GG_{total})$ vs distance, where

GG_n is the amount of damage at GG_n, GG_{total} is the sum of the damage at all GG steps , and the distance between the 5'-G of each GG step is 13.6 Å assuming 3.4 Å per base stack (Figure 4.12). Fitting the plot with a best fit line indicates the efficiency of charge migration through DNA 1-3 is equivalent, with a decrease based upon distance. If the charge migration was faster than trapping at the GG steps, the slope of the best fit line would be approximately 0, indicating all GG steps reacted to the same extent. In contrast, if the charge migration is slower than the trapping reaction, the slope of the line will be more negative, indicating more reaction at the GG steps closest to the AQ. The latter is the trend shown here for DNA (1-3), where the decrease in charge migration with distance is consistent with earlier reports of DNA with the same sequence.[10]

Interestingly, the oxidation reaction with H_2O or O_2 at GG_2 was considerably affected by the change from C to 3-deazacytidine, as seen in Figure 4.11. The total amount of damage at GG_2 appears to be unaffected; however, the distribution of damage at this site is changed. The distribution of oxidative damage on the 5' and 3' G's at GG_2 of DNA (1) and DNA (2) is approximately 10:1 in favor of reaction at the 5'-G. However, for DNA (3) the ratio of oxidative damage at the 5'-G vs 3'-G is approximately 1:1. This distribution of damage is a direct result of the 3-deazacytidine, and is not caused by the methoxy group at the 2'-position of the sugar.

Recent evidence suggests that inhibition of proton transfer from N1-H of G to N3 of C diminishes the amount of reactivity at the G.[10] Therefore, the structural distortions caused by deazacytidine are believed to be the influencing factor on reactivity. It has also

been reported that the bases to the 3'-side of the G greatly affect the rate of reaction of the $G^{\bullet+}$. It has been proposed that this 3' influence could result either from structural rearrangement to accommodate the H_2O molecule involved in reaction, or through changes in cation distribution.[29] From these experiments we are unable to determine the extent of structural distortion, nor the effect this distortion has on solvent molecules as well as neighboring bases. However, it can be reasoned that changes in the local structure of the DNA will alter the cation distribution around the distorted base pairs.

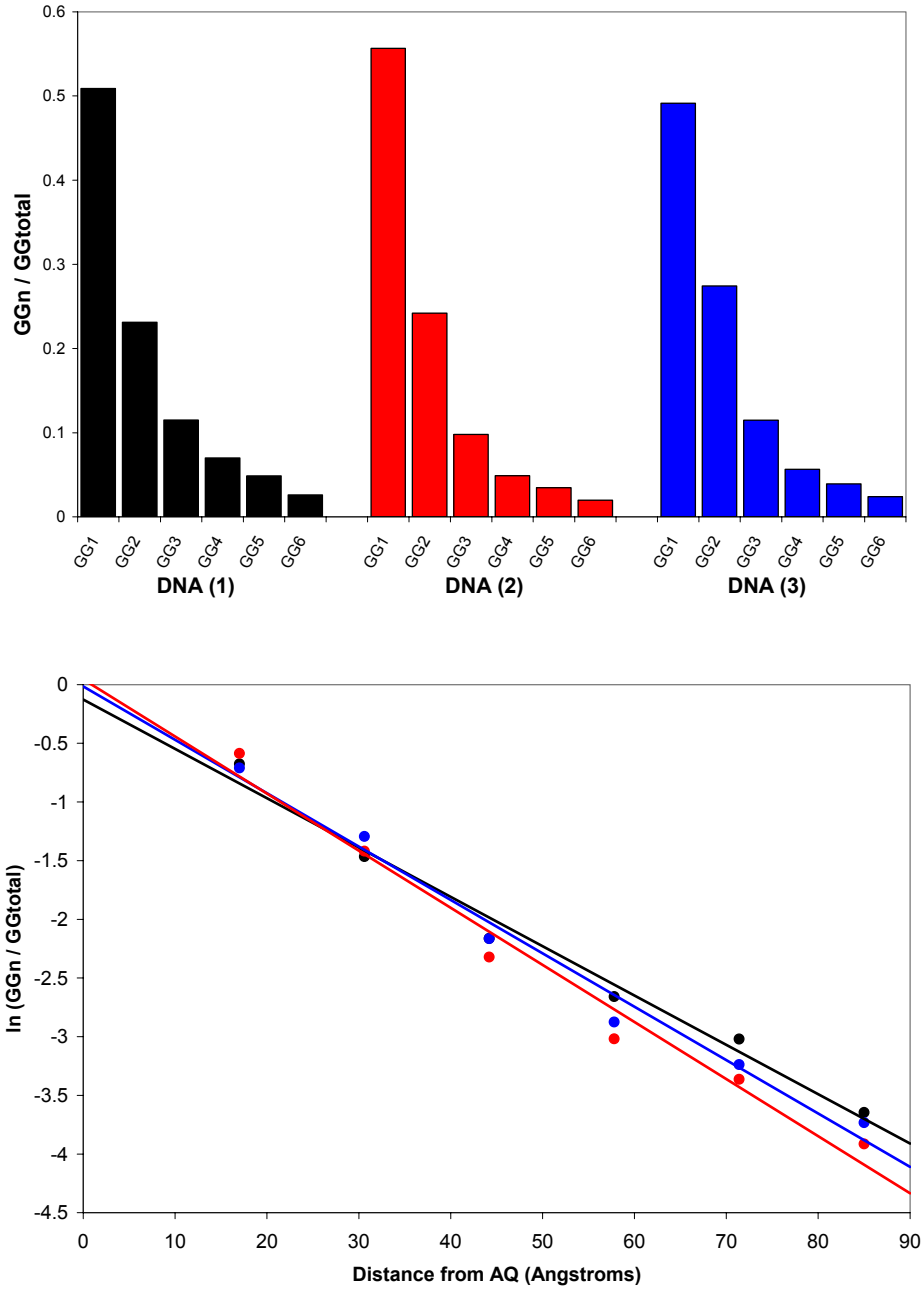

Figure 4.13. Fuji Phosphorimagery Results for DNA 1-3. Top view: ratio of damage at GG_n / GG_{total}. Bottom view: ln (GG_n / GG_{total}) at each GG step.

Conclusions

Oxidative damage at guanine in DNA as a result of charge migration leads to strand scission after piperidine treatment. It has been suggested that the N1-H of G plays a critical role in the mechanism of oxidative damage at guanine. Recent studies suggest the role of the proton transfer from G to C is critical in oxidative damage at G, but has no affect on the rate of hopping through the DNA[10]. The incorporation of a cytidine base analogue, 3-deazacytidine **25**, and its affects on charge migration as well as oxidative damage at the opposite GG step has been examined.

Incorporation of a deazacytidine is expected to destabilize the DNA through structural distortion caused by steric interactions between the N1-H of G and C3-H of deazacytidine. Thermal denaturation studies have shown that the addition of two consecutive deazacytidine analogues reduces the melting temperature of the duplex DNA by up to 10 ºC depending on the salt concentration. However, the decrease in structure stability isn't revealed in the circular dichroism experiments where the dsDNA appears to adopt a B-DNA conformation. This can be somewhat misleading as CD is an average of the entire molecules secondary structure, and modifications at only two consecutive bases out of a total of 60 bases for the two DNA oligomers may not cause enough of a structural distortion to affect the overall secondary structure of the dsDNA.

In addition to decreasing the melting temperature of the dsDNA, the deazacytidine molecule dramatically changes the pattern of oxidative damage at the GG step opposite **25**. Base pairing of G to c_3C altered the ratio of 5' to 3' damage at the GG_2

step from 13:1 for the complementary DNA to 1:1 for the G:c_3C paired DNA. However, the amount of damage at the GG steps before and after the G:c_3C base pairs is the same as the complementary DNA. This indicates the rate of hopping was unaffected by the introduction of a deazacytidine analogue.

The extent of structural distortion caused by the deazacytidine analogue is unclear from these experiments. However, the decrease in Tm as well as the change in oxidative damage is clear indicator that an alteration in structure is present, and this distortion has no affect on either the rate of hopping or the rate of trapping. It does however affect the distribution of damage across the 5'and 3' G of the GG_2 step by allowing each G to react equivalently. This study indicates that slight structural distortions in DNA secondary structure can have a dramatic affect on the oxidative damage properties of GG steps. Interestingly, minor fluctuations in DNA secondary structure as a result of 3-deazacytidine base pairing with G have no significant affects on the charge migration efficiency and trapping at each GG step.

REFERENCES

[1] Steenken, S.; Jovanovic, S. V., How Easily Oxidizable Is DNA? One-Electron Reduction Potentials of Adenosine and Guanosine Radicals in Aqueous Solution. *J. Am. Chem. Soc.* 1997, 119, (3), 617-618.

[2] Demple, B.; Harrison, L., Repair of Oxidative Damage to DNA - Enzymology and Biology. *Annual Review of Biochemistry* 1994, 63, 915-948.

[3] Kanvah, S.; Schuster, G. B., One-Electron Oxidation of DNA: The Effect of Replacement of Cytosine with 5-Methylcytosine on Long-Distance Radical Cation Transport and Reaction. *J. Am. Chem. Soc.* 2004, 126, (23), 7341-7344.

[4] Poulsen, H. E.; Prieme, H.; Loft, S., Role of Oxidative DNA Damage in Cancer Initiation and Promotion. *European Journal of Cancer Prevention* 1998, 7, (1), 9-16.

[5] Burrows, C. J.; Muller, J. G., Oxidative Nucleobase Modifications Leading to Strand Scission. *Chem. Rev.* 1998, 98, (3), 1109-1152.

[6] Cadet, Jean; Douki, Thierry; Gasparutto, Didier; Ravanat, Jean-Luc, Oxidative Damage to DNA: Formation, Measurement and Biochemical Features. *Mutation Research/Fundamental and Molecular Mechanisms of Mutagenesis* 2003, 531, (1-2), 5-23.

[7] Candeias, L. P.; Steenken, S., Structure and Acid-Base Properties of One-Electron-Oxidized Deoxyguanosine, Guanosine, and 1-Methylguanosine. *J. Am. Chem. Soc.* 1989, 111, 1094-1099.

[8] Gervasio, Francesco Luigi; Laio, Alessandro; Iannuzzi, Marcella; Parrinello, Michele, Influence of DNA Structure on the Reactivity of the Guanine Radical Cation. *Chemistry - A European Journal* 2004, 10, (19), 4846-4852.

[9] Gervasio, Francesco Luigi; Laio, Alessandro; Parrinello, Michele; Boero, Mauro, Charge Localization in DNA Fibers. *Physical Review Letters* 2005, 94, (15), 158103-4.

[10] Ghosh, Avik K.; Schuster, Gary B., Role of the Guanine N1 Imino Proton in the Migration and Reaction of Radical Cations in DNA Oligomers. *J. Am. Chem. Soc.* 2006, 128, (13), 4172-4173.

[11] Kasai, Hiroshi; Yamaizumi, Ziro; Berger, Maurice; Cadet, Jean, Photosensitized Formation of 7,8-Dihydro-8-oxo-2'-deoxyguanosine (8-hydroxy-2'-

deoxyguanosine) in DNA by Riboflavin: a Nonsinglet Oxygen-mediated Reaction. *J. Am. Chem. Soc.* 1992, 114, (24), 9692-9694.

[12] Li, X.; Cai, Z.; Sevilla, M. D., Investigation of Proton Transfer within DNA Base Pair Anion and Cation Radicals by Density Functional Theory (DFT). *J. Phys. Chem. B* 2001, 105, (41), 10115-10123.

[13] Misiaszek, Richard; Crean, Conor; Joffe, Avrum; Geacintov, Nicholas E.; Shafirovich, Vladimir, Oxidative DNA Damage Associated with Combination of Guanine and Superoxide Radicals and Repair Mechanisms via Radical Trapping. *J. Biol. Chem.* 2004, 279, (31), 32106-32115.

[14] Shafirovich, V.; Dourandin, A.; Geacintov, N. E., Proton-Coupled Electron-Transfer Reactions at a Distance in DNA Duplexes: Kinetic Deuterium Isotope Effect. *J. Phys. Chem. B* 2001, 105, (35), 8431-8435.

[15] Steenken, S., Electron Transfer in DNA? Competition by Ultra-fast Proton Transfer? *Biological Chemistry* 1997, 378, (11), 1293-1297.

[16] Weatherly, S. C.; Yang, I. V.; Armistead, P. A.; Thorp, H. H., Proton-Coupled Electron Transfer in Guanine Oxidation: Effects of Isotope, Solvent, and Chemical Modification. *J. Phys. Chem. B* 2003, 107, (1), 372-378.

[17] Wu, Zhengrong; Ono, Akira; Kainosho, Masatsune; Bax, Ad, H···N Hydrogen Bond Lengths in Double Stranded DNA from Internucleotide Dipolar Couplings. *Journal of Biomolecular NMR* 2001, 19, (4), 361-365.

[18] Drew, Horace R.; Dickerson, Richard E., Structure of a B-DNA Dodecamer , : III. Geometry of Hydration. *Journal of Molecular Biology* 1981, 151, (3), 535-556.

[19] Shui, X.; McFail-Isom, L.; Hu, G. G.; Williams, L. D., The B-DNA Dodecamer at High Resolution Reveals a Spine of Water on Sodium. *Biochemistry* 1998, 37, (23), 8341-8355.

[20] Bloch, A.; Dutschman, G.; Currie, Bruce L.; Robins, Roland K.; Robins, Morris J., Preparation and Biological Activity of Various 3-Deazapyrimidines and Related Nucleosides. *Journal of Medicinal Chemistry* 1973, 16, (3), 294-297.

[21] Khare, G. P.; Sidwell, R.W.; Huffman, J. H.; Tolman, R. L.; Robins, R. K., Inhibition of RNA Virus Replication in vitro by 3-Deazacytidine and 3-Deazauridine. *Proc. Soc. Exp. Biol. Med.* 1972, 140, 880-884.

[22] Searls, Tim; McLaughlin, Larry W., Synthesis of the Analogue Nucleoside 3-Deaza-2'-deoxycytidine and its Template Activity with DNA Polymerase. *Tetrahedron* 1999, 55, (41), 11985-11996.

[23] Morales, Juan C.; Kool, Eric T., Efficient Replication between Non-hydrogen-bonded Nucleoside Shape Analogs. *Nature Structural Biology* 1998, 5, 950-954.

[24] Currie, Bruce L.; Robins, Roland K.; Robins, Morris J., The Synthetis of 3-Deazapyrimidine Nucleosides Related to Uridine and Cytidine and their Derivatives (1a,b). *Journal of Heterocyclic Chemistry* 1970, 7, 323-329.

[25] Cook, P. Dan; Day, Robert T.; Robins, Roland K., An Improved Synthesis of 3-Deazacytosine, 3-Deazauracil, 3-Deazacytidine, and 3-Deazauridine. *Journal of Heterocyclic Chemistry* 1977, 14, 1295-1298.

[26] Dove, W. F.; Davidson, N., Cation Effects on Denaturation of DNA. *Journal of Molecular Biology* 1962, 5, (5), 467-468.

[27] Petruska, John; Goodman, Myron F., Enthalpy-Entropy Compensation in DNA Melting Thermodynamics. *J. Biol. Chem.* 1995, 270, (2), 746-750.

[28] Rouzina, Ioulia; Bloomfield, Victor A., Heat Capacity Effects on the Melting of DNA. 2. Analysis of Nearest-Neighbor Base Pair Effects. *Biophys. J.* 1999, 77, (6), 3252-3255.

[29] Liu, Chu-Sheng; Schuster, Gary B., Base Sequence Effects on Hole Trapping Sites in Long Distance Charge Migration through Duplex DNA: A Good Correlation with Sodium Cation Distribution. *Unpublished results* 2006.

VITA

NATHAN WILLIAM SCHLIENTZ

Nathan William Schlientz was born in Conway, Arkansas on May 24, 1978 to parents William and Mary Ann Schlientz. He was raised with his 5 siblings, Dejah, Jason, Christa, Graham, and his twin sister Anna. His family has always been an instrumental part in raising Mr. Schlientz to work hard and always respect the people around him. His twin sister Anna has always been there for him, as a best friend and inspiration for him to succeed. He attended public schools in Conway, Arkansas, and received a B.A. in Chemistry from Hendrix College, Conway, Arkansas in May of 2000.

In high school, Mr. Schlientz lettered in tennis for four years. He continued playing tennis at Hendrix College, as well as managing the women's volleyball team for several years. While managing the volleyball team, he met and fell in love with his future wife Leah Hybl. While at Hendrix College, Mr. Schlientz majored in chemistry with a minor in mathematics. His desire to understand the fundamental properties of science led Mr. Schlientz to pursue a Ph.D. at Georgia Institute of Technology.

While at Georgia Tech, Mr. Schlientz enjoyed his research under the guidance of Professor Gary B. Schuster. During his life he has made many incredible friendships, and plans to enjoy every moment in life and love his friends and family to the best of his ability.